INVESTIGATION OF A PROTON EXCHANGE MEMBRANE FUEL CELL

by

Manogran Govender

Submitted in fulfilment of the academic requirements
for the degree of
Masters of Science
in the
School of Chemical Engineering,
University of Natal
2001

Supervisor: Prof. CA Buckley
Date of Submission : December 2001

ACKNOWLEDGEMENTS

I would like to acknowlegde the following people and companies,

My supervisor, Prof C.A Buckley, for his time, assistance and advice.

Dr Bavanethan Pillay, my co-supervisor, for his help in initially directing me in this project, and his advice throughout the project.

Eskom, for their financial assistance and Mr Gerhard Gericke at TRI for his assistance.

ElectroChem Inc. for their technical support.

Numerous other fuel cell companies for their technical information and advice.

Dr John Marsh from Anglo American Research Laboratories, for the discussions we had, which proved very helpful.

Dr Fiona Graham of the Electron Microscope Unit for taking the micrographs.

The workshop staff of the chemical engineering department, at the University of Natal, for building the equipment.

PREFACE

The whole thesis, unless otherwise stated, is my own work, and has not been submitted in part, or in whole to any other University.

This study was carried out at the University of Natal (Durban), under the supervision of Prof C. A Buckley and Dr Bavanethan Pillay. The work was financially supported by Eskom as part of their Tertiary Education Support Programme (TESP).

GLOSSARY

AFC	alkaline fuel cell
FEP	fluoroethylene polymer
MCFC	molten carbonate fuel cell
MEA	membrane electrode assembly
PAFC	phosphoric acid fuel cell
PEMFC	proton exchange membrane fuel cell
PFSI	polyflurosulphonic ionomer
PTFE	polytetrafluoroethylene
SOFC	solid oxide fuel cell
VOC	volatile organic compounds

ABSTRACT

This thesis involved the study of a proton exchange membrane fuel cell (PEMFC). The main aims of the study were to test, build and model a PEMFC. The tests were performed on a PEMFC purchased from ElectroChem Inc. (an overseas fuel cell company). The effects of temperature, pressure, humidification, oxidant (air *vs.* pure oxygen), and carbon dioxide dilution on the performance of the fuel cell were tested.

Results showed that increasing the temperature of the fuel cell increases the performance. There was an average increase of 1.6 % in the maximum current density and 1.5 % in the maximum power density for a 10 °C increase in temperature. Increasing the cell pressure by 1 atm resulted in an average increase in the maximum current density of 9 % and 15 % in the maximum power. Humidification resulted in a 10 % increase in the maximum current density and a 26 % increase in the maximum power density at 60 °C. The performance of the cell was very dependant on the state of humidification of the membrane and severe drop in performance was observed with the unhumidified cell run at temperatures greater than 60 °C. The air *vs.* pure oxygen test showed that the use of pure oxygen improved the cell performance significantly. There was a 21 % increase in the maximum current density and a 50 % increase in the maximum power density when oxygen was used as compared to air.
An increase in the carbon dioxide concentration resulted in a decrease in cell performance. An increase in carbon dioxide concentration from 0 % to 50 % resulted in a 17 % decrease in the maximum current density and 31 % decrease in the maximum power density.

A method for the preparation of the catalyst paste and the electrode was selected and modified after initial tests of various other methods. The main change made to the original method was that of lowering the solvent and Nafion® content by 50 % and 50 % respectively. This resulted in a catalyst paste that was thicker and easier to apply. A hot-press, used for assembling the membrane-electrode-assembly (MEA), was manufactured. The hot-press consisted of a G-clamp, with two metal plates placed in-between the clamp. The MEA was placed in-between the metal plates. A procedure for hot-pressing was developed. MEA's were manufactured and tested. The main problems encountered during the manufacturing process were cracking of the

catalyst layer and twisting of the MEA during hot-pressing. The manufactured MEA showed an average decrease of 23 % in the maximum current density and 26 % in the maximum power density as compared to commercial MEA's.

A one dimensional, multicomponent model describing the performance of the fuel cell was developed and a simulation programme written. The model was used to simulate the performance of the cell under various operating conditions. The predicted profiles and the experimental results showed the same trends.

TABLE OF CONTENTS

		Page Number
Acknowledgements		ii
Preface		iii
Glossary		iv
Abstract		v
Table of Contents		vii
Breakdown of Thesis Structure		xi
Chapter 1	Introduction	1-1
Chapter 2	Literature Review	2-1
Chapter 3	Theory	3-1
Chapter 4	Hydrocarbon Reforming	4-1
Chapter 5	Landfill Sites	5-1
Chapter 6	Market for Fuel Cells	6-1
Chapter 7	Fuel cells in South Africa	7-1
Chapter 8	Experimentation	8-1
	8.1 Experimental Equipment	
	8.1.1 Test Station	8-1
	8.1.2 ElectroChem (FCO5) cell	8-1
	8.1.3 Dais cell	8-2
	8.1.4 Humidification unit	8-2
	8.2 Experiments	8-3
	8.3 Experimental Procedure	8-4
	8.4 Safety Precautions	8-5

Chapter 9	Manufacturing	9-1
	9.1 Equipment	9-1
	9.2 Catalyst and Electrode Preparation Methods	9-2
	9.2 Hot-Pressing Procedure	9-5
Chapter 10	Modelling	10-1
Chapter 11	Results	11-1
	11.1 Effects of Temperature on ElectroChem cell	11-1
	11.2 Effects of Pressure on ElectroChem cell	11-2
	11.3 Effects of Humidification on ElectroChem cell	11-3
	11.4 Effect of Oxidant on ElectroChem cell	11-5
	11.5 Effects of CO_2 Dilution on ElectroChem cell	11-6
	11.6 Effect of Humidification on Dais cell	11-7
	11.8 Effect of Air flow on Dais cell	11-8
	11.9 Comparison of ElectroChem MEA and manufactured MEA	11-9
	11.10 Fuel Cell Model	11-10
Chapter 12	Discussion	12-1
	12.1 Experimentation	12-1
	12.2 Manufacturing	12-9
	12.3 Modelling	12-17
Chapter 13	Conclusion and Recommendations	13-1
Appendix A	Calibration Charts	A-1
Appendix B	Specification Sheets	B-1
Appendix C	Electrode Loading Calculations	C-1
Appendix D	Photographs	D-1
Appendix E	Scanning Electron Micrographs	E-1
Appendix F	Fuel Cell Model Program	F-1
Nomenclature		N-1
References		R-1

Tables

1.1	characteristics of the different types of fuel cells	1-3
8.1	experiments carried out on ElectroChem fuel cell (E-cell)	8-3
8.2	experiments carried out on Dais fuel cell (D-cell)	8-4
9.1	materials required for manufacturing process	9-1
9.2	equipment required for manufacturing process	9-2
B1	spefiication of Nafion® solution	B-1
B2	spefiication of Nafion® 117 membrane	B-1
C1	catalyst loading of the manufactured electrodes	C-1

Diagrams/ Figures

3.1	assembly of a PEMFC	3-1
3.2	cell reactions and flow of reactants and products	3-1
3.3	components of a fuel cell	3-2
3.4	cross sectional view of an electrode	3-3
3.5	polarisation curve	3-6
8.1	flow channel	8-1
8.2	humidification unit	8-3
8.3	test station	8-6
8.4	schematic drawing of ElectroChem cell	8-7
9.1	G-clamp hot-press	9-5
10.1	cross section of fuel cell showing direction of model dimension	10-1
10.2	flow diagram for model algorithm	10-20

Photographs

D1	ElectroChem FC05 cell	D-1
D2	gas flow channel	D-2
D3	test station	D-3
D4	humidification unit	D-4
D5	ElectroChem MEA	D-5
D6	manufactured MEA	D-6
D7	paint brushes	D-7
D8	G-clamp hot-press	D-8

SEM - Micrographs

E1	cross section of manufactured MEA & ElectroChem MEA	E-1
E2	surface view of manufactured MEA & ElectroChem MEA	E-2
E3	catalyst powder	E-3
E4	cross section of Nafion® 117 membrane	E-3
E5	backing material (carbon paper)	E-4

THESIS STRUCTURE

A breakdown of the chapters in this thesis is as follows

Chapter 1 gives a background into fuel cells and looks at the different types of fuel cells. The advantages and disadvantages of fuel cells are discussed. The aims of this study are detailed.

Chapter 2 is a literature review of journal papers and books.

Chapter 3 looks at the theory of fuel cells, and in particular the operation of a fuel cell and materials selection.

Chapter 4 looks at the theory of hydrocarbon reforming

Chapter 5 looks at the potential of landfill sites to supply fuel for fuel cells.

Chapter 6 deals with the potential application of fuel cells.

Chapter 7 looks at the potential of the fuel cell in South Africa.

Chapter 8 deals with the experimental section of the work, looking at the equipment used and experiments carried out.

Chapter 9 deals with the manufacturing section. The methods for catalyst, electrode and MEA preparation are detailed.

Chapter 10 looks at the modelling of the fuel cell. The model development is detailed in this section.

Chapter 11 shows the results of the experiments carried out.

Chapter 12 involves a discussion of the work done.

Chapter 13 lists the conclusions reached from this study and the recommendations made.

CHAPTER 1 : INTRODUCTION

Fuel cells have recently (over the past decade) received increasing attention world-wide, and research into fuel cells has increased significantly. A fuel cell is an electrochemical device that converts the chemical energy of fuel into electrical and thermal energy. The concept of the fuel cell is an old one. The first fuel cell (acid fuel cell) was built by Sir William Grove in 1859 (Appleby and Foulkes, 1993). The principle of the operation of a fuel cell is as follows. The fuel, hydrogen, is oxidised at a catalysed electrode called the anode. Protons travel through the electrolyte, from the anode to the cathode. The oxidant, oxygen, is reduced at similar electrode called the cathode. Electrons travel through an external load, thus accomplishing work, from the anode to the cathode. The by-product of this reaction is water.

Fuel cells were used in the first space missions (Gemini mission, which used PEMFCs, and the Apollo mission, which used an alkaline fuel cell) in the 1960's to provide onboard power requirements (Appleby and Foulkes, 1993). Commercialisation of the fuel cell was not viable at that time due to numerous problems. One of the main problems encountered was that of cost. Platinum was used as the catalyst in order to obtain sufficiently high reaction rates, and platinum loading was very high, approximately 25 mg/cm^2 (Appleby and Foulkes, 1993). Hence, interest and thus research into fuel cells declined. Due to stricter pollution and environmental laws, the attention has once again turned to the fuel cell. Research in fuel cells have seen major improvements, the main one being the reduction in the catalyst loading on the electrodes. Platinum loading has been reduced from about 25 mg/cm^2 to about 0.2 mg/cm^2 without reducing performance (Appleby and Foulkes, 1993).

1.1 Types of Fuel Cells

There are different types of fuel cells and the fuel that can be used and the products are different for these different types. There are two main differences between the various types of fuel cells, viz. the electrolyte used and the operating temperature.

There are 5 main types of fuel cells:

- phosphoric acid fuel cell (pafc)
- alkaline fuel cell (afc)
- proton exchange membrane fuel cell (pemfc) / polymer electrolyte fuel cell (pefc)
- molten carbonate fuel cell (mcfc)
- solid oxide fuel cell (sofc)

1.1.1 Phosphoric Acid Fuel Cell

The electrolyte is concentrated phosphoric acid. The acid is maintained in a matrix made of silicon carbide. Platinum catalysts are used for both the anode and the cathode. The operating temperature is 150 to 220 °C. Lower temperatures result in poor ionic conductivity of the acid. A major problem with pafc is carbon monoxide poisoning. Small amounts of carbon monoxide poisons the platinum catalyst (Appleby and Foulkes, 1993).

1.1.2 Alkaline fuel cell

Alkaline fuel cells use Potassium hydroxide (KOH) as the electrolyte. The electrolyte is kept in a matrix (which is usually asbestos). The concentration of KOH depends on the operating temperature. At temperatures of around 250 °C, a 85 weight percent KOH solution is used whereas for lower temperatures (<120 °C), 35 to 50 weight percent KOH solutions are used. A wide range of catalyst can be used, e.g. Ni, Ag, noble metals (Appleby and Foulkes, 1993).

1.1.3 Polymer Electrolyte Fuel Cell

The electrolyte is a polymer membrane. The polymer is a protonic conductor and the commonly used membrane is Nafion®. This is a perfluorinated sulphonic acid polymer. The membrane must be kept sufficiently hydrated since proton conductivity is dependant on water content of membrane. The operating temperature is < 120 °C. Platinum is generally used as the catalyst. Carbon monoxide (< 10 ppm) poisons the platinum catalyst (Appleby and Foulkes, 1993).

1.1.4 Molten Carbonate Fuel Cell

The electrolyte used is a combination of alkali (Na, K) carbonates. The electrolyte is immobilised in a ceramic matrix made of $LiAlO_2$. The operating temperature is around 600 to 700 °C, at which temperature the alkali carbonates form a highly conductive molten salt and is sufficiently conductive to the carbonate ions. The anode is made from porous sintered nickel and the cathode consists of nickel oxide. Sulphur is a contaminant and concentrations of hydrogen sulphide above 10 ppm affects performance significantly (Appleby and Foulkes, 1993).

1.1.5 Solid Oxide Fuel Cell

The electrolyte used is a solid, nonporous metal oxide. Yttria-stabalised zirconia is normally used. The operating temperature is between 650 to 1000 °C. At these high temperatures the solid oxide electrolyte becomes sufficiently conductive to oxide ions. The anode consists of metallic nickel or cobalt with yttria-stabilised zirconia. The cathode is made of porous strontia-doped lanthanum manganite (Appleby and Foulkes, 1993).

Table 1.1 : Characteristics of the different types of fuel cells

	AFC	**PAFC**	**PEMFC**	**MCFC**	**SOFC**
Anode	$H_2 + 2OH^- \rightarrow 2H_2O + 2e$	$H_2 \rightarrow 2H^+ + 2e^-$	$H_2 \rightarrow 2H^+ + 2e^-$	$H_2 + CO_3^{2-} \rightarrow H_2O + CO_2 + 2e^-$	$H_2 + O^{2-} \rightarrow H_2O + 2e^-$
Cathode	$1/2O_2 + H_2O + 2e^- \rightarrow 2OH^-$	$1/2O_2 + 2H^+ + 2e^- \rightarrow H_2O$	$1/2O_2 + 2H^+ + 2e^- \rightarrow H_2O$	$1/2O_2 + CO_2 + 2e^- \rightarrow CO_3^{2-}$	$1/2O_2 + 2e^- \rightarrow O^{2-}$
Overall	$H_2 + 1/2O_2 \rightarrow H_2O$	$H_2 + 1/2O_2 \rightarrow H_2O$	$H_2 + 1/2O_2 \rightarrow H_2O$	$H_2 + 1/2O_2 \rightarrow H_2O$	$H_2 + 1/2O_2 \rightarrow H_2O$
Op.Temp ^0C	100 - 250	150 - 220	<120	600 - 700	650 - 1000
Electrolyte	alkaline solution (KOH)	phosphoric acid	polymer membrane	alkali carbonate	solid nonporous metal oxide

1.2 Advantages of Fuel Cells

Reduced air pollution - produce lower levels of air pollution than other energy converters.

Higher efficiency - Fuel cells operate electrochemically and hence are not restricted by Carnot cycle. Fuel efficiencies of around 80 % and higher are obtainable as compared to about 30 % from other energy converters (Hirschenhofer *et al*, 1994).

The high efficiency are as a result of cogeneration, that is, the heat generated can be used for heating purposes.

Fuel supply - can operate on hydrogen derived from a variety of fuels and depending on the fuel cell, relatively impure hydrogen can be used (Appleby and Foukles, 1993).

Reduced noise pollution - the noise levels during fuel cell operation are lower than that of normal internal combustion engines. The noise from fuel cell operated vehicles is a result of the electrical motor (Appleby and Foulkes , 1993).

Reliability and maintenance - electrochemical power sources are potentially more reliable than internal combustion engines (Hirschenhofer *et al*, 1994). The fuel cell itself does not consist of any moving parts.

Portable - units (depending on size) are portable and can be transported with relative ease.

1.3 Disadvantage of fuel cells

Cost - the main disadvantage of fuel cells is the high cost. Fuel cells are presently not as economic as existing energy converters. This is mainly due to the fact that the fuel cell is in the development or initial stages of commercialisation. With the advancements made in terms or lower catalyst loading, cheaper catalysts and combined with increased production rate, the cost would be reduced significantly.

1.4 Fuels used

(i) pure hydrogen

(ii) hydrogen derived from the following fuels:

- alcohols (usually methanol)
- hydrocarbons (methane, naphtha, natural gas)
- coal (gasification of coal)
- hydrazine

Fuel cells can also operate on fuels such as hydrocarbons and methanol directly, that is, without external reforming (Appleby and Foulkes, 1993). These are referred to as direct fuel cells. The reforming is achieved within the cell with the use of appropriate reforming catalysts.

The fuel cell currently receiving the bulk of the attention is the PEMFC. The PEMFC is preferred to the other low temperature fuel cells (viz. AFC and PAFC) because the electrolyte is a polymer and not a liquid, hence there is no electrolyte loss due to evaporation or spillage. Also, PEMFC's offer good load characteristics, that is, the response to load variations. There is ongoing research to try to improve the performance, lower the catalyst loading, and find a cheaper alternative to Platinum as a catalyst. Studies looking at alternative fuels to pure hydrogen gas (Wang *et al*, 1995), reforming of fuel as well as direct PEMFC (Ren *et al*, 1996), electrode and MEA preparation methods (Cha and Lee, 1999), and the effect of impurities in the fuel, on cell performance are ongoing.

This study investigates the PEMFC. The study was in three parts. **Firstly**, a commercial fuel cell was tested under various operating conditions to observe the effects on the performance of the fuel cell. The effects of carbon dioxde as an impurity in the anode fuel stream was tested. The carbon dioxide tests were linked to the use of impure fuels as opposed to pure hydrogen. The main aim of the carbon dioxide tests was to experimentally observe the effects of CO_2 on performance of the fuel cell and hence get some idea of the extent of the reformation. It was basically a performance vs. cost trade-off, to determine the concentration of carbon dioxide that would affect performance of the fuel cell significantly. Naturally, more reformation means a higher reformation cost.

Secondly, a PEMFC was manufactured and, the main problems facing the manufacturing process were identified.

Thirdly, modelling of the fuel cell performance was undertaken so as to be able to predict the fuel cell performance under various operating conditions.

Eskom, as an energy provider, is looking into fuel cell technology. This project was financially supported by Eskom as part of its TESP funding programme. Fuel cell technology and research is very limited in South Africa. Fuel cells are only obtainable overseas, mostly in USA. The aim of this project and other such projects was to increase local knowledge on fuel cell technology.

CHAPTER 2 : LITERATURE REVIEW

The following aspects of the proton exchange membrane fuel cell (PEMFC) are reviewed:

- catalyst and electrode preparation
- fuel impurities
- membrane
- direct methanol fuel cell (DMFC)
- modelling

2.1 Catalyst and Electrode Preparation

Research in the catalyst and electrode preparation areas of the PEMFC have dealt mainly with attempts to lower the catalyst loading, and improve catalyst utilisation, find substitutes for platinum, and improve the diffusion of reactants both in the diffusion layer of the electrode backing and in the catalyst layer. All of the research looks at improving the performance of the fuel cell. The performance of the fuel cell is determined by the voltage and current density that it produces. Hence a cell with a higher cell voltage at the same current density would have a higher performance.

2.1.1 Catalyst and Catalyst Preparation Techniques

Ticianelli *et al* (1988) used electrodes with a platinum loading of 0.35 mgPt/cm^2 as compared to previous loading of 4 mgPt/cm^2. They incorporated Nafion® solution in the reaction zone by painting Nafion® solution onto the catalysed area. The performance of the lower platinum loading electrodes was similar to the higher loading one. The Nafion® in the electrode enhanced catalyst utilisation and protonic transport between the electrode and the membrane. Several methods including electrodepositing, chemical deposition and sputter deposition, which were used to localise platinum at surface of electrode, were reviewed by Srinivasan *et al* (1990). A loading of approximately 0.05 mgPt/cm^2 was deposited on the surface of the electrode, in addition to existing catalyst in the electrode. The results indicated that there was little improvement when using these methods. Wilson and Gottesfeld (1992 a) used a different technique, applying the catalyst directly to the membrane, instead of applying the catalyst onto a catalyst-backing layer and then hot-pressing the electrodes onto the membrane. The catalyst paste was applied onto Teflon sheets, hot

pressed and then peeled of. Platinum loadings of 0.15 and 0.22 mgPt/cm^2 were used. A higher catalyst loading increases the catalyst area and hence results in better performance at low current densities but the thicker layer causes diffusion problems at high current densities and, hence the performance drops. The performance of the 0.15 mgPt/cm^2 electrode was slightly lower than the conventional electrode with a catalyst loading of 0.45 mgPt/cm^2, but had a higher catalyst activity due to higher catalyst utilisation, that is, higher percentage of catalyst particles in contact with the reactant gases. Wilson and Gottesfeld (1992 b) improved on their method (Wilson and Gottesfeld, 1992 a) by simplifying the fabrication process. In the new method the catalyst was cast directly onto the membrane at elevated temperatures ranging from 150 to 190 °C. The new method improved the interfacial continuity between the ionomer in the membrane and in the catalyst layer. The catalyst loading was reduced to 0.12 mgPt/cm^2. An electrochemical catalysation technique was evaluated by Taylor *et al* (1992). The technique involved the impregnation of Nafion® solution onto uncatalysed carbon paper electrode. The platinum particles were then electrodeposited from a plating bath, through the Nafion®, into the electrode. The technique results in the deposition of platinum particles in regions of the electrode that are in ionic contact with the membrane and electronic contact with carbon support. A platinum loading of 0.05 mgPt/cm^2 was used. Performances higher than conventional electrodes with 0.5 mgPt/cm^2 was reported. Poltarzewski *et al* (1992) prepared electrodes using a method involving flocculate formation of the catalyst paste and a screen printing technique for application of the catalyst paste onto the carbon paper. The catalyst powder was mixed with PTFE, which served as a catalyst binder, and was converted to a flocculate by addition of isopropyl alcohol. The flocculate was screen printed onto the electrode. Nafion® solution is impregnated by floating the electrode on Nafion® solution. Catalyst loading of 0.5 mgPt/cm^2 are used. Tamizhmani and Capuano (1994a) investigated the effect of base metal oxide (nonnoble metal oxide) in a Pt-Cr-Cu alloy catalyst for the oxygen reduction reaction. Pt, Pt-Cr, Pt-Cr-Cu and mixture of Pt-Cr-Cu alloy with base metal oxide (copper oxide) were compared. The mixture of ternary catalyst with metal oxide yielded the highest performance as a result of having the highest electrocatalytic activity. The metal oxide catalyst had a six times greater cathode mass activity that the platinum catalyst, and a two times greater cathode mass activity that the platinum alloy catalysts. However, the

preparation method for the platinum alloy and metal oxide catalysts were more involved than that for the pure platinum catalyst. Kumar *et al* (1995) used electrodes with a loading of 0.1 mgPt/cm^2 applied by using a spraying technique. Higher performances were reported than the conventional 0.4 mgPt/cm^2 electrodes. Lalande *et al* (1995) investigated a new catalyst, cobalt phthalocyanine. The cobalt loading was investigated and found that a loading of 3.5 % w cobalt to support gave the best result. Uchida *et al* (1995) introduced a catalyst preparation method based on the formation of a perfluorosulphonate-ionomer colloid. Certain solvents, depending on the dielectric constant of the solvent, form colloids when mixed with Nafion® solution. The colloidal catalyst paste was applied to electrodes and hot-pressed onto a membrane. The methods results in the formation of uniform network of ionomer on the platinum particles. Catalyst loading of 0.5 mgPt/cm^2 were used and higher performance is reported than the conventional electrodes using Pt/C and PTFE/C. Wilson *et al* (1995) investigated transforming the ionomer to a thermoplastic form by an ion-exchange process. The ionomer are more melt-processable. A loading of 0.12 mgPt/cm^2 was used. The durability of the cell was tested by running the cell for 4000 hours during which time a 10 % loss in performance was noticed. The previous thin film methods (Wilson *et al*, 1992 a, b) were not very durable and the performance over time dropped because of poor binding in the catalyst layer. Ralph *et al* (1997) developed a high volume, low cost, electrode manufacturing process. A catalyst loading of 0.6 mgPt/cm^2 for the cathode and 0.25 mgPt/cm^2, 12 mgRu/cm^2 for the anode was used. A higher platinum to support ratio than the conventional value of 20 % w was suggested. The optimum platinum content of the Pt/C mixture was found to be 40 % w Pt. Uchida *et al* (1998) improved on their previous colloidal method (Uchida *et al*, 1995). The new method involved adding Pt/C to the solvent and then dropping PFSI into it while mixing, instead of adding the solvent to the Pt/C and ionomer mixture. The new method improved the reaction area and lowered the internal resistance. The catalyst loading was reduced from 0.5 mgPt/cm^2 to 0.1 mgPt/cm^2 while also improving the performance slightly.

2.1.2 Nafion® Loading

Paik *et al* (1989) investigated the effects of Nafion® thickness on the kinetics of the oxygen reaction on a platinum gauze electrode. Authors used Ticianelli's (Ticianelli *et al*, 1988) method of applying Nafion® solution to the electrode. The experimental observations were that a thin coating of Nafion® gave an oxygen reduction current that rose continuously but relatively slowly while the thicker layer gave a current thatrose sharply at low overpotentials but was limited by diffusion at large overpotentials. Poltarzewski *et al* (1992) investigated the effects of the Nafion® loading on the performance of the electrode. The study showed that at low loading, the Nafion® solution uniformly fills the micro and macropores of the electrode structure and increase its ionic conductivity. The pores were completely filled when the Nafion® loading was between 0.8 to 1 mg/cm^2. Higher loading resulted in the formation of a film on the external surface of the electrode, which increased the resistance of the electrode and decreased performance. A similar finding was reported by Watanabe *et al* (1995) who investigated the effect of the thickness of the Nafion® layer on the catalytic activity. The critical thickness of the Nafion® layer was found to be 0.2 μm, above which the diffusion of reactants becomes a limiting factor in cell performance. The investigations into the effect of Nafion® in the catalyst layer suggested that increasing the Nafion® content over a critical value decreased the performance.

2.1.3 Catalyst/Substrate Formation

Fournier *et al* (1997) studied two methods of catalyst/carbon substrate formation, *viz*. the inclusion and the supported methods. The inclusion method requires a more involved procedure. Fournier *et al* showed that in the high current region, the inclusion method yielded better results when the specific area of the carbon substrate was large and poorer results when the specific area was small. They found that the inclusion method with loading of 0.07 and 0.11 mgPt/cm^2 showed similar performance to supported catalysts with a loading of 0.287 mgPt/cm^2. Faubert *et al* (1998) investigated platinum inclusion in two types of carbon substrate. The results indicated that the inclusion method yielded better results in the high current region than the supported method. Electrodes with loading of 0.13 mgPt/cm^2 using the inclusion method performed better than electrodes with a loading of 0.15 mgPt/cm^2

using the supported method. Faubert *et al* findings are similar to that by Fournier *et al* (1997). The inclusion method resulted in lower platinum loading and higher performance than the supported method, but had a more involved preparation method than the supported method.

Uchida *et al* (1995) studied the influence of the carbon support on the microstructure of the catalyst layer. Their results indicated that acetylene black support (such as Vulcan XC-72R) gave the best results in terms of performance of the electrode. Uchida *et al* observed that the carbon support with large pore volumes performed the best. According to the authors, the large pore volume was needed to sufficiently distribute the ionomer over the platinum. It was observed that the ionomer was distributed in pore sizes of 0.04 to 0.1 μm. The platinum particles within this pore size contributed to the reaction, any platinum particles below this size distribution was wasted. Ye *et al* (1996) used a new type of catalyst support, porous carbonised polyacrylonitrile (PAN) foam. The PAN had a higher specific area than other support material, which resulted in a higher catalyst utilisation. Platinum loading of 13 $\mu g/cm^2$ were used. The catalytic activity was higher than with conventional support material. The preparation of the PAN was quite an involved procedure though. Uchida *et al* (1996) tested various carbon supports. The colloid method as developed by Uchida *et al* (1995) was used. It was observed that the acetylene blacks were best support material results. Acetylene blacks had a larger pore volume than the other carbon supports. A larger pore volume gave better performance as a result of better distribution of the PFSI over the platinum particles inside the agglomerate. Their findings were in aggreance to a similar study by Uchida *et al* (1995). The findings of support material studies were that PAN yielded higher performance than carbon blacks but required a more involved preparation method. Support material with a higher pore volume yielded higher performance.

2.1.4 Diffusion of Reactants

The diffusion of reactants, both through the catalyst backing layer and the catalyst layer had been investigated. Fisher *et al* (1998) looked at increasing the porosity of the catalyst layer of the cathode for air operated cells. The porosity was increased by use of a hot spraying method and addition of pore formers to the catalyst slurry. The higher porosity allows for increased access for oxygen from air to the cathode surface.

This resulted in improved performance and higher utilisation. Lufrano *et al* (1999) investigated a new method of electrode fabrication. A carbon layer was added between the catalyst and carbon paper substrate. The carbon layer provided a microporous hydrophobic layer to optimise the gas distribution. They investigated the Teflon content in this layer and reported that the optimum Teflon content was 20 % w. Nguyen (1993) developed a new gas distribution design. The new design improved mass transport rates from the flow channel to the catalyst layer of the electrode and reduced flooding in the cathode. In the new design the inlet and outlet flow channels were dead-ended. Reactants were forced to flow through the electrode to the exit. The transport of reactants was transformed from the conventional diffusion mechanism to a convection mechanism. Results with the new design were better than that with the conventional design.

2.2 Membrane

The membrane generally used in PEMFC was a perfluorosulfonic acid polymer. Various types of membranes were available and determination of the transport properties of some of these membranes were determined. Literature dealing with water management and humidification was also reviewed. The performance of the membrane was determined by its conductivity such that a higher conductivity would result in lower ohmic losses through the membrane and increased performance of the fuel cell in terms of voltage produced.

2.2.1 Types of Membranes and Measurement of Transport Properties

Chen *et al* (1995) investigated the effect of pressure on Nafion® 117. The results showed that the conductivity decreased with increasing pressure. The thermal stability of Nafion® 117 was investigated by Samms *et al* (1996). Their studies showed that the membrane was stable up to 280 °C. Okada *et al* (1997) investigated the impurity of Ca^{+} ions in Nafion® 117 membrane. The results showed that the impurity decreased the water content of the membrane and hence decrease the performance. Impurities could beintroduced as a result of the catalyst preparation methods.

Fuller and Newman (1992) used a concentration cell to measure the transport properties of Nafion® 117. A transport number or drag coefficient of 1.4 water

molecules per proton was reported. Zawodzinski *et al* (1993 a) investigated water uptake, water diffusion coefficient and drag coefficient of Nafion® 117. A water content of 22 molecules per sulphonic acid group for immersion in liquid water and 14 with saturation in water vapour was reported. The diffusion coefficient increased with increasing water content. A linear increase in conductivity with water content was observed. A drag coefficient of 2.5 to 2.9 for immersion in liquid water was measured. The drag coefficient shows a marked difference with the drag coefficient for the membrane saturated with water vapour as measure by Fuller and Newman (1992). Zawodzinski *et al* (1995) investigated the drag coefficient for Nafion® 117 and reported a drag coefficient of 1 for Nafion® 117 at saturated water vapour and 2.5 for liquid water. Results of the drag coefficient of the membrane saturated in liquid water were similar to the study by Zawodzinski *et al* (1993 a) but the drag coefficient with membrane saturate with water vapour showed a difference to the value measured by Fuller and Newman (1992). Zawodzinski *et al* (1995) reported that the drag coefficient was independent of the water content of the membrane over a wide range of membrane water content. Fuller and Newman (1992) reported similar trends with the independence of the drag coefficient on the water content of the membrane.

Srinivasan *et al* (1990) investigated the Dow Nafion® membranes. Tests showed that the Dow membrane performed better than the Nafion® membrane. This was due to the greater number of sulphonic acid groups in the Dow membrane, resulting in a lower equivalent weight. Zawodzinski *et al* (1993 b) measured the water transport properties of three perfluorosulfonic acid membranes, Nafion® 117, Dow and membrane C (from Chlorine Engineers). The Dow membrane had the highest water uptake value, the best rehydration characteristics and the highest conductivity. The performance or conductivity of membrane C was slightly lower than that of the Dow membrane, with the Nafion® membrane having the lowest performance. Zawodzinski *et al* findings were similar to that by Srinivasan *et al*. Eisman (1990) also investigated the Dow membrane and found that the Dow membrane to performed better than the Nafion® membrane as reported by Zawodzinski *et al* and Srinivasan *et al*. Wakizoe *et al* (1995) investigated Dow, Aciplex-S and Nafion® membranes and also reported that the Dow membrane yielded the highest performance. Wang *et al* (1996) used a new type of membrane, polybenzimidazole (PBI). The membrane was operated at a

temperature of 150 °C, which was much higher than the perfluorinated membranes which were usually run at 80 to 100 °C. The PBI was a polymer, doped with phosphoric acid and had the advantage of a very low drag coefficient which resulted in reduced dehydration of the anode.

2.2.2 Membrane Humidification

Watanabe *et al* (1996) proposed a thin membrane (50 μm) containing 0.07 mgPt/cm^2 and few weight percent hygroscopic materials such as silica or titania. The platinum catalysed the oxidation of crossover hydrogen and oxygen to generate water, which was absorbed by the oxide particles, thus humidifying the membrane. The new membrane showed better performance than normal membranes due to a lower resistance. Watanabe *et al* (1998) used a similar approach as Watanebe *et* al (1996) by using nanocyrstals highly dispersed in Nafion® 112 (50 μm) to catalyse the recombination of the crossover hydrogen with oxygen and water generated was found to humidify the membrane directly. Their findings were similar to Watanabe *et al* (1996). Büchi and Srinivasan (1997) investigated operating a PEMFC without external humidifcation and investigated controlling the operating conditions, like gas flowrates, to allow the water produced by the reaction to keep the membrane hydrated. A counter flow of gases such that inlet of one crosses outlet of other was investigated. The results however showed that humidification, as opposed to their approach, gave a higher performance. Voss *et al* (1995) also looked at optimising operating conditions to allow self humidification. They investigated a technique where the fuel flow was optimised such that a pressure drop along the flow channel is obtained, which enhanced back diffusion of water from the cathode to the anode. Ticianelli *et al* (1988) optimised the humidification temperature and recommended humidification temperatures of 5 °C higher than the cell temperature for the cathode and 10 to 15 °C higher than the cell temperature for the anode. Humidification investigations showed that external humidification of the gases were necessary for good performance, especially at high temperatures. Thinner membranes, with hygroscopic particles and platinum particles gave higher performance but the reaction of crossover reactants reduced fuel efficiency.

2.3 Fuel Impurities

The review deals mainly with carbon monoxide and carbon dioxide, which are the most common fuel impurities, since these are the products of hydrocarbon reforming. Hydrocarbons are reformed to produce hydrogen for the fuel cell.

Dhar *et al* (1986) studied the effects of carbon dioxide and carbon monoxide on the platinum catalyst in a phosphoric acid cell. Since platinum was also used in PEMFCs, the results of their study were of relevance to this review. The result indicated that carbon dioxide acted as a diluent and carbon monoxide poisoned the platinum catalyst. They found that carbon monoxide poisoning was logarithmically dependent on the ratio of CO/H_2 concentration. This dependence indicated the replacement of hydrogen by carbon monoxide molecules. Gottesfeld and Pafford (1988) introduced the concept of adding oxygen to the anode stream in PEMFC to breakdown the carbon monoxide. The oxygen oxidises the carbon monoxide to carbon dioxide. The PEMFC was reported to be tolerant to carbon dioxide. A ratio of 2 to 5 % oxygen to hydrogen resulted in almost complete recovery for 100 to 500 ppm carbon monoxide. Schmidt *et al* (1997) proposed adding liquid hydrogen peroxide to the anode humidifier. The hydrogen peroxide decomposes to oxygen, which oxidises the carbon monoxide to carbon dioxide. The principle was the same as that used by Gottesfeld and Pafford (1988). Complete recovery for 100 ppm carbon monoxide concentration was reported. Bellows *et al* (1998) used a method similar to Schmidt and Gottesfeld, by using less than 1 % hydrogen peroxide in anode humidifier and also found minimal loss with 100 ppm carbon monoxide. They noticed that when the hydrogen peroxide decomposition was stopped the oxidation of the carbon monoxide to carbon dioxide also stopped.

Oetjen *et al* (1996) investigated the effect of carbon monoxide, in the concentration range of 25 to 250 ppm carbon monoxide, on Pt and Pt-Ru catalysts with a platinum loading of 1 $mgPt/cm^2$. The results showed that the Pt-Ru catalyst gave the best results but still showed a decrease in performance even with 25 ppm carbon monoxide. A similar study was undertaken by Ianniello *et al* (1995), who investigated carbon monoxide adsorption and oxidation on Pt and Pt-Ru. Ianniello suggested that the oxygen containing species bound preferentially to ruthenium rather than the platinum, which was used for hydrogen oxidation. Their results were similar to Oetjen

et al. Schmidt *et al* (1998) investigated the use of a binary colloid catalyst for the oxidation of carbon monoxide. The colloid catalysts gave higher performance than the Pt-Ru catalyst.

The articles reviewed above all indicated that carbon monoxide poisons the platinum catalyst. Carbon monoxide poisoning caused by chemisorption of carbon monoxide onto the platinum catalyst forming nearly complete carbon monoxide monolayer, which blocked the reaction sites for oxidation of hydrogen. Carbon dioxide was a diluent in the system and as such did not poison the catalyst.

2.4 Direct Fuel Cells

Direct fuel cells use fuels containing hydrogen, such as hydrocarbons and alcohols directly, without external reformation.

2.4.1 Direct Methanol Fuel Cell

The direct methanol fuel cell (DMFC) is receiving increasing attention due to the advantages of using liquid methanol over gaseous hydrogen or hydrocarbons. The various areas of research in DMFC are reviewed here. Fuel cells using ethanol are also discussed.

Verbrugge (1989) investigated methanol diffusion through Nafion® membrane using a model and reported that methanol readily diffuse through perfluorosulphonic acid membranes. This crossover of methanol from the anode to the cathode caused a chemical short and lowered fuel utilisation. Verbrugge suggested that perfluoronated membranes could be used as an electrochemical sensor to measure methanol concentration. Verbrugge suggested investigation of new membranes or use of membrane incorporating a layer that is impervious to methanol. Barton *et al* (1998) developed an aqueous methanol sensor using Nafion®. Arico` *et al* (1999), studied the morphology of both supported and unsupported catalysts and found that unsupported catalysts gave better performance. Schmidt *et al* (1999) investigated Pt-Ru catalyst produced by colloidal Pt-Ru precursors supported on carbon support. Pt-Ru-colloid based catalyst showed similar activity towards methanol oxidation as other conventional Pt-Ru. Anderson *et al* (1996) theoretically investigated alloying various atoms with platinum. The results indicated that the elements from the first and second transition series to the left of the platinum group attract and activate water with

comparable or greater effectiveness than ruthenium, which was the most commonly used alloying material. Sun *et al* (1998) investigated carbon supported FeTMPP as the catalyst for cathode reaction in polybenzimidazole polymer electrolyte fuel cell run at 150 °C. The result showed that the new membrane was methanol tolerant. Gupta *et al* (1998) investigated catalysts other than platinum for oxygen reduction reaction. Methanol crossover decreases the activity of platinum. Various catalysts tested report similar performance to platinum but were methanol insensitive. Arico` *et al* (1996) studied the structure and morphology of the Pt-Ru/C catalyst by various methods and report improved methanol oxidation than with pure platinum. Ravikumar and Shukla (1996) investigate methanol crossover and found that methanol concentrations above 2 M affects performance of cell significantly, particularly at high temperatures. Ren *et al* (1996) investigated the performance of a DMFC using Pt-Ru catalyst with a loading of 2.2 $mgPt/cm^2$ in the anode and pure platinum with a loading of 2.3 $mgPt/cm^2$ for the cathode. Catalyst was applied directly to the membrane. This method was similar to that by Wilson and Gottesfeld (1992 b). The results showed that high performance was obtained if the cell was run at high temperatures at around 110 to 130 °C. Scott *et al* (1998 a) used vapourised aqueous methanol with Pt-Ru catalyst. Carbon cloth was investigated as the electrode backing and reported comparable or better results than with carbon paper. Scott *et al* (1998 b) investigated the effects of flow channel design and Teflon content and recommend a Teflon content of 13 to 20 % w. Argyropoulos *et al* (1999) investigated carbon dioxide removal in DMFC by analysing flow channel and exhaust manifold designs and compared carbon cloth and carbon paper as backing material. Reported findings similar to Scot *et* al (1998 a) in that the carbon cloth gave a higher performance. Arico` *et al* (1998) compared methanol and ethanol in a direct fuel cell. A composite membrane made of Nafion® ionomer and silica for water retention was used. Pt-Ru was used as the catalyst with a platinum loading of 2 $mgPt/cm^2$. The results indicated that methanol gave a higher performance than ethanol. Patel (1994) investigated using ethanol from agricultural source (corn) in direct MCFC and reports technical and economic feasibility. Delime *et al* (1998) investigated improving the dispersion of the platinum particles without increasing the loading. Ethanol was used as the fuel. Ren *et al* (1997) used a new method based on DMFC, to investigate transport properties of

membranes and reported transport properties of Nafion® 117 similar to existing literature.

2.5 Modelling

The modelling of PEMFCs is reviewed below. The models are divided into two sections, the one-dimensional and two-dimensional models.

2.5.1 One-Dimensional Models

The one-dimensional models reviewed below were all isothermal models. The dimension taken into account was the co-ordinate along the cross section of the MEA. Springer *et al* (1991) developed a model that included the diffusion layers, catalyst layers and the membrane. The values for the water diffusion coefficient, drag coefficient and membrane conductivity were obtained by experimental measurements. The porosity of the carbon paper backing was taken into account by the use of a porosity factor. There was no comparison with experimental data. Bernardi and Verbrugge (1991) modelled the cathode electrode. Model considered the catalyst layer, diffusion layer and membrane. The model included velocity and transport terms in the membrane. A good fit with experimental data was reported. Bernardi (1990) developed a model that identified the operating conditions that a cell should be run at to achieve water balance. The model was confined to the diffusion layers. Model predicted operating condition were found for experimental result but the experiment using their predicted operating conditions was not conducted. Bernardi and Verbrugge (1992) developed a model taking all the layers into account. The model used velocity and transport equations for the membrane as used in their previous model (Bernardi and Verbrugge, 1991). They reported a good fit with experimental data.

Springer *et al* (1993) developed a model that incorporates the entire range of the polarisation curve. The model was based on the cathode only, since authors assumed that the anode overpotential was negligible. Protonic conductivity and oxygen permeability in the cathode catalyst layer were modelled. The effect of catalyst distribution in the catalyst layer was also investigated. The model assumes the membrane was always saturated. Model results indicated that a distributed catalyst layer increased the effective conductivity and permeability. The fit to the experimental data was good. Amphlett *et al* (1995 a, b) took a parametric approach to

the modelling of the fuel cell. The first paper (1995 a) dealt with the model development. The model assumed that the net flux of water was zero and hence water transport through the membrane was ignored. The equations for the cell voltage, overpotentials and equilibrium potential were developed and written in parametric form by linear regression of these equations. The second paper (1995 b) dealt with the experimental section, where the parameters of the equations developed in the first paper were found. This was achieved by fitting the experimental data to the parametric equations. The paper reported a good fit between experimental data and model prediction.

Kim *et al* (1995) suggested an empirical equation to fit experimental data. The model incorporated a term for the mass transport losses. The mass transport term was obtained through curve fitting experimental data and had no theoretical backing. The parameters were obtained by non-linear regression analysis. Broka and Ekdunge (1997) compared two models, pseudohomogenous film and an agglomerate model, for the cathode. The pseudohomogenous film model assumed that the active layer consisted of four media, that is, a diffusion, ionic (proton) conduction, electronic (electron) conduction and reaction medium. The agglomerate model assumed the active layer contained small agglomerates consisting of carbon, platinum and Nafion® solution mixture, separated by gas pores. From scanning electron microscope studies, simulations and experimental data, Broka and Ekdunge have concluded that the agglomerate model was a better representation of the active catalyst layer than the pseudohomogenous film model.

2.5.2 Two-Dimensional Models

The two-dimensional models took the distance along the flow channel as the second co-ordinate. The first dimension was the same as that in the one-dimensional models. Fuller and Newman (1993) developed a non-isothermal model that was based on concentrated solution theory. Fuller investigated the transport number of water across the membrane and experiments to calculate the diffusion coefficient of water in the membrane are conducted. The model also looked at utilisation of reactants and showed that heat removal was important in the operation of the cell. There was no comparison with experimental data. Nguyen and White (1993) developed a non-isothermal model in which diffusion through the electrode was ignored since the

authors assumed the electrode is ‘ultrathin’ and thus the diffusion layer was of negligible thickness. There was no comparison with experimental data. Gurau *et al* (1998) developed an isothermal model using nondimensional transport equations. The model showed a good fit with experimental.

A non-isothermal model was developed by Yi and Nguyen (1998). The model included convective water transport across the membrane by a pressure gradient, temperature distribution in solid phase along flow channel, heat removal by natural convection and heat exchangers based on coflow and counterflow. They sugested a pressure differential between the cathode and the anode to increase the back transport of water from the cathode to the anode. The results indicated that effective heat removal was necessary to prevent excessive temperature increase leading to local membrane dehydration, which was similar to finding by Fuller and Newman (1993). Yi and Nguyen reported that the counter flow heat exchanger yielded the best result for heat management.

CHAPTER 3 : THEORY

The PEMFC, as its name suggests, uses a polymer electrolyte membrane, which selectively allows protons to pass through it. The following diagram shows the basic assembly of a PEMFC (Fuller, 1993).

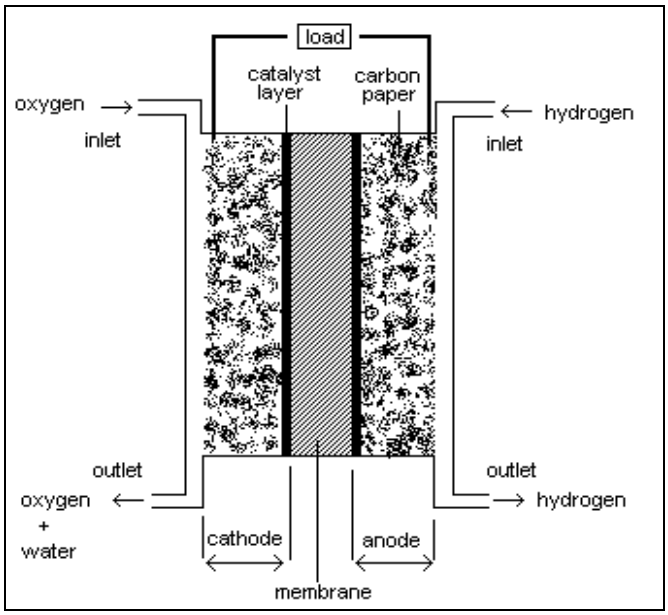

Figure 3.1 : Fuel cell assembly

3.1 Cell Reactions and Operation

Anode: $H_2 <=> 2H^+ + 2e^-$ (3.1)

Cathode : $1/2\ O_2 + 2H^+ + 2e^- <=> H_2O$ (3.2)

Overall: $H_2 + 1/2\ O_2 <=> H_2O$ (3.3)

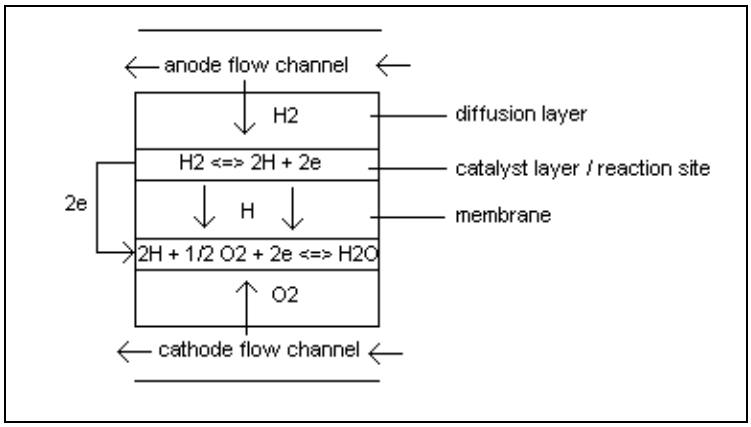

Figure 3.2 : cell reactions

The basic operation of the fuel cell is as follows:

Hydrogen gas enters at the anode and diffuses through the porous carbon paper electrode to the catalyst layer, where the hydrogen is oxidised to hydrogen ions. The hydrogen ions travel across the proton exchange membrane to the cathode. The electrons, unable to pass through the membrane travel from the anode, through an external circuit, to the cathode. At the cathode, O_2 gas diffuses through to the reaction site where the O_2 atoms combine with the hydrogen ions and electrons to form water.

3.2 Cell Components

The components of fuel cell are shown in the diagram below (Ticianelli *et al*, 1988):

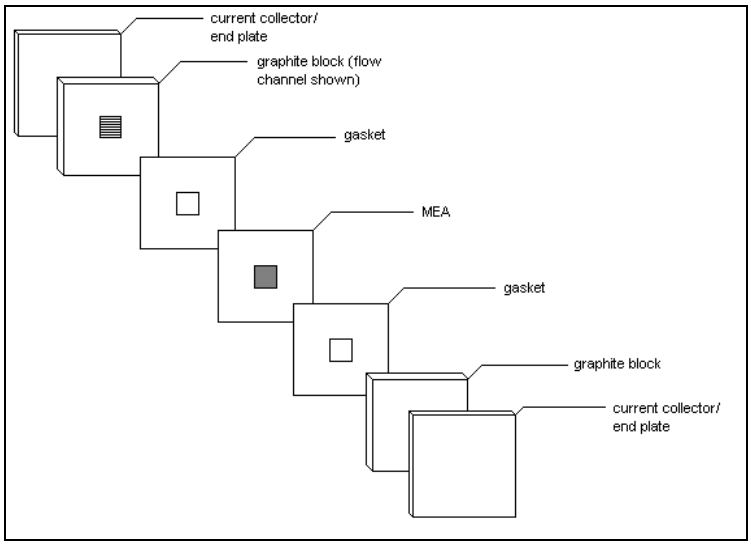

Figure 3.3 : Fuel cell components

The cell consists of a membrane electrode assembly (MEA). The MEA consists of two electrodes, called the anode and the cathode, sandwiching a polymer membrane. The electrodes are made of porous carbon paper with the catalyst layer impregnated onto one side. The MEA is placed in-between two graphite blocks which have flow channels machined into them. The flow channel represents the flow pathway for reactants and products. Metal plates, called current collectors, are placed on either side of the graphite blocks. Current collectors are usually made of copper or gold plated metal. They serve as collection terminals for the current. End plates, which are usually made from stainless steel are used to hold the entire cell together. Current collectors can also be used as end plates. Gaskets, which are made of silicone, are used to ensure proper sealing of the cell and prevent gas leakage. These are placed

between the graphite block and the MEA. The gaskets also prevent the graphite blocks from making contact and thus shorting out the cell.

A closer look at the electrode shows the reaction zone and diffusion layers more clearly (Taylor *et al*, 1992).

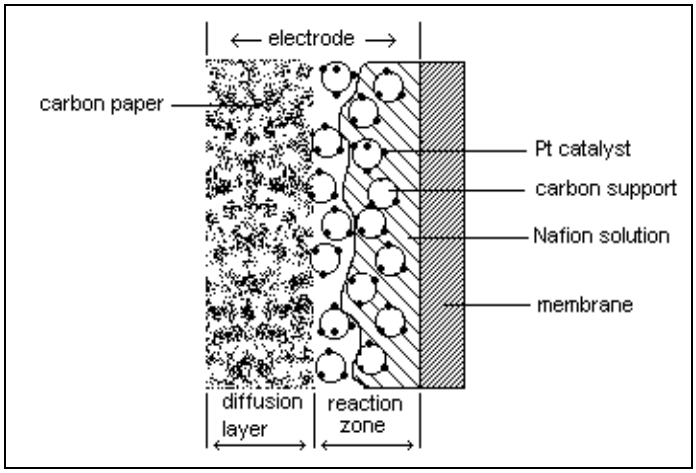

Figure 3.4 : electrode structure

3.3 MEA Components

3.3.1 Electrode Backing

The electrode backing serves to support the catalyst paste. It constitutes the diffusion layer. The basic requirements of the backing are that it allows diffusion of reactants and products through them and is electronically conductive. Carbon paper, usually Toray®, is most commonly used though carbon cloth is also used (Appleby and Foulkes, 1993).

3.3.2 Catalyst

The function of the catalyst, or rather electrocatalyst since the reactions are electrochemical in nature, is to increase the reaction rates. This is done by providing the reaction with an alternative path that has a lower activation energy as compared to the uncatalysed reaction.

3.3.2.1 Requirements of the electrocatalyst (Appleby and Foulkes, 1993):

Stability:- the electrocatalyst must be stable in the operating environment of the fuel cell, that is, the electrocatalyst must not corrode.

Electrocatalytic activity:-Naturally the electrocatalyst need to have a sufficiently high activity. The Tafel equation (see equation 1 in chapter 10 "Modelling") represents the relation between current density and activation overpotential. The activation overpotential is simply the deviation of the cell potential from the equilibrium potential. The exchange current density is the maximum current that can be achieved at negligible overpotential. The exchange current density gives us an indication of the activity of the electrocatalyst. Electrocatalysts with a high exchange current density have high catalytic activity (Appleby and Foulkes, 1993). See chapter 10 'Modelling' for more detail on reaction kinetics.

Electronic conductivity:-the electrocatalyst must be electronically conductive to ensure good conduction of electrons to the current collector. If the electrocatalyst has a poor electronic conductivity, it must be supported on or dispersed within a conducting support, such as graphite.

Adsorption characteristics - since the reactants and/or reactant intermediates adsorb onto the catalyst surface, the electrocatalyst needs to have suitable adsorption characteristics.

The catalyst used in PEMFC is usually platinum since it meets all of the above criteria. Other catalysts have been successfully used, the most common one being ruthenium. Platinum/Ruthenium alloys have been successfully used and are less prone to catalyst poisoning due to carbon monoxide than pure platinum (Appelby and Foulkes, 1993).

3.3.3 Catalyst Support

The function of the catalyst support is to ensure maximum activity of the electrocatlayst (Appleby and Foulkes, 1993). The requirements of the support material are that it is electronically conductive, stable and has a sufficiently high surface area, to allow effective dispersion of the catalyst particles.

The platinum catalyst is supported on a carbon support. A commonly used support is Vulcan XC-72R, which has a specific surface area of about 254 g/m^2 (Fournier *et al*, 1997).

The reaction zone shown in figure 1 is the catalysed region. The catalyst layer is impregnated with Nafion® solution, which helps provide better proton conduction from reaction site to the membrane.

3.3.4 Membrane

The proton exchange membrane is a transparent polymer film also referred to as perfluoro-sulphonic acid polymer (Pyle *et al*, 1994). The most commonly used membrane in fuel cells is the Nafion® 117 membrane from DuPont®. See table B2 (page B-1) for properties on Nafion 117. Nafion® 117 is 175 microns (0.007 inches) thick.

The basic structural unit of the Nafion® 117 membrane is as shown below (Pyle *et al*, 1994)

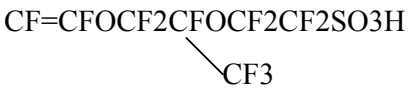

The unit consists of a number of carbon, fluorine, and oxygen atoms with an SO3H group at the end. The membrane is made up of a number of these units. The hydrogen atom from the SO3H group is free to detach from the SO3 site and the H^+ ion is able to hop from one SO3 site to the next, thus conducting (exchanging) the proton through the membrane, hence the name proton exchange membrane.

An important property of the membrane is its ability to absorb water. The membrane needs to be in a hydrated state for good proton conductivity. The performance of the membrane is defined by its conductivity, such that a higher conductivity results in a lower ohmic loss through the membrane thus increasing the performance of the membrane.

The membrane serves a dual purpose. Firstly, it serves as the electrolyte, permitting the transfer of protons from anode to cathode and secondly, it serves as a separator to prevent the anode and cathode reactant gases from mixing.

3.4 Polarisation curve

A theoretical graph of the polarisation curve (cell potential *vs*. current density) is shown below.

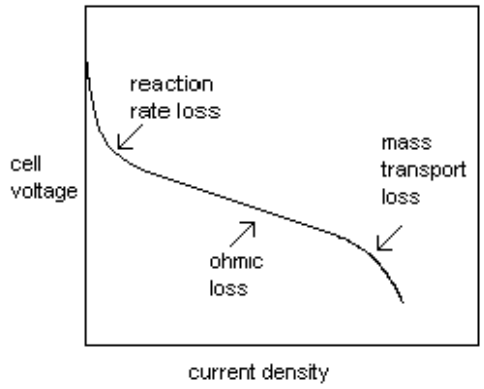

Figure 3.5 : Polarisation curve

The curve shows the main losses occurring in the cell. The initial part of the curve represents the reaction rate losses, which are called activation losses. These are due to slow electrode kinetics and occur predominantly at low current densities. The linear region of the curve represents the ohmic losses within the cell. These include the resistance of the membrane and the contact resistance. The final part of the curve represents the mass transport losses, which predominate at high current densities. Mass transport losses are caused by the increased difficulty of the reactant gases in reaching the reaction sites.

A more detailed look at the equation representing the polarisation curve is discussed in the modelling section in chapter 10.

CHAPTER 4 : HYDROCARBON PROCESSING

Fuel cells usually use hydrogen as the fuel. Hydrocarbons are a source of hydrogen. The hydrocarbons are processed to produce hydrogen, which is then used as the fuel in fuel cells. There are many processes for treatment of hydrocarbons, such as *steam reforming, partial oxidation, pyrolysis etc.* Steam reforming yields the best results with higher mole fraction of hydrogen and lower mole fractions of carbon monoxide in the product stream than the alternative processes (Appleby and Foulkes, 1993).

Steam reforming

Steam reforming refers to the reaction of hydrocarbon with steam to produce a hydrogen rich gaseous product. Excess steam and hydrocarbon in a mole ratio of 2 moles water to 3 moles carbon are reacted over a catalyst at a temperature between 450 and 800 °C. The product of this reaction is hydrogen, carbon dioxide, carbon monoxide, methane and steam (Appleby and Foulkes, 1993).

The reaction at high temperature can be written as:-

$$C_nH_{2n+2} + nH_2O \rightarrow (2n+1)H_2 + nCO \qquad (4.1)$$

assuming for the moment that all carbon product gas in carbon monoxide.

To increase the hydrogen yield and simultaneously decrease the concentration of carbon monoxide, which poisons the noble metal catalysts, the carbon monoxide is reacted further with steam via the water-gas shift reaction:-

$$CO + H_2O \leftrightarrow H_2 + CO_2 \qquad (4.2)$$

The above reaction is exothermic and reversible and carried out over a catalyst at about 500 °C. The shift reaction is sometimes carried out in more than one stage depending on the level of purity desired. Catalysts used are iron-chromium and copper based catalysts (Appleby and Foulkes, 1993).

The combined reforming and shift reactions results in the following reaction:-

$$C_nH_{2n+2} + 2nH_2O \rightarrow (3n+1)H_2 + nCO_2 \qquad (4.3)$$

Even further reduction in carbon monoxide concentration can be achieved by methanation, whereby the carbon monoxide is converted to methane:-

$$CO + 3H_2 \rightarrow CH_4 + H_2O \qquad (4.4)$$

Typical results (Appleby and Foulkes, 1993) show that after reforming, shift reaction and methanation of natural gas, the resulting gas stream has a composition by volume of 78 % hydrogen, 19.7 % carbon dioxide, 0.3 % methane, 2 % water, and 8 ppm carbon monoxide.

Methanol

The most convenient fuel for automative application is methanol. It s offers advantage of convenience and existing infrastructure for refueling. Methanol can be formed from methane gas from landfill sites and from chemical processes where methane is formed. A reformer would be fitted to the fuel cell to reform the methanol and produce hydrogen gas or the methanol can be used in direct fuel cells.

CHAPTER 5 : LANDFILL SITES

Landfill sites are a source of methane (CH_4). Methane exists as a gas and is a major component of landfill gas. Bacteria decompose the waste in a landfill site and the main by-product of this degradation is methane gas. Carbon dioxide and other gases are also produced. The methane gas, which is usually flared, can be reformed (as explained in chapter 5 'Fuels') and the hydrogen product used in a fuel cell, or used directly in a direct fuel cell.

Table 5.1: Typical landfill gas composition (Lombard *et al*, 1999)

Component	**Vol. %**
methane	64
carbon dioxide	34
nitrogen	2

A local landfill site over a 50 year period, cumulatively produces 321 m^3 of landfill gas per ton of waste (Lombard *et al*, 1999). The rate of gas production varies each year due to the amount of waste added. This site produces a minimum of 1000 to a maximum of 4000 m^3/hour of landfill gas that contains 50 %, by volume, methane (Lombard *et al*, 1999). Thus, there is a substantial amount of fuel available from landfill sites.

CHAPTER 6 : POTENTIAL MARKET FOR FUEL CELLS

This chapter looks at the potential application of the different types of fuel cells and the advantages and disadvantages of each type of fuel cell.

6.1 PAFC

PAFC's can be used for grid and a wide range of non-grid purposes. Large power units (12.5 kW and 4.5 MW PAFC) having been successfully used in the past (Appleby and Foulkes, 1993). The cells run on reformed natural gas. The disadvantages of the PAFC are that due to low operating temperature of PAFC's, noble metals, which are relatively expensive, are used as catalysts. The noble metals are poisoned by carbon monoxide and hence the fuel has to be relatively clean.

6.2 MCFC

MCFC's are typically used with hydrogen derived from hydrocarbons and coal. Also, the high temperature allows for internal reforming of the hydrocarbon fuel. This increases overall efficiency of the system as well as lowering cost by eliminating the need for external reformers. Catalyst choices are not significant due to the high temperatures. Due to higher power ratings of MCFC's, their potential lies mainly with power generation for power stations and industrial applications (Appleby and Foulkes, 1993).

6.3 SOFC

The SOFC's applications are similar to that of the MCFC.

6.4 PEMFC

PEMFC's are expected to be used mainly for non-grid purposes, for low to medium power requirements (Appleby and Foulkes, 1993). The main potential use at present is in the automotive application, in the production of electric vehicles. Due to stricter pollution laws, normal internal combustion engines, which produce large amounts of toxic fumes, are put under greater pressure to be less polluting. A number of automotive manufacturers are extensively involved in PEMFC studies and PEMFC cars have been built (The Chemical Engineer, 1999). Space programmes are also a potentail application,

with PEMFC's already having been used in the Gemini space mission (Appleby and Foulkes, 1993)

At present the main disadvantage of fuel cells is the high cost of production.

CHAPTER 7 : FUEL CELLS IN SOUTH AFRICA

The potential of fuel cells in South Africa is investigated from two points of view. Firstly, the potential of South Africa as a materials supplier is explored. Secondly, the areas of application of fuel cells and the specific type of fuel cell for each application are discussed.

South Africa is the leading producer of platinum, currently supplying 75 % of world consumption (Creamer, 1999). Platinum is the most widely used catalyst in fuel cells, especially in PEMFC's and PAFC's. South Africa also mines ruthenium (Creamer, 1999), which is also used as a fuel cell catalyst, usually alloyed with platinum. Platinum/Ruthenium catalysts are used in direct PEMFC and are less prone to poisoning by carbon monoxide than platinum. Being the leading platinum producer, as well as a major ruthenium producer, South Africa could potentially be an important country in the fuel cell market.

As explained in chapter 1 'Introduction', there are two main purposes for fuel cells, viz.

- large scale power requirements
- low to medium scale power requirements

The type of fuel cell used depends on the power required.

7.1 Large Scale Power Requirements

7.11 Power Stations

For large power generation, as in grid purposes and supplying of electricity on a large scale, SOFC and MCFC are used. The main advantage of fuel cell over existing technology, especially coal stations, is the reduced pollution and increased efficiency. The fuel cell can be run directly on hydrocarbon fuel or gassified coal.

7.2 Low to Medium Scale Power Requirements

7.2.1 Power for remote areas

Fuel cells can be used in remote areas that are not connected to a grid line. Fuel cells (depending on the size) have the advantage of being relatively mobile or transportable.

Hence, units can be placed in rural areas for example. PAFC or PEMFC are best suited for this purpose. They can be run of reformed gas from refuse dump sites or landfill sites, or even without reformation in direct fuel cells. The fuel cells require little maintenance and manpower for operation and have been proved to be reliable (Appleby and Foulkes, 1993).

7.2.2 Community Application

Fuel cells have been used successfully overseas to supply power requirements for small community buildings and sections of hospitals (Appleby and Foulkes, 1993). The fuel cell can also provide useful heat energy (cogeneration). This heat can be used to provide hot water for normal household applications. PAFC and PEMFC are expected to be used for this application.

7.2.3 Industrial Application

Industries, especially ones producing hydrocarbons and alcohols, are potential users of fuel cells. The industries producing hydrocarbons and alcohols are in effect manufacturing the fuel for fuel cells and can potentially supply their own electrical and heating (depending on the amount of electrical and thermal energy required) requirements. Depending on the power requirement of the industry, the main types of fuel cells that would be used are PAFC, PEMFC, and MCFC.

7.2.3.1 Automotive Industry

South Africa has a number of automotive manufacturing sites or assembling plants. With the automotive industry looking at fuel cell vehicles, particularly the PEMFC (The Chemical Engineer, 1999), South Africa could be involved in the manufacturing and/or assembling of fuel cell vehicles.

Thus, there would definitely seem to be a potential market for fuel cells in South Africa, both as a consumer and as a materials (catalyst) supplier.

CHAPTER 8 : EXPERIMENTATION

The aims of the investigation were:

- to build a test station and develop an operating procedure
- to test the effects of various operating conditions, viz. temperature, pressure, humidification, oxidant (air *vs.* pure oxygen)
- to test the effect of carbon dioxide dilution of the anode stream

8.1 Experimental Equipment

The equipment used for the experiments conducted are detailed below.

8.1.1 ElectroChem Cell

The ElectroChem cell (FC05) was a single test cell (see photograph D1 on page D-1). A schematic drawing of the cell is shown in figure 8.4 on page 8-7. The cell had an electrode area of 5 cm^2 and a catalyst loading of 1 $mgPt/cm^2$. The cell was equipped with heating pads and had a maximum temperature rating of 130 °C, controlled by a thermostat. It had a maximum pressure rating of 5 atm (abs). A Pin-stripe flow pattern (figure 8.1) was used in the flow channels. The anode and cathode were fitted with thermocouple wells.

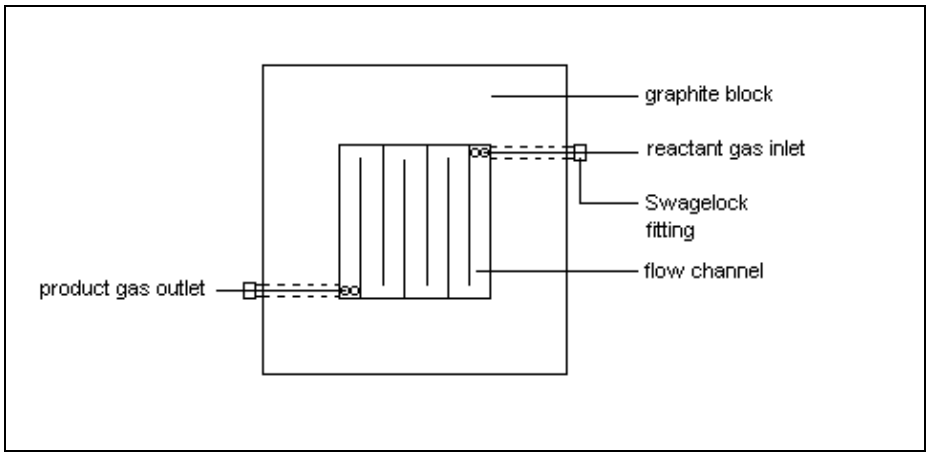

Figure 8.1: Flow channel pattern for ElectroChem cell

8.1.2 Dais cell

The Dais PEMFC was a single cell. The cell dimensions were 7 cm by 5 cm. The cell operated on air, at atmospheric pressure, as the oxidant. The MEA was an enclosed unit. The cathode electrode was visible and open to the atmosphere. The anode electrode was an enclosed compartment with an inlet and an outlet. Two ribbed metal plates were placed on top of the cathode and served to create a flow path for the air. Metal plates were placed on either sides of the MEA and served as current collectors. Stainless steel endplates held the cell together using two bolts, one at each end. The current collectors were separated from the end-plate by a piece of plastic insulator.

8.1.3 Experimental set-up

The experimental set-up (test station) is shown in figure 8.3 (see photograph D3 on page D-3). The test station was situated in a fume-cupboard. The test station consisted of a stainless steel sheet riveted onto a metal frame made from hollow, square metal tubing. The flowmeters, pressure gauges, eurotherm and temperature selector were mounted onto the stainless steel sheet. Copper tubing was used for connections from the gas cylinders to the flowmeters. Polyflow tubing was used for lines directly entering or leaving the fuel cell. Pt-100 thermocouples were used for temperature measurement. The computer, multimeter, load box and voltac were situated next to the fume cupboard.

8.1.4 Humidification unit

The humidification unit consisted of stainless steel water containers. The containers were filled with distilled water and the gases are bubbled through. The containers had a capacity of 500 ml. The unit consisted of a stainless steel tube, 5 cm in diameter and 26.5 cm in height, with stainless steel discs welded at both ends. Stainless steel tubes, 0.5 cm in diameter, which were used for the inlet and the outlet, were inserted and welded onto the discs. The inlet tube went down to a depth 25 cm. The outlet tube extended 0.5 cm below the top disc. Fittings for polyflow tubing were fitted onto the stainless steel tubing. The containers were filled through a threaded hole drilled into the top disc. A screw sealed the filling hole. A 23 cm long stainless steel tube was inserted through the filling screw and served as a thermocouple well. A Pt-100 thermocouple was inserted into the well and connected to the temperature selector.

The containers were placed on a heating pad, thus allowing the temperature of the water to be adjusted. The design is shown below (see photograph D4 on page D-4).

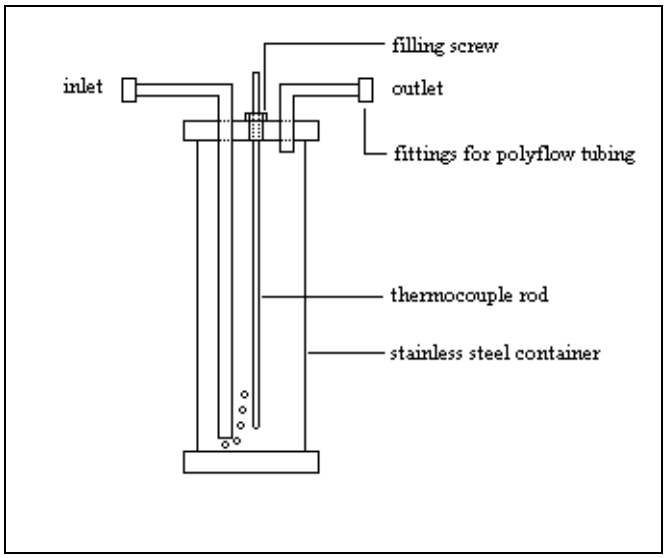

Figure 8.2 : Humidification unit

8.2 Experiments

Experiments were carried out on the two fuel cells, the FC05 from ElectroChem and the Dais cell. The tables below detail the experiments carried out for each cell.

Table 8.1: Experiments carried out on the ElectroChem cell

Temperature	**Pressure**	**Humidification**	**Carbon Dioxide Dilution**
P = 1atm, humidified	*T = 40 °C humidified*	*P = 1 atm*	*P = 1 atm, T = 40 °C, humidified*
°C	atm (abs)	°C	mole % CO_2
30	1	30	0
40	2	60	10
60	3		20
80			30
			50

Table 8.2*:* Experiments carried out on the Dais cell

Humidification	**Air Flow**
P = 1 atm	*P = 1 atm, 25 ℃*
25 °C	stagnant (fan off)
	high (fan on)

8.3 Experimental Procedure

Start-up

- open gas cylinder valves and feed line valves
- set required pressure and temperature of the cell
- set reactant gas flowrates
- humidify cell (under open circuit conditions) for 1 hour at 40 °C and 1atm
- do a run under varying load settings to saturate membrane

Run

- start data logging programme
- start 'load' run (starting at a low current, step the load and wait for stability of the current and voltage before changing the load setting)
- do an open circuit run to measure equilibrium potential

Shut-down

- stop logging programme
- switch off heaters and computer
- for high temperature runs, temperature greater than 40 °C, allow the cell to run under open circuit conditions for a few minutes to allow the cell to cool down
- close all flowmeters and valves, and switch off temperature display unit
- switch on the extractor fan for a few minutes

8.4 Safety Precautions

The main safety hazard anticipated with the experimental work was fire or explosion. Since we were working with hydrogen, which is a potentially explosive gas, the following safety precautions are taken.

- flashback arrestor on hydrogen regulator
- extraction fan in fume cupboard

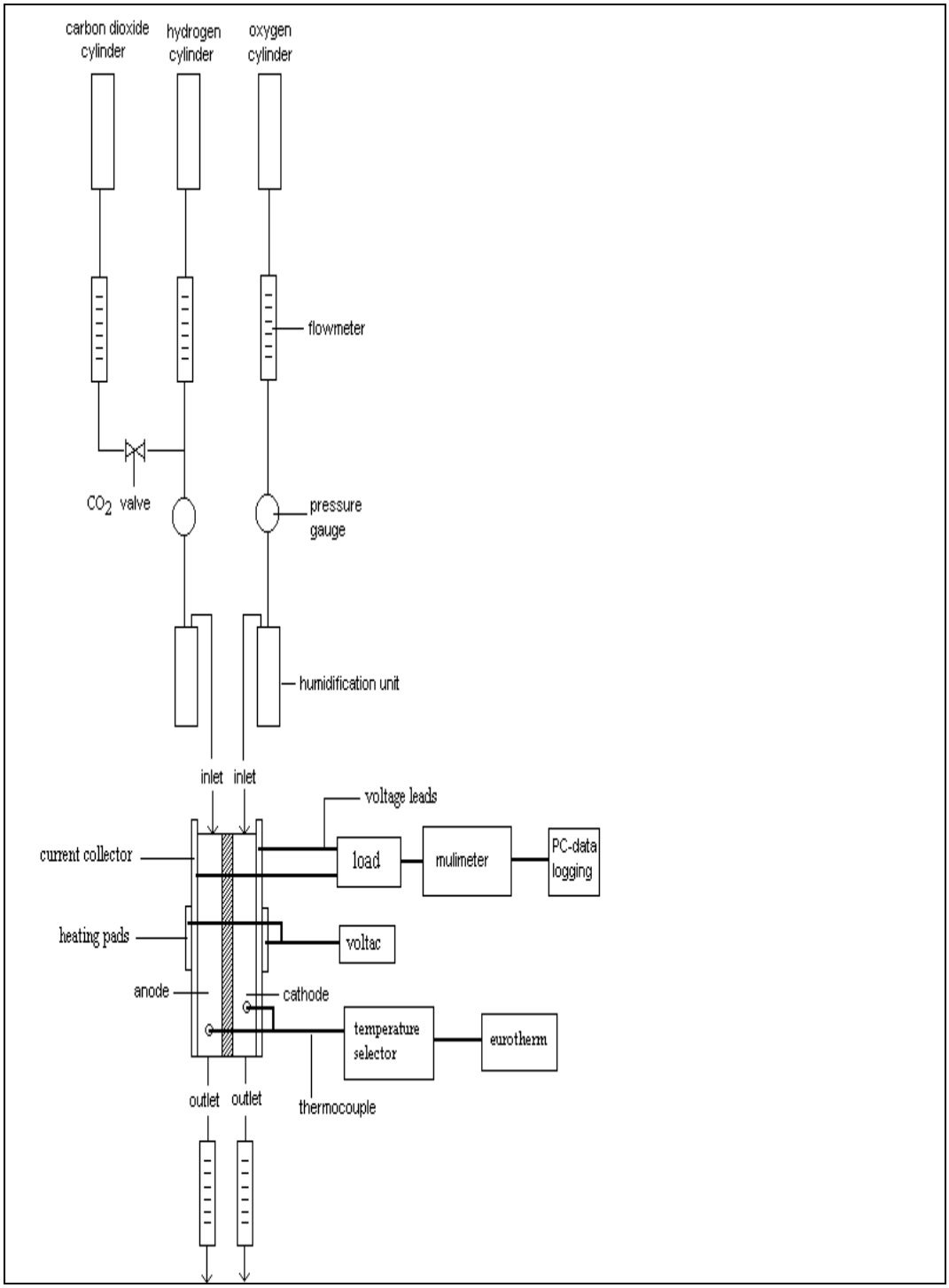

Figure 8.3 : test station

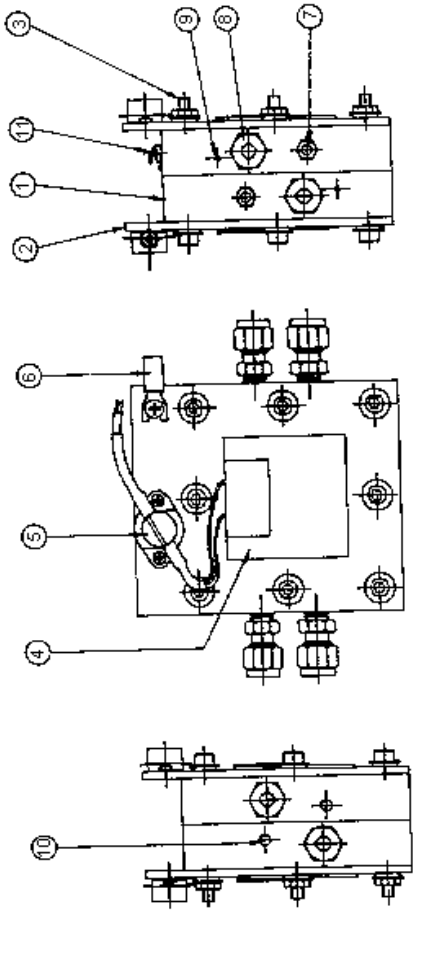

Figure 8.4: Diagram of ElectroChem cell (FC05) - (obtained from ElectroChem)

CHAPTER 9 : FUEL CELL MANUFACTURING

This part of the research details the manufacturing of a PEMFC, from the preparation of the catalyst mixture and the electrodes, to assembling the MEA and machining of the flow channels. The cost of manufacturing a fuel cell is analysed.

The main aims in manufacturing were to:-

- ascertain the availability of materials required for manufacturing a cell locally
- obtain a simple catalyst and electrode manufacturing technique
- manufacture a hot-press and develope a procedure for hot-pressing of the MEA
- identify the main problems in manufacturing a fuel cell

Table 9.1 : Materials required

Material	**Purpose**
platinum	catalyst
carbon support (Vulcan® XC-72R)	support for catalyst particle
nafion® solution	catalyst preparation method (improves proton conductivity from electrode to membrane)
nafion® 117 membrane	electrolyte
carbon paper (Toray®)	backing for the catalyst
fluoroethylene propylene polymer (FEP)	wet-proofing of carbon paper
polytetrafluoroetylene (PTFE)	binder for the catalyst
silicon rubber gaskets	sealing of the cell (prevent gas leaks)
graphite blocks	machining of flow channels
current collector (copper)	terminal for current collection
stainless steel end plates	holds the entire cell together

Table 9.2 : Equipment required

Equipment	Purpose
hot-press	to assemble the MEA. Allows the electrode/membrane/electrode sandwich to be compressed together at high pressure and at high temperature

9.1 Preparation Methods

While there were numerous catalyst and electrode preparation methods, the methods selected for this study had to be simple and not require any specialised equipment.

9.1.1 Carbon Paper Preparation

(Poltarzewski *et al*, 1992)

- carbon paper (Toray® TGP 90) was wet-proofed with a solution of fluoroethylene propylene polymer (FEP T 1200)
- dried at 70 °C for 1 hour
- sintered at 340 °C for 15 minutes

9.1.2 Membrane Preparation

(Poltarzewski *et al*, 1992)

- Nafion® membrane was treated with 5 weight percent H_2O_2/H_2O solution heated to boiling point to oxidise organic impurities
- rinsed in deionised water
- immersed in hot dilute sulphuric acid to remove metallic impurities
- treated several times in boiling deionised water to remove traces of the acid

9.1.3 Catalyst and Electrode Preparation

Method 1

(Poltarzewski *et al*, 1992)

- catalyst and aqueous dispersion of PTFE (61% Teflon®) were mixed and stirred at 50 to 60 °C for 15 minutes (the catalyst layer contains 40 weight percent PTFE and catalyst loading of 0.5 mgPt /cm^2)
- isopropyl alcohol was added to the cold solution and the flocculate screen printed onto the carbon paper

- the electrodes with the catalyst impregnated were dried in air at 120 °C for 1 hour, at 280 °C for 1/2 hour and then sintered in air at 340 °C for 1/2 hour
- the electrolyte (Nafion®) was impregnated onto the catalyst layer by floating the electrodes on a 5 weight percent Nafion® 1100 EW solution. Electrolyte loading was altered by varying the contact times with the electrolyte
- the impregnated electrodes were dried at room temperature for 12 to 15 hours and then heated at 130 °C under vacuum for 1 hour

Method 2

(Fournier *et al*, 1997)

- 12.9 mg of catalyst (Pt-C), 0.5 ml of distilled water and 0.3 ml of 5 weight percent Nafion® recast solution were blended ultrasonically for 1 hour
- 80 μl of catalyst was uniformly spread over 1 cm^2 of electrode material. This resulted in a Pt loading of 0.24 mg/cm^2 for 20 weight percent Pt-C
- a hot plate was used to accelerate the drying of catalyst on electrode
- the electrode was then dried in a vacuum oven at 75 °C for 1 hour

Method 3

(Uchida *et al*, 1995)

- perfluorosulphonate-ionomer (PFSI) solution in isopropanol (Nafion®) was added to a specific organic solvent e.g. alcohols, ketones, acids. A weight ratio of 1:60 PFSI dry weight to solvent was used. Certain solvents (depending on the dielectric constant of the solvent) formed colloids
- the colloids were mixed with Pt-C and treated ultrasonically to form a paste
- carbon paper was wet proofed with 40 weight FEP
- the catalyst paste was uniformly spread over the carbon paper. Most of the solvent passed through the carbon paper by filtration
- two electrodes were hot pressed to PFSI membrane (Nafion® 117) at 150 °C and 5 MPa for 1 minute

Method 4

(Ticianelli *et al*, 1988)

- Nafion® solution was brushed onto electrodes that have been catalysed

- evaporation of the solvent from the Nafion® solution (85 weight percent isopropanol/water) in the electrode under ambient conditions followed by vacuum drying at 70 °C for 1 hour
- hot-pressing a pair of electrodes onto membrane

Conventional Method

(Uchida *et al*, 1995)

- Pt-C and PTFE-loaded carbon (PTFE-C) were mixed and hot pressed onto carbon paper at 360 °C and 5 MPa.
- the steps from method 3 for applying Nafion® solution and hot pressing the electrodes were taken

Method 2(modified)

- 25 mg Pt-C catalyst powder was ground to a fine powder
- 0.1 ml Nafion® solution and 0.4 ml distilled water were added to the catalyst powder
- mixture was blended ultrasonically for 15 minutes
- catalyst paste was painted onto wet-proofed carbon paper (5 cm^2) using a soft paint brush (a single, thin coat of catalyst paste was applied)
- electrodes were dried at room temperature and ambient pressure
- successive coats of catalyst were applied depending on the required loading

9.2 Equipment : Hot-Press

A hot-press was used to assemble the MEA under high temperature and high pressure. Good MEA contact was very important since this lowers the resistance of the MEA by allowing an easy flow of protons from between the membrane and the reaction.

A hot-press had to be made since one was not available, and the cost of purchasing one was too high. A G-clamp with two metal plate in-between the clamp was suggested. The MEA was placed in-between the plates. A nut was welded onto the end of the turning shaft of the clamp so that a torque wrench can be used to tighten the cell. The diagram is shown below (see photograph D8 on page D-8).

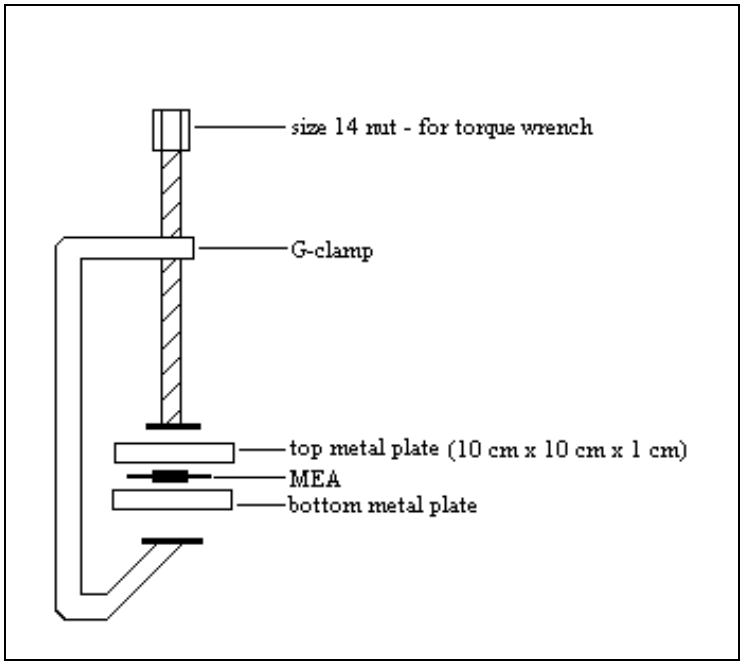

Figure 9.1: 'G-clamp' hot-press

9.3 Hot-Pressing Procedure

Conventional Hot-Press

(Ticianelli *et al*, 1988)

- two Nafion® impregnated electrodes were placed on either side of a wet Nafion® membrane
- the MEA was placed into the two platens of the hot-press set at 100 °C
- the temperature of the hot press was raised to 120 to 130 °C and a pressure of 50 to 60 atm was applied for 30 to 40 seconds

Note: The membrane dries up during hot pressing, hence the MEA must be hydrated before use.

9.3.2 G-clamp hot-press

- membrane was placed in boiling water for 30 minutes to hydrate the membrane
- first electrode was placed centrally on the bottom plate
- the membrane was placed on top of the electrode taking note to align the membrane centrally
- second electrode was placed on top of the membrane making sure the electrode was aligned with the bottom electrode

- top plate was placed onto the MEA, taking care not to shift the MEA
- G-clamp was tightened using 35 N.m torque
- clamp was placed in preheated oven set at 120 °C, for 1 hour
- clamp was allowed to cool and opened

9.4 Gasket Manufacturing

Gaskets were used to seal the cell, preventing gas leaks. It was attempted to manufacture the silicon rubber gaskets. Silicon rubber solution consisting of an elastomer base and catalyst was used to make the gaskets. The procedure was as follows:

- silicon catalyst and base were stirred before use
- catalyst and base were mixed in a ratio of 5 weight percent catalyst to base.
- mixture was stirred for 2 minutes, trying not to entrap too much air
- mixture was poured into the gasket mould and left to cure for 48 hours

CHAPTER 10 : MODELLING

This chapter details the model development. The main aims in modelling were to:-

- develop a model of the fuel cell
- simulate the experiments carried out on a commercial fuel cell
- give a theoretical explanation for the experimental results

Model Development

The fuel cell was divided into four regions:

- flow channel
- diffusion layer
- reaction site
- membrane

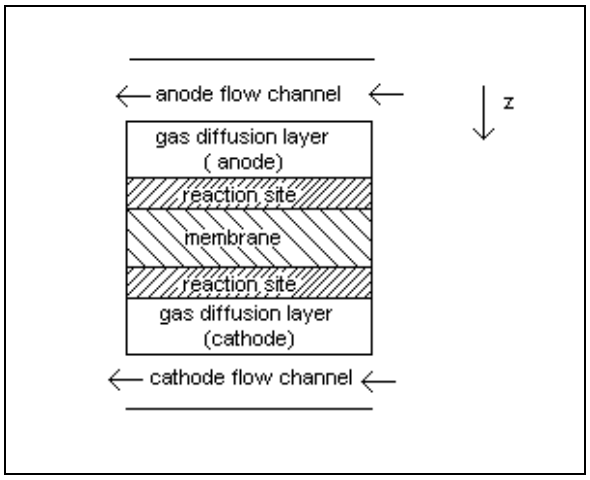

Figure 10.1 : Cross section of fuel cell showing direction of model dimension

The main investigation in these regions were:

- utilisation of reactants in the flow channel
- diffusion of reactants through porous electrode backing
- reaction kinetics at the reaction site
- net flux of water through the membrane

The assumptions of the model are:

- gases are ideal
- reactant gases are humidified to saturation
- variables are one dimensional and functions of z co-ordinate only, that is, constant over the surface
- isothermal and constant pressure operation
- linear concentration gradient of water across the membrane

The model allows us to predict the voltage and power of the fuel cell as a function of the current density, under various operating conditions, such as temperature, pressure, and reactant composition. Naturally, the complexity of the model will differ depending on the inlet gas composition and whether the net water flux through the membrane is taken into account. The most complex case is discussed here.

The model developed is for the case where the anode inlet stream is composed of H_2, CO_2 and H_2O (saturated) and the cathode inlet stream composed of O_2, N_2 and H_2O (saturated). The water flux is non-zero.

10.1 Flow channel

The saturated vapour pressure of water is a function of temperature and is given by the Antoine equation,

$$\log p_i^{sat} = A - \frac{B}{(t + C)}$$

$$for water, \qquad (10.1)$$

$$p_w^{sat} = 8.046 + \frac{1713.72}{(t + 231.83)}$$

The mole fraction of the binary mixture before entering the humidifier, $x`_{in,i}$, is given by,

$$x'_{in,i} = \frac{n_{in,i}}{n_{in}},$$

$$n_{in} = \sum_{i=1}^{2} n_{in,i} \qquad (10.2)$$

The mole fraction of water in the gas stream after humidification is given by,

$$x_{in,w} = \frac{p_w^{sat}}{P} = \frac{n_{in,w}}{n_{in} + n_{in,w}} \tag{10.3}$$

The resulting mole fraction of components after humidification is given by,

$$x_{in,i} = \frac{n_{in,i}}{n_{in} + n_{in,w}} \tag{10.4}$$

dividing both numerator and denominator by $1/n_{in}$ yields,

$$x_{in,i} = \frac{x'_{in,i}}{1 + \frac{n_{in,w}}{n_{in}}} \tag{10.5}$$

substituting for $n_{in,w}$ from equation 10.3 yields expression for x_i,

$$x_{in,i} = x'_{in,i}\left(1 - x_{in,w}\right) \tag{10.6}$$

The component molar flowrate of the binary mixture before humidification is given by,

$$F'_{in,i} = x'_{in,i} F'_{in} \tag{10.7}$$

where $F`_{in}$ is the total molar flowrate of the binary mixture entering the humidifier. After humidification the molar flow of water $F_{in,w}$ is calculated from the mole fraction equation for water,

$$x_{in,w} = \frac{F_{in,w}}{F_{in}} = \frac{F_{in,w}}{F'_{in} + F_{in,w}} \tag{10.8}$$

The remaining component molar flowrate after humidification is given by,

$$F_{in,i} = x_{in,i} F_{in} \tag{10.9}$$

where, $F_{in} = F`_{in} + F_{in,w}$

Component fluxes

The molar flux of hydrogen is given by,

$$N_{H_2} = \frac{i}{nF} \tag{10.10}$$

The molar flux of the other components are related to the hydrogen flux by the stoichiometry of the overall reaction,

$$H_2 + 1/2\, O_2 \Leftrightarrow H_2O \tag{10.11}$$

Hence,

$$\begin{aligned} N_{O_2} &= \frac{N_{H_2}}{2} \\ N_{H_2O} &= N_{H_2} \end{aligned} \tag{10.12}$$

The molar flux of water in the anode and cathode is given as follows,

$$\begin{aligned} N^a_{H_2O} &= N_{H^+}\alpha \\ N^c_{H_2O} &= -\left(N_{H^+}\alpha + N_{H_2}\right) \end{aligned} \tag{10.13}$$

The variable α represents the net flux of water molecules across the membrane per flux of hydrogen ions. The calculation of α is detailed further on in the model development.

The flux of water from the anode is in the positive z-direction, that is, entering the anode. The flux of water in the cathode, which is the combination of the water due to migration as well as that produced by reaction 10.11, is in the negative z-direction, that is, leaving cathode.

Since CO_2 and N_2 are inerts in the system, the flux of these species is zero,

$$N_{CO_2} = 0 = N_{N_2} \tag{10.14}$$

The consumption rate of the species is given by Faraday's law,

$$F_{cons,H_2} = \frac{I}{nF} = N_{H_2} A_e \tag{10.15}$$

where A_e is the area of the electrode

Thus, a component mass balance over the anode gives the hydrogen outlet flowrate as,

$$\begin{aligned} F_{out,H_2} &= F_{in,H_2} - F_{cons,H_2} \\ F_{out,inert} &= F_{in,inert} \end{aligned} \tag{10.16}$$

The average or bulk flow of hydrogen was calculated using a log-mean average as suggested by Amphlett *et al* (1995).

$$\begin{aligned} F_{avg,H_2} &= \frac{F_{in,H_2} - F_{out,H_2}}{\ln\left(F_{in,H_2} \Big/ F_{out,H_2} \right)} \\ F_{avg,inert} &= F_{in,inert} \end{aligned} \tag{10.17}$$

Thus the mole fractions of each species in the flow channel is given by,

$$x_{i\_fc} = \frac{F_{avg,i}}{\sum_{1}^{n} F_{avg,i}} \tag{10.18}$$

10.2 Diffusion Layer

Diffusion through the porous electrodes was modelled using the Stefan-Maxwell equation for multicomponent diffusion (Bird *et al*, 1960),

$$\nabla x_i = \sum_{j=1}^{n} \frac{RT\left(x_i N_j - x_j N_i\right)}{D_{ij}^{eff} P} i = 1,2,...,n \tag{10.19}$$

The effective binary diffusion coefficient (Amphlett *et al*, 1995) is given as,

$$D_{ij}^{eff} = 0.0002745\left(\frac{T}{\sqrt{T_i^{crit}T_j^{crit}}}\right)^{1.832}\left(p_i^{crit}p_j^{crit}\right)^{1/3}\left(T_i^{crit}T_j^{crit}\right)^{5/12}\left(\frac{1}{M_i}+\frac{1}{M_j}\right)^{1/2}\varepsilon \qquad (10.20)$$

The parameter ε takes into account the porosity of the electrode, which is between 0.25 and 0.35 for carbon fibre-paper electrodes (Amphlett *et al*, 1995). An arithmetic average value of 0.3 was used.

Equation 10.19 can be written for all components and hence for each electrode we have three equations with three unknowns, that is, the component mole fractions at the reaction site. The equation relating the mole fractions is,

$$\sum_1^n x_i = 1 \qquad (10.21)$$

Thus we need only two diffusion equations and the mole fraction relation to solve for the unknowns.

Using the above equations we solve for the anode mole fractions.

The diffusion equation for each component in the anode is given below,

$$\nabla x_{H_2} = \frac{RT\left(-x_{CO_2}N_{H_2}\right)}{D_{H_2,CO_2}^{eff}P} + \frac{RT\left(x_{H_2}N_{H_2O}^a - x_{H_2O}^a N_{H_2}\right)}{D_{H_2,H_2O}^{eff}P}$$

$$\nabla x_{CO_2} = \frac{RT\left(x_{CO_2}N_{H_2}\right)}{D_{H_2,CO_2}^{eff}P} + \frac{RT\left(x_{CO_2}N_{H_2O}^a\right)}{D_{CO_2,H_2O}^{eff}P} \qquad (10.22)$$

$$\nabla x_{H_2O} = \frac{RT\left(x_{H_2O}^a N_{H_2} - x_{H_2}N_{H_2O}^a\right)}{D_{H_2,H_2O}^{eff}P} + \frac{RT\left(-x_{CO_2}N_{H_2O}^a\right)}{D_{CO_2,H_2O}^{eff}P}$$

integrating the equation for carbon dioxide yields,

$$\int \frac{1}{x_{CO_2}}dx_{CO_2} = \int \frac{RT}{P}\left(\frac{N_{H_2}}{D_{H_2,CO_2}^{eff}} + \frac{N_{H_2O}^a}{D_{CO_2,H_2O}^{eff}}\right)dz_a \qquad (10.23)$$

yielding the mole fraction of CO_2 as a function of z_a. Using the boundary condition,

$$x_{CO_2\_z_a} = x_{CO_2\_fc} \quad at\ z_a = 0$$

$$x_{CO_2\_z_a} = x_{CO_2\_fc} \exp\left(\frac{RT}{P}\left(\frac{N_{H_2}}{D^{eff}_{H_2,CO_2}} + \frac{N^a_{H_2O}}{D^{eff}_{CO_2,H_2O}} \right) z_a \right) \tag{10.24}$$

using the equation for hydrogen, from equation 10.22, and substituting for x_{CO_2} from equation 10.21 yields,

$$\nabla x_{H_2} = \frac{RT\left(N^a_{H_2O} + N_{H_2}\right)}{D^{eff}_{H_2,H_2O}P} x_{H_2} + \frac{RT}{P}\left(\frac{-1}{D^{eff}_{H_2,CO_2}} + \frac{1}{D^{eff}_{H_2,H_2O}} \right) N_{H_2} x_{CO_2} - \frac{RTN_{H_2}}{D^{eff}_{H_2,H_2O}P} \tag{10.25}$$

To solve the above equation, the Euler method was used,

$$\begin{aligned} x_{n+1} &= x_n + f'(x)\Delta z \\ f'(x) &= dx/dz \\ z_{n+1} &= z_n + \Delta z \end{aligned} \tag{10.26}$$

Δz is a step change in z, the smaller the steps the more accurate the result but of course the longer the iteration.
With the initial condition,

$$x_{H_2\_z_a} = x_{H_2\_fc} \quad at \;\; z_a = 0$$

equation 10.25 can be solved for the mole fraction of hydrogen at the reaction site or interface, $x_{H_2\_\text{int}}$. The interfacial mole fraction of the remaining component, $x_{H_2O\_\text{int}\_a}$, can be calculated using equation 10.21.

A similar calculation procedure is used for the cathode and yields the following equations,

$$x_{N_2\_z_c} = x_{N_2\_z_c} \exp\left(\frac{RT}{P}\left(\frac{N_{O_2}}{D^{eff}_{O_2,N_2}} + \frac{N^c_{H_2O}}{D^{eff}_{N_2,H_2O}} \right) z_c \right) \tag{10.27}$$

$$\nabla x_{O_2} = \frac{RT\left(N^c_{H_2O} + N_{O_2}\right)}{D^{eff}_{O_2,H_2O}P} x_{O_2} + \frac{RT}{P}\left(\frac{-1}{D^{eff}_{O_2,N_2}} + \frac{1}{D^{eff}_{O_2,H_2O}} \right) N_{O_2} x_{N_2} - \frac{RTN_{O_2}}{D^{eff}_{O_2,H_2O}P} \tag{10.28}$$

The above equations are solved as explained for the anode.

Calculation of the net water flux

Looking closer at the flux of water through the anode,

$$N^{a}_{H_2O} = \alpha\, N_{H^+} = n_{drag} N_{H^+} - D_{H_2O} \frac{dC_{H_2O}}{dz_m} \tag{10.29}$$

The first term in equation represents the migration effect, that is, the flux of water molecules 'dragged' with the protons as the protons travel from the anode to the cathode. n_{drag} is the electro-osmotic coefficient. The second term represents the back diffusion of water from the cathode to the anode.

Nguyen and White (1993) assumed that the concentration gradient of water across the membrane is constant. Hence, with this assumption, the change in concentration of water across the membrane can simply be expressed as,

$$\frac{dC_{H_2O}}{dz} = \frac{C^{c}_{H_2O} - C^{a}_{H_2O}}{t_m} \tag{10.30}$$

hence, equation 10.29 simplifies to,

$$\alpha = n_{drag} - \frac{D_{H_2O} F}{i} \left(\frac{C^{c}_{H_2O} - C^{a}_{H_2O}}{t_m} \right) \tag{10.31}$$

n_{drag} is a function of the activity of water at the anode and is given by (Nguyen and White, 1993),

$$\begin{aligned} n_{drag} &= 0.0049 + 2.02 a_{H_2O} - 4.53 a^2_{H_2O} + 4.09 a^3_{H_2O} \quad (a_{H_2O} \le 1) \\ n_{drag} &= 1.59 + 0.159 \left(a_{H_2O} - 1 \right) \quad (a_{H_2O} > 1) \end{aligned} \tag{10.32}$$

The activity of water, a_{H_2O}, is given by (Nguyen and White, 1993),

$$a_{H_2O} = \frac{x_{H_2O} P}{p^{sat}_{H_2O}} \tag{10.33}$$

The diffusion coefficient for water (Nguyen and White, 1993), is given by,

$$D_{H_2O} = n_{drag} D^o \exp\left(2416\left(1/303 - 1/T\right)\right) \tag{10.34}$$

The concentration of water at the surface of the membrane at each electrode is given by (Nguyen and White, 1993),

$$\begin{aligned} C_{H_2O,k} &= \frac{\rho_{m,dry}}{M_{m,dry}}\left(0.043 + 17.8a_{H_2O,k} - 39.8a_{H_2O,k}^2 + 36a_{H_2O,k}^3\right)\left(a_{H_2O,k} \le 1\right) \\ C_{H_2O,k} &= \frac{\rho_{m,dry}}{M_{m,dry}}\left(14 + 1.4\left(a_{H_2O,k} - 1\right)\right)\left(a_{H_2O,k} > 1\right) \end{aligned} \tag{10.35}$$

where the subscript *k* refers to either the anode or the cathode.

The solution for the interfacial mole fraction is an iterative one. An initial value for α is chosen and a new α value is calculated from equation. This is then used as the α for next iteration. Iteration stops when a pre-set tolerance value is achieved.

Concentration Overpotential

Concentration overpotential is due to a concentration difference between the bulk concentration of reactants and the surface (reaction site) concentration. This concentration difference results in an overpotential.

Fick's first law of diffusion gives the rate of mass transport of reactants to reaction site (Hirschenhofer *et al*, 1994).

$$N_i = \frac{D_i\left(C_i - C_{i\_s}\right)}{\delta} \tag{10.36}$$

For the anode,

$$N_{H_2} = \frac{i}{nF} = \frac{D_{H_2}\left(C_{H_2\_b} - C_{H_2\_s}\right)}{t_a} \tag{10.37}$$

The limiting current density occurs when the concentration of the reactant at the surface is zero.

$$i_L^a = \frac{nFD_{H_2} C_{H_2\_b}}{t_a} \tag{10.38}$$

Using the Nernst equation, the difference in potential at the bulk and surface gives the concentration overpotential,

$$\eta_{conc}^{a} = \Delta E = RT \ln\left(C_{H_2\_s} \Big/ C_{H_2\_b} \right) \tag{10.39}$$

Equations 10.38 and 10.39 can be combined to yield,

$$\frac{C_{H_2\_s}}{C_{H_2\_b}} = 1 - \frac{i}{i_L^a} \quad hence$$
$$\eta_{conc}^{a} = RT \ln\left(1 - \frac{i}{i_L^a}\right) \tag{10.40}$$

A similar analysis yields following expression for cathode,

$$i_L^c = \frac{2nFD_{O_2} C_{O_2\_b}}{t_c}$$
$$\eta_{conc}^{c} = \tfrac{1}{2} RT \ln\left(1 - \frac{i}{i_L^c}\right) \tag{10.41}$$

assuming the gases are ideal, the gas concentration is calculated from the ideal gas law,

$$C_i = \frac{p_i}{RT} \tag{10.42}$$

10.3 Reaction Site

Equilibrium Potential

For a general electrode reaction which can be represented by the form (Newman, 1991),

$$\sum_i s_i A_i^{z_i} \Leftrightarrow ne^- \tag{10.43}$$

The condition for equilibrium is given by (Newman, 1991),

$$\sum_i s_i \mu_i = n\mu_{e^-} \tag{10.44}$$

where the chemical potential, μ, is defined by (Newman, 1991),

$$\mu_i = RT \ln(\lambda_i) \tag{10.45}$$

The activity, λ_i, is given by,

$$\lambda_i = C_i f_i a_i^{\theta} \tag{10.46}$$

where C_i is the molarity, f_i is the activity coefficient and a_i^{θ} is a proportionality constant for species i.

The fuel cell can be expressed as,

γ	φ	δ	φ`	γ`
carbon paper	Pt, H_2	electrolyte	Pt, O_2	carbon paper

(10.47)

(the vertical lines represent phase boundaries)

The equilibrium cell potential is related to the difference in the electric potential between the phases γ and γ` , which is related to the difference in the chemical potential of the electrons in these two phases (Newman, 1991),

$$nFE = z_{e^-} F\left(\Phi^{\gamma} - \Phi^{\gamma`}\right) = \mu^{\gamma}_{e^-} - \mu^{\gamma`}_{e^-} \tag{10.48}$$

Considering the reactions at both electrodes, written in the form of reaction 10.43,
Anode:

$$H_2 - 2H^+ \Leftrightarrow 2e^- \tag{10.49}$$

Cathode:

$$H_2O - \tfrac{1}{2}O_2 - 2H^+ \Leftrightarrow 2e^- \tag{10.50}$$

Writing the equilibrium potential (equation 10.48) for these electrode reactions,

$$2FE = \mu_{H_2} - 2\mu_{H^+} + \tfrac{1}{2}\mu_{O_2} + 2\mu_{H^+} - \mu_{H_2O} \tag{10.51}$$

for ideal gases, $\mu_i = \mu_i^* + RT \ln p_i$ and for a pure substance $\mu_i = \mu_i^o$ (Newman, 1991)
Hence, with these simplifications the cell potential reduces to,

$$2FE = (\mu_{H_2}^* + \tfrac{1}{2}\mu_{O_2}^* - \mu_{H_2O}^o) + RT \ln p_{H_2} + \tfrac{1}{2} RT \ln p_{O_2} \tag{10.52}$$

Thus, the equilibrium potential is defined as,

$$\begin{aligned} E_{eqm} &= E^o + \frac{RT}{2F} \ln\left(p_{H_2} p_{O_2}^{\frac{1}{2}}\right) \\ E^o &= \frac{\mu_{H_2}^* + \tfrac{1}{2}\mu_{O_2}^* - \mu_{H_2O}^o}{2} \end{aligned} \tag{10.53}$$

This is called the Nernst equation. The first term, E^o, is the standard electrode potential for the overall reaction and has a value of 1.229 V at 25 ^oC (Newman, 1991).

Reaction kinetics

The rate of the elementary step, as given by equation 10.43, is given by the following equation (Newman, 1991),

$$r = \frac{i}{nF} = k_a \exp\left[\frac{(1-\beta)nF}{RT} V\right] \prod_i C_i^{pi} - k_c \exp\left[\frac{-\beta nF}{RT} V\right] \prod_i C_i^{qi} \tag{10.54}$$

$$k_{a,c} = A \exp\left(\frac{-\Delta E_{a,c}}{RT}\right) \tag{10.55}$$

The first term in equation 10.54 represents the anodic reaction and the second the cathodic reaction. k_a and k_c are the rate constants for anodic and cathodic reactions respectively. Equation 10.55 expresses the rate constants as a function of temperature. $\Delta E_{a,c}$ represents the activation energy for anodic and cathodic reactions respectively. The parameter β is a symmetry factor and represents the fraction of the potential, V, which promotes the cathodic reaction. *pi* and *qi* are the reaction orders for the anodic and cathodic reactions respectively.

The kinetics at the electrodes are modelled using the Butler-Volmer equation (Newman, 1991),

$$i = i_o\left[\exp\left(\frac{(1-\beta)nF}{RT}\eta_s\right) - \exp\left(\frac{-\beta nF}{RT}\eta_s\right)\right] \tag{10.56}$$

Equation 10.56 gives a relation between the current density and surface overpotential at the electrode.

Development of Butler-Volmer equation for anode and cathode reactions

Cathode:

Writing equation 10.54 for the cathode reaction 10.50,

$$r = \frac{i}{2F} = k_a \exp\left(\frac{(1-\beta)2F}{RT}V\right)C_{H_2O} - k_c \exp\left(\frac{-\beta 2F}{RT}V\right)C_{H^+}^2 C_{O_2}^{1/2} \tag{10.57}$$

at equilibrium, $i=0$ and $V=V^o$, hence equation 10.57 becomes,

$$\begin{aligned} k_a \exp\left(\frac{(1-\beta)2F}{RT}V^o\right)C_{H_2O} &= k_c \exp\left(\frac{-\beta 2F}{RT}V^o\right)C_{H^+}^2 C_{O_2}^{1/2} \\ \exp\left(\frac{2FV^o}{RT}\right) &= \left(\frac{k_c}{k_a}\right)\left(\frac{C_{H^+}^2 C_{O_2}^{1/2}}{C_{H_2O}}\right) \\ \frac{2FV^o}{RT} &= \ln\left(\frac{k_c}{k_a}\right) + 2\ln C_{H^+} + \tfrac{1}{2}\ln C_{O_2} - \ln C_{H_2O} \end{aligned} \tag{10.58}$$

Thus the equilibrium potential can be expressed as,

$$V^o = \frac{RT}{2F}\ln\left(\frac{k_c}{k_a}\left(\frac{C_{H^+}^2 C_{O_2}^{1/2}}{C_{H_2O}}\right)\right) \tag{10.59}$$

When the anodic and cathodic currents are equal, the resulting current is called the exchange current density,

$$\frac{i_o}{2F} = k_a \exp\left(\frac{(1-\beta)2F}{RT}V^o\right)C_{H_2O} = k_c \exp\left(\frac{\beta 2F}{RT}V^o\right)C_{H^+}^2 C_{O_2}^{1/2} \tag{10.60}$$

expanding the cathodic expression of equation 10.60 and substituting for the equilibrium potential from equation 10.59, yields an expression for the exchange current density,

$$\frac{i_o}{2F} = k_a^{\beta} k_c^{1-\beta} C_{H^+}^{2(1-\beta)} C_{O_2}^{1/2(1-\beta)} C_{H_2O}^{\beta} \tag{10.61}$$

The surface overpotential, η_s, is defined as the departure from equilibrium (Newman, 1991),

$$\eta_s = V - V^o \tag{10.62}$$

Writing equation 10.54 , substituting for V in terms of η_s from equation 10.62, yields,

$$\frac{i}{2F} = k_a \exp\left(\frac{(1-\beta)2F}{RT}\left(\eta_s + V^o\right)\right) C_{H_2O} - k_c \exp\left(\frac{-\beta 2F}{RT}\left(\eta_s + V^o\right)\right) C_{H^+}^2 C_{O_2}^{1/2} \tag{10.63}$$

expanding equation 10.63 and substituting for V^o from equation 10.59, equation 10.63, after some manipulation becomes,

$$\frac{i}{2F} = k_a^{\beta} k_c^{(1-\beta)} C_{H^+}^{2(1-\beta)} C_{O_2}^{1/2(1-\beta)} C_{H_2O}^{\beta} \left[\exp\left(\frac{(1-\beta)2F}{RT}\eta_s\right) - k_c \exp\left(\frac{-\beta 2F}{RT}\eta_s\right)\right] \tag{10.64}$$

The first part of equation 10.64 is the exchange current density term (equation 10.61). Thus equation 10.64 finally becomes,

$$i = i_o \left[\exp\left(\frac{(1-\beta)2F}{RT}\eta_s\right) - \exp\left(\frac{-\beta 2F}{RT}\eta_s\right)\right] \tag{10.65}$$

which is the Butler-Volmer equation (equation 10.56).

For large overpotentials, as is found with the oxygen electrode, the second term in equation 10.65 becomes negligible and thus can be written as,

$$i = i_o \exp\left(\frac{(1-\beta)2F}{RT}\eta_s\right) \tag{10.66}$$

Rearranging equation 10.66, results in an equation for the surface overpotential in terms of the current density,

$$\eta_s = \frac{RT}{(1-\beta)2F}\ln\left(\frac{i}{i_o}\right) \tag{10.67}$$

Equation 10.67 is referred as the general form of the Tafel equation. The Tafel equation is usually written as (Hirschenhofer *et al*, 1994),

$$\begin{aligned}\eta_s &= a + b\log(i)\\ a &= \frac{-2.3RT}{(1-\beta)2F}\log(i_o)\\ b &= \frac{2.3RT}{(1-\beta)2F}\end{aligned} \tag{10.68}$$

The term b is referred to as the Tafel slope and obtained from a plot of η *vs.* log(i). The equation for i_o is given by 10.61. Parthasarathy *et al* (1992a,b) experimentally investigated the effects of temperature and pressure on i_o for the oxygen electrode. Their data was fitted to an equation and used for the calculation of i_o.
The temperature dependence of i_o is given by,

$$\log(i_o) = 0.0372T - 20.929 \tag{10.69}$$

and the pressure dependence is given by,

$$\log(i_o) = 0.3453\ln(p_{O_2}) - 7.8749 \tag{10.70}$$

<u>Anode</u>

Writing equation 10.54 for the anode reaction (equation 10.49) gives,

$$r = \frac{i}{2F} = k_a \exp\left(\frac{(1-\beta)2F}{RT}V\right)C_{H_2} - kc\exp\left(\frac{-\beta nF}{RT}V\right)C_{H^+}^2 \tag{10.71}$$

A similar analysis as with the cathode yields the following expressions for the anode.

The equilibrium potential is given by,

$$V^o = \frac{RT}{2F}\ln\left(\frac{k_c}{k_a}\left(\frac{C_{H^+}^2}{C_{H_2}}\right)\right) \tag{10.72}$$

The exchange current density is given by,

$$\frac{i_o}{2F} = k_a^{\beta} k_c^{1-\beta} C_{H^+}^{2(1-\beta)} C_{H_2}^{\beta} \tag{10.73}$$

For small surface overpotentials, as is found with the hydrogen electrode, a Taylor series expansion of the Butler-Volmer equation yields,

$$i(\eta_s) = i(\eta_s)\Big|_{\eta_s \to 0} + \left.\frac{di(\eta_s)}{d\eta_s}\right|_{\eta_s \to 0} \eta_s \tag{10.74}$$

Thus, the Butler-Volmer expression becomes,

$$i = i_o\left(\frac{(1-\beta)2F}{RT} + \frac{\beta 2F}{RT}\right)\eta_s \tag{10.75}$$

Rearranging results in the expression for η_s,

$$\eta_s = \frac{RT}{F}\left(\frac{i}{i_o}\right) \tag{10.76}$$

10.4 Membrane

Ohmic Overpotential

The internal ohmic loss is due to the resistance of the electrolyte and is obtained as follows. The ohmic potential can be expressed as (Newman, 1991),

$$\eta_{ohmic}^{Internal} = \frac{1}{\kappa}\int_{anode}^{cathode} i \qquad dz \tag{10.77}$$

Since the current density is assumed to be constant and not a function of channel length,

$$\eta_{ohmic}^{Internal} = \frac{it_m}{\kappa} \tag{10.78}$$

The conductivity of the membrane is given by the following correlation (Springer *et al*, 1991),

$$\begin{aligned} \kappa &= \exp\left(1268\left(1/303 - 1/T\right)\right)\kappa_{30} \\ \kappa_{30} &= 0.005139\lambda - 0.00326 \\ \lambda &= 0.043 + 17.81\left(a_{H_2O}^a\right) - 37.85\left(a_{H_2O}^a\right)^2 + 36\left(a_{H_2O}^a\right)^3 \end{aligned} \tag{10.79}$$

where κ_{30} is the conductivity of the membrane at temperature of 30 °C and λ represents the water content of the membrane.

Cell Potential

The overall cell potential is a sum of the equilibrium potential and the overpotentials

$$V_{cell} = E_{eqm} - \eta_{conc}^a - \eta_{conc}^c - \eta_s^a - \eta_s^c - \eta_{ohm} \tag{10.80}$$

Cell Power Density

The cell power density of cell of simply the product of cell potential and current density.

$$P_{cell} = V_{cell}\, i \tag{10.81}$$

A flow diagram of the model algorithm is shown in figure 10.1 (page 10.-20).

Non-isothermal

From the thermodynamic relationship (Smith and Van Ness, 1987),

$$\Delta H = \Delta G + T\Delta S \tag{10.82}$$

The Gibbs free energy, ΔG, of reaction 10.11 results in the electrical energy part of the enthalpy change, ΔH, of the reaction. The second term, $T\Delta S$, is the entropy change and this results in a change in thermal energy. Since the enthalpy change is more negative than the Gibbs free energy change, this results in a negative entropy change. This implies that energy is leaving the system, in the form of heat. Thus, the fuel cell increases in temperature.

Writing a heat balance over the fuel cell gives,

$$F_i C_{p_i} T_{in} + F_{H_2O}\left(T_{in}\Delta S\right) = F_i C_{p_i} T_{out} \tag{10.83}$$

The heat capacities, C_{p_i} are given by (Perry and Green, 1984),

$$\begin{aligned} C_{p_{H_2}} &= 6.62 + 0.00081T \\ C_{p_{O_2}} &= 8.27 + 0.000258T - \frac{187700}{T^2} \\ C_{p_{H_2O}} &= 8.22 + 0.00015T + 0.00000134T^2 \\ C_{p_{CO_2}} &= 10.34 + 0.00274T - \frac{195500}{T^2} \\ C_{p_{N_2}} &= 6.5 + 0.001T \end{aligned} \tag{10.84}$$

Efficiency

The maximum efficiency of common energy converter (heat engines) is governed by the Carnot cycle (Appleby and Foulkes, 1993),

$$\varepsilon_c = \frac{T_h - T_c}{T_h} \tag{10.85}$$

Where T_h represents the temperature of the heat source and T_c represents temperature of the heat sink. Due to heat losses and losses through mechanical transfer of this work, the maximum practical efficiency is less than 40 percent (Appleby and Foulkes, 1993).

The fuel cell is not governed by the Carnot cycle limitations. The energy of the fuel is electrochemically converted in useful energy. The electrical efficiency of the fuel cell is higher and the heat produced by the fuel cell can also be used, hence fuel cells have a much higher efficiency.

The theoretical maximum electrical efficiency of the cell resulting from reaction 10.11 is defined as (Barbir and Gomez, 1996),

$$\varepsilon_e = \frac{\Delta G}{\Delta H} \tag{10.86}$$

ΔG for reaction 10.11 at standard conditions of 1 atm and 25 °C is -57.798 Cal/mol.K and ΔH is -54.635 Cal/mol.K (Perry and Green, 1984). Thus the maximum electrical efficiency of the fuel cell is 94.6 %.

The electrical efficiency of the fuel cell in terms of the fuel

$$\varepsilon_{fc} = \frac{electrical\ energy\ produced}{energy\ of\ \ fuel} \tag{10.87}$$

The electrical energy produced is the power which is the product of cell voltage and current

$$P_{cell} = V_{cell} \times I \tag{10.88}$$

The energy of the fuel, hydrogen, is the enthalpy $(\Delta H)_{H2}$ or higher heating value of the fuel. The total energy, E_{H_2}, available is a product of the hydrogen consumption, as given by Faraday's law , and the enthalpy,

$$\begin{aligned} E_{H_2} &= G_{cons,H_2} \times (\Delta H)_{H_2} \\ &= \frac{M_{H_2} I}{nF} \times (\Delta H)_{H_2} \end{aligned} \tag{10.89}$$

Thus the efficiency of the fuel cell is given by,

$$\varepsilon_{fc} = \frac{V_{cell} I}{\left(\frac{M_{H_2}(\Delta H)_{H_2}}{nF}\right) I} = \frac{V_{cell}}{\left(\frac{M_{H_2}(\Delta H)_{H_2}}{nF}\right)} \tag{10.90}$$

The denominator has a value of 1.482 and is referred to as the reversible potential corresponding to the maximum possible energy (Barbir and Gomez, 1996). The maximum potential of reaction 10.11 at standard conditions is 1.229 volts. Hence, the maximum fuel efficiency of the fuel cell is 83 %.

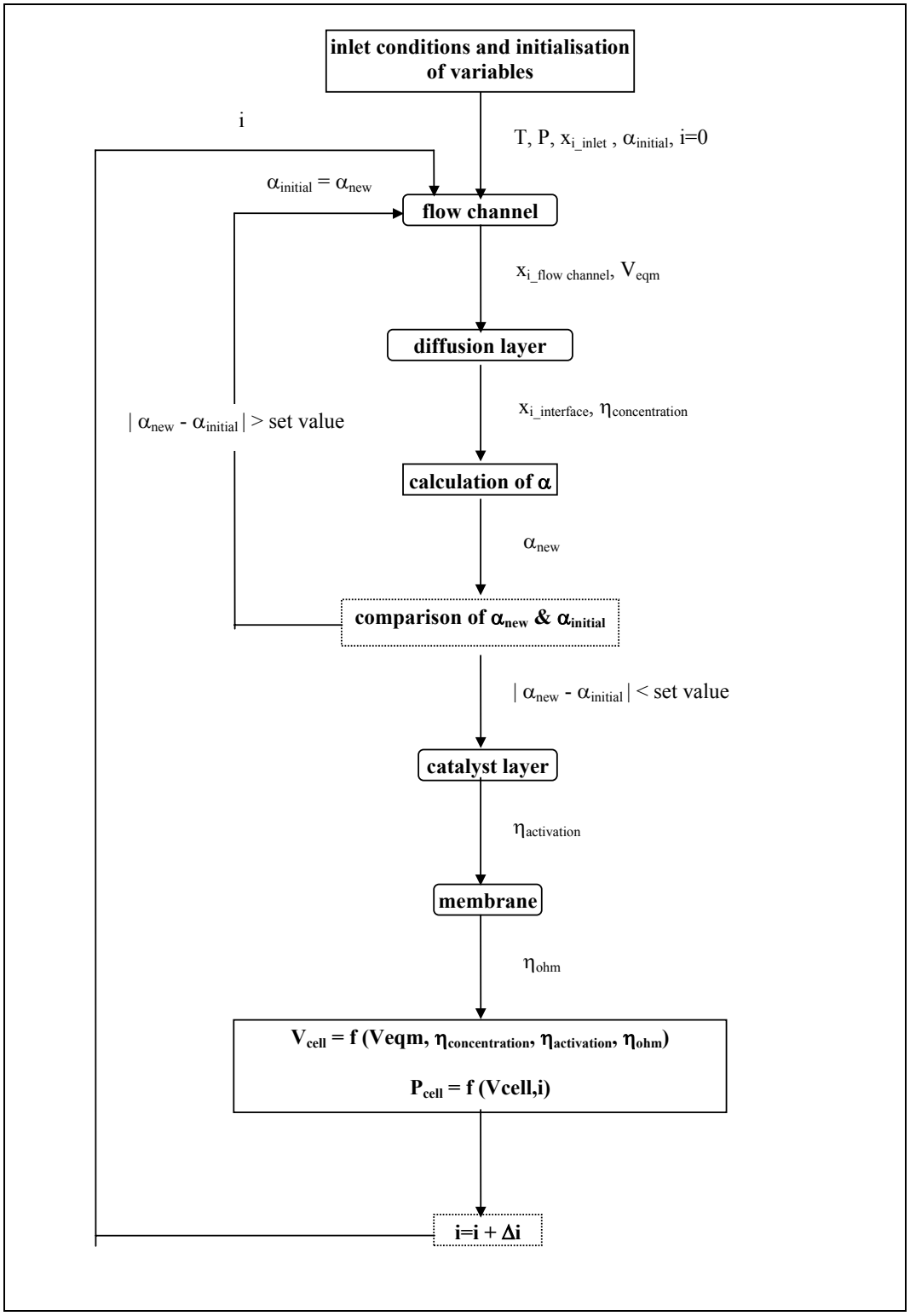

Figure 10.2 : Flow diagram for model algorithm

CHAPTER 11 : RESULTS

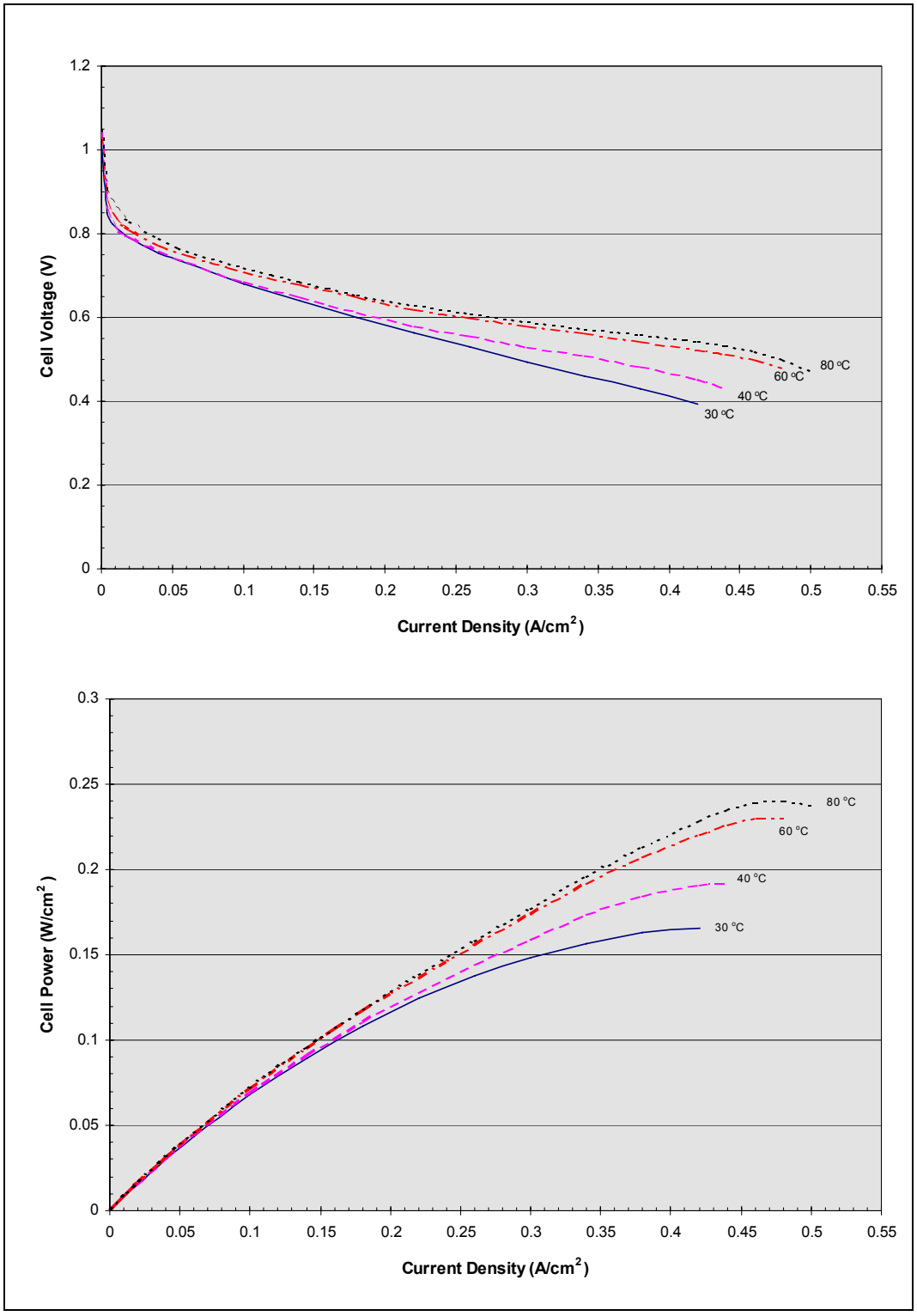

Figure 11.1 : Effect of temperature on the performance of ElectroChem cell using H_2 (humidified) and O_2 (humidified) at 1atm (abs).

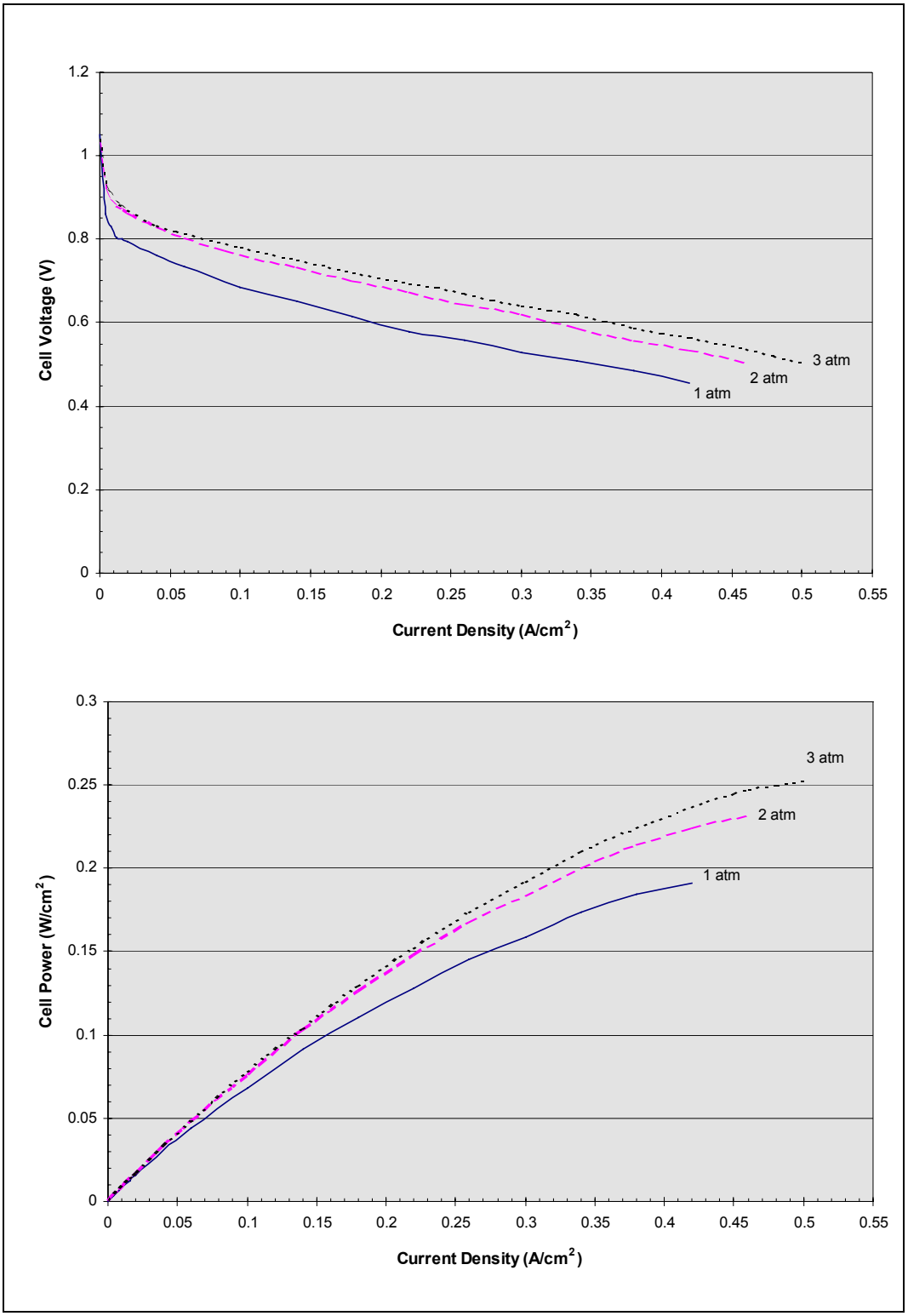

Figure 11.2 : Effect of pressure on the performance of ElectroChem cell using H_2 (humidified) and O_2 (humidified) at 40 °C

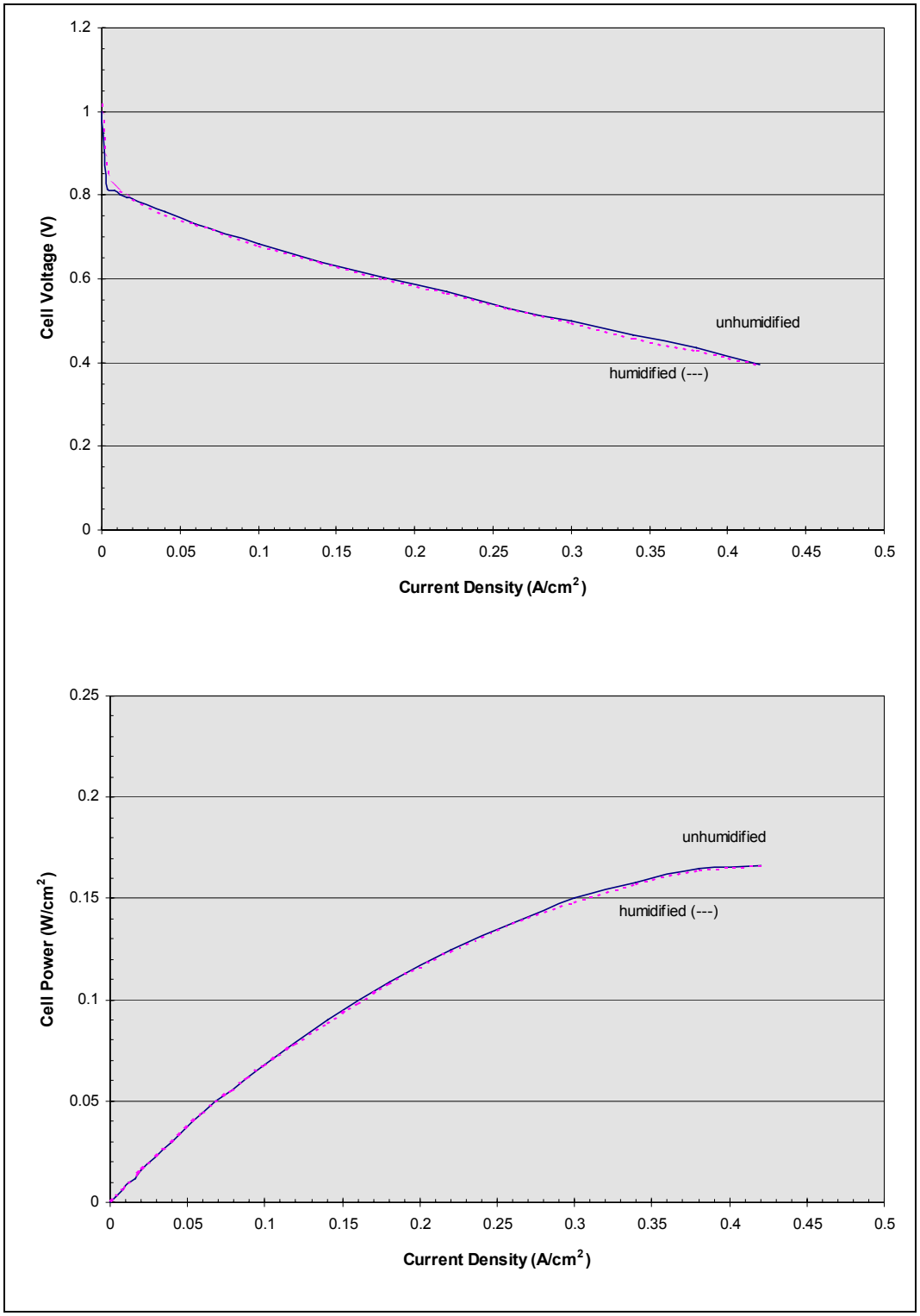

Figure 11.3 : Effect of humidification on the performance of ElectroChem cell using H_2 and O_2 at 1atm (abs) and 30 °C

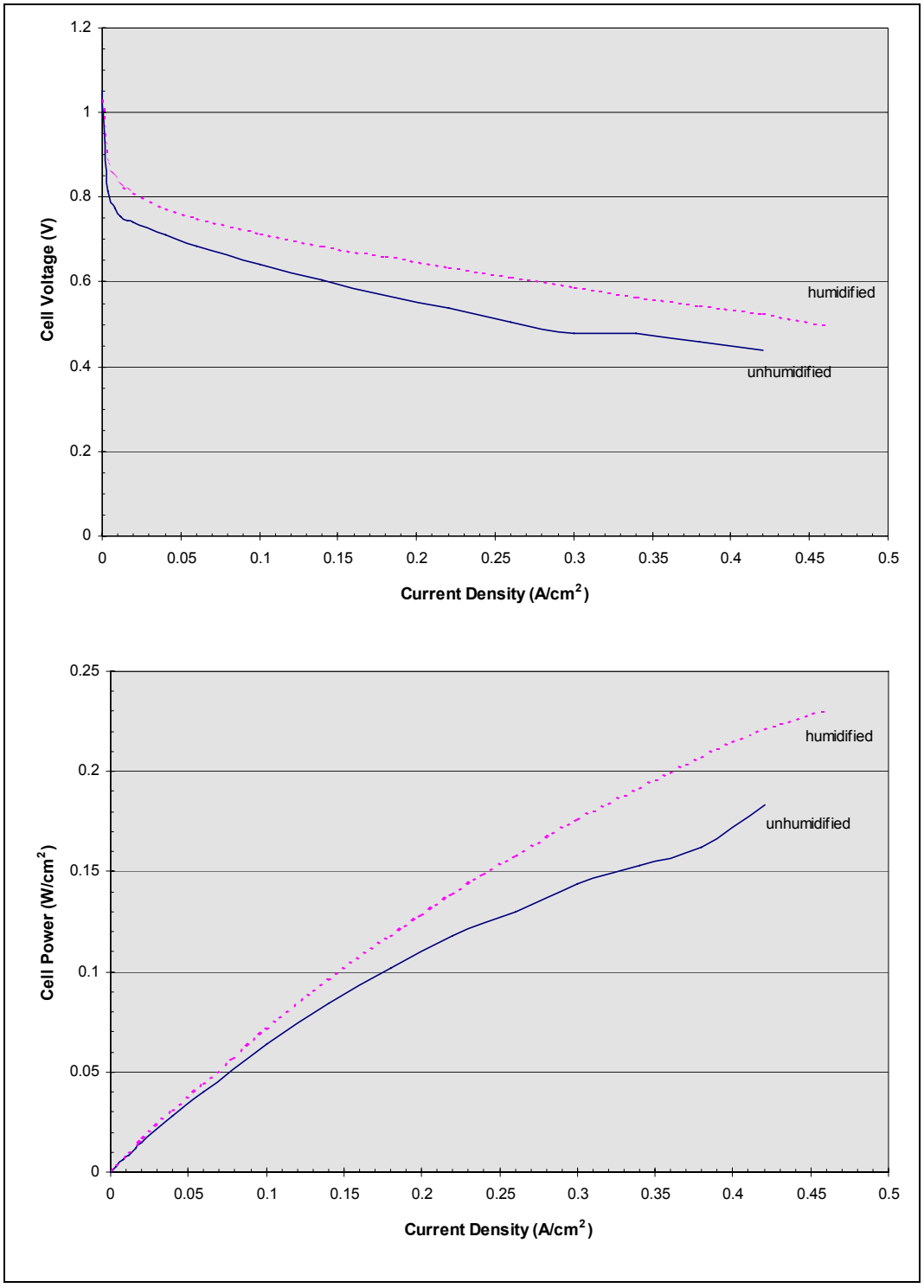

Figure 11.4 : Effect of humidification on the performance of ElectroChem cell using H_2 and O_2 at 1atm (abs) and 60 °C

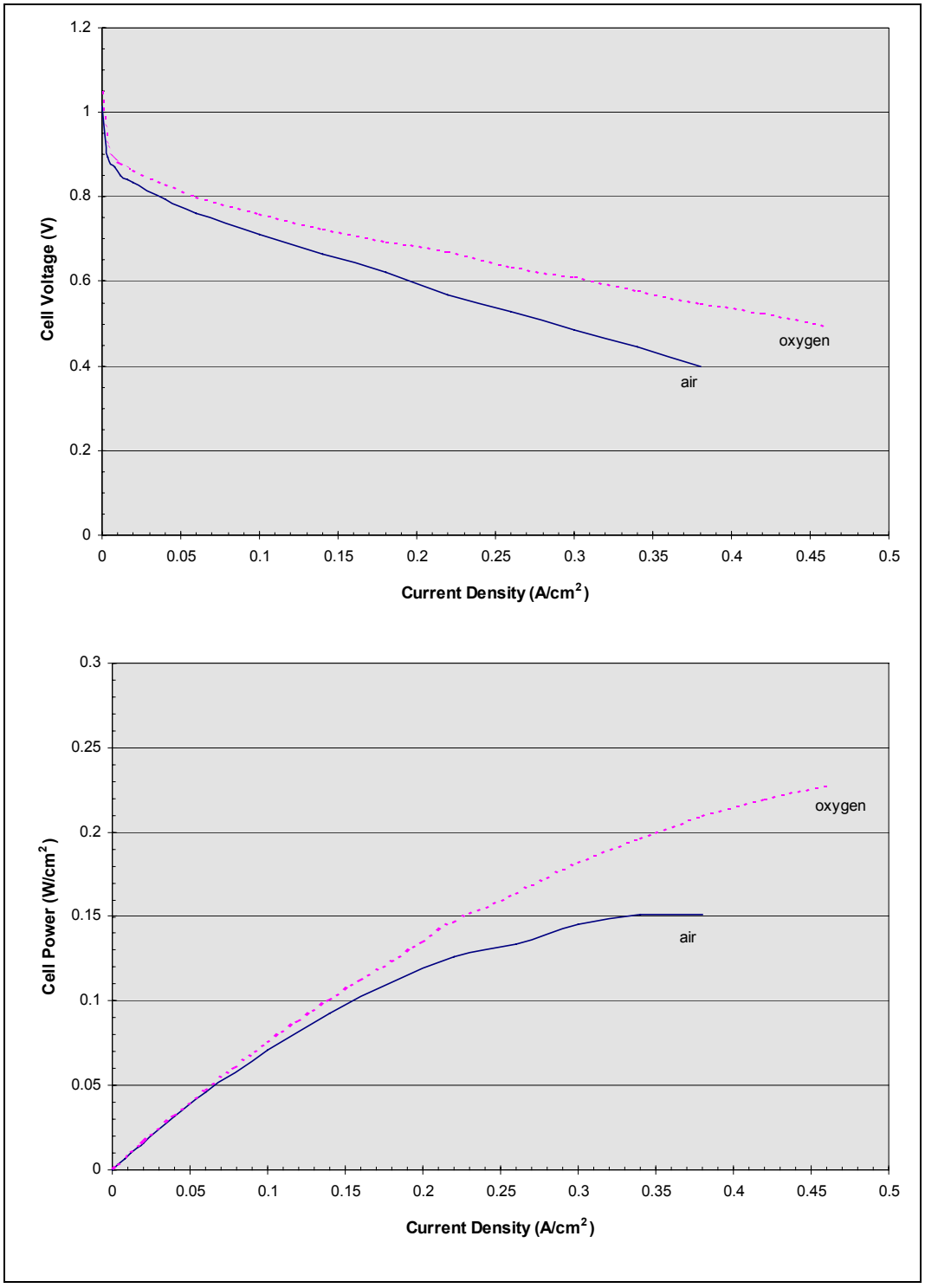

Figure 11.5 : Effect of oxidant (humidified) on the performance of ElectroChem cell using H_2 (humidified) at 1atm (abs) and 40 °C

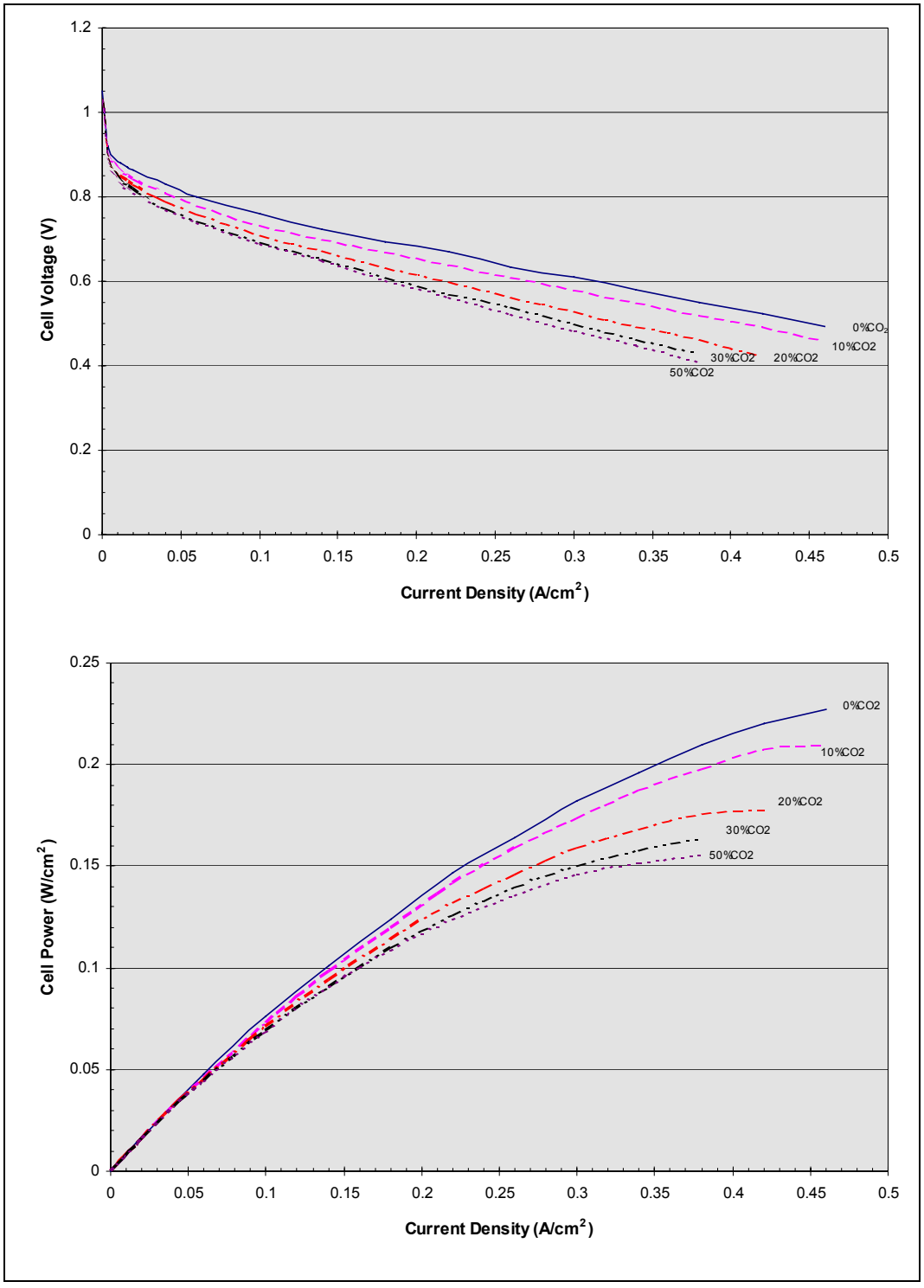

Figure 11.6 : Effect of carbon dioxide dilution of anode (humidified) on the performance of ElectroChem cell using O_2 (humidified) at 1atm (abs) and 40 °C

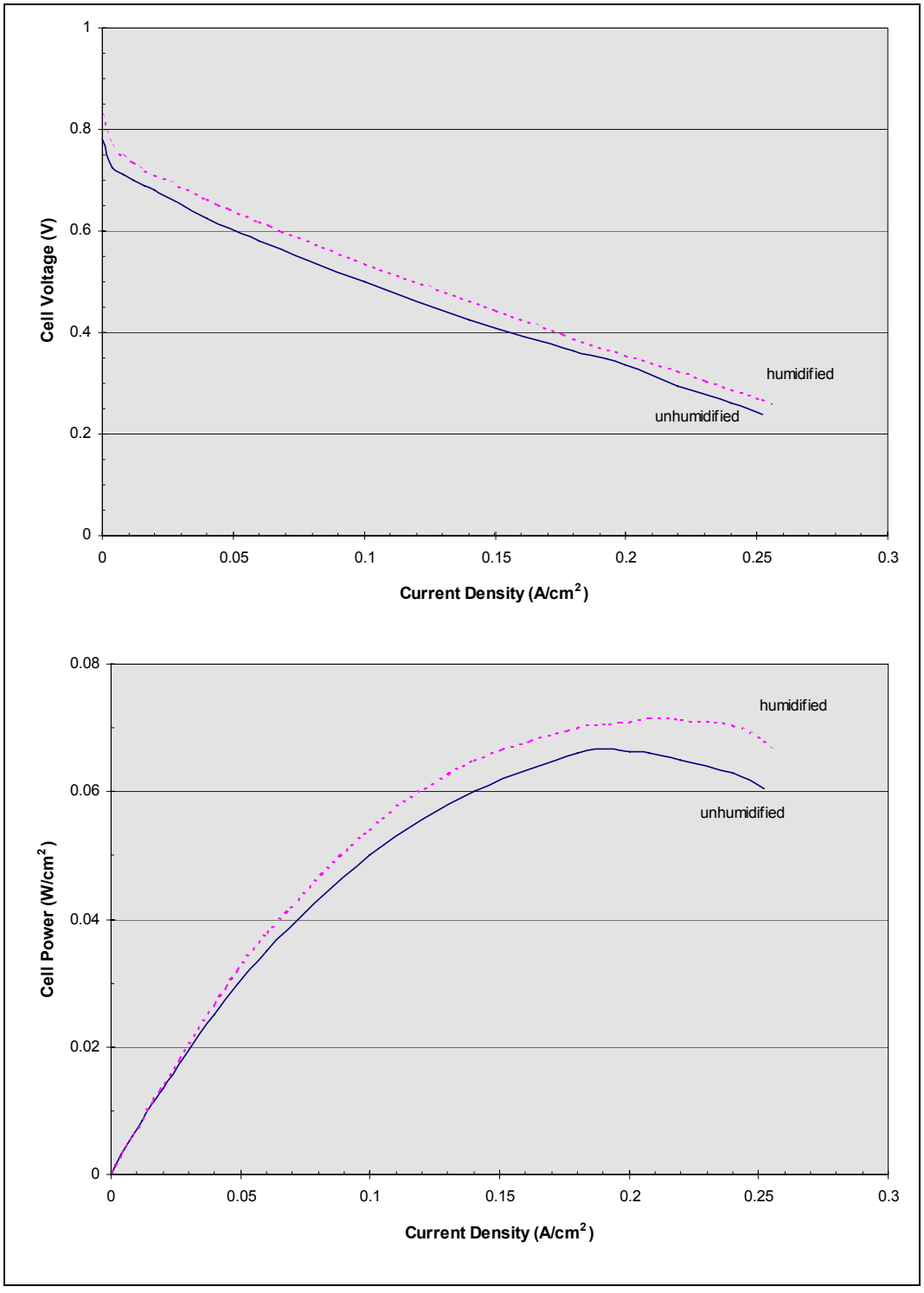

Figure 11.7 : Effect of humidification of anode on the performance of Dais cell using H_2 and Air at 1atm (abs) and 25 °C

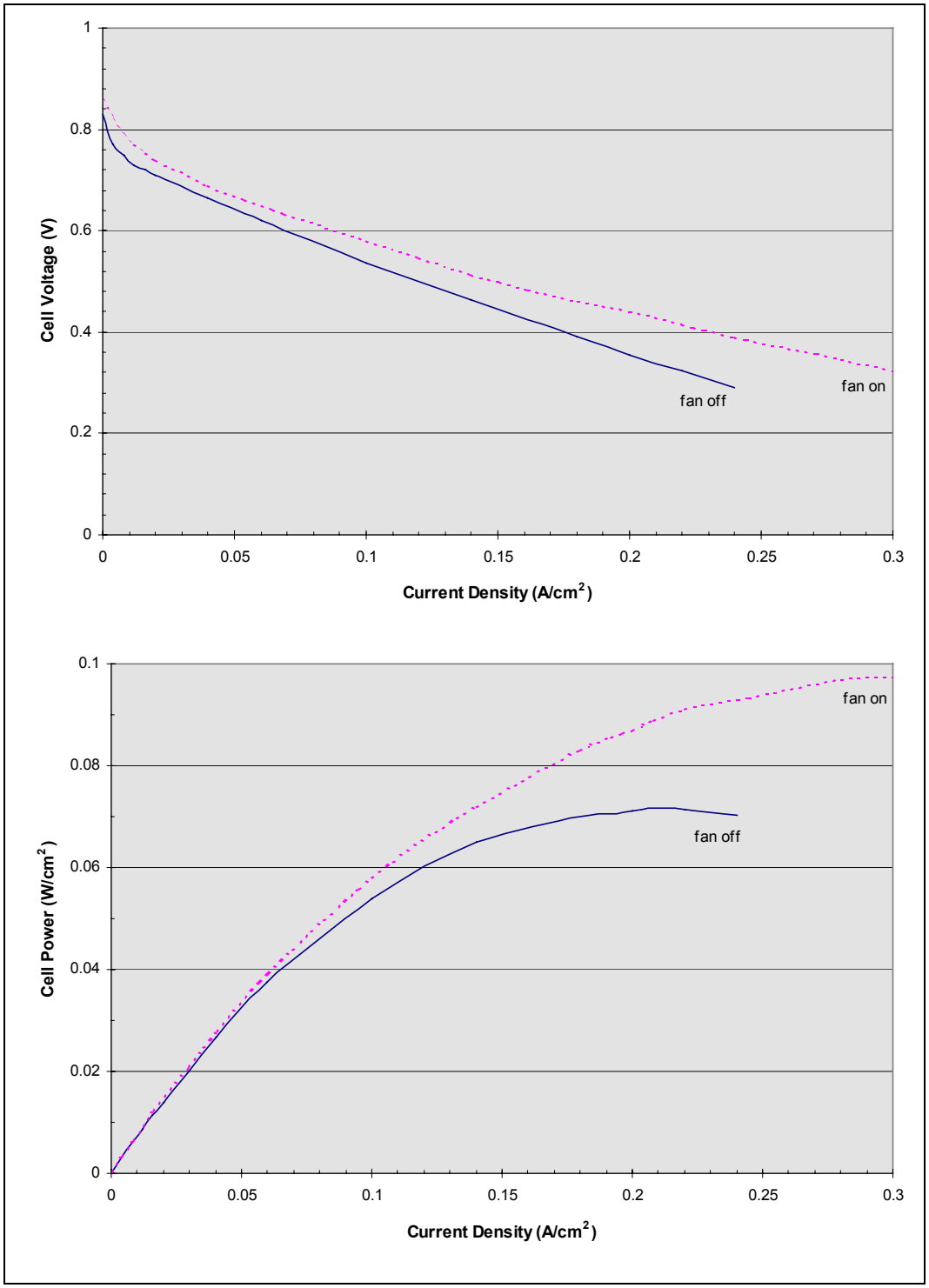

Figure 11.8 : Effect of Air flow on the performance of Dais-cell using H_2 (humidified) and Air at 1atm (abs) and 25 °C

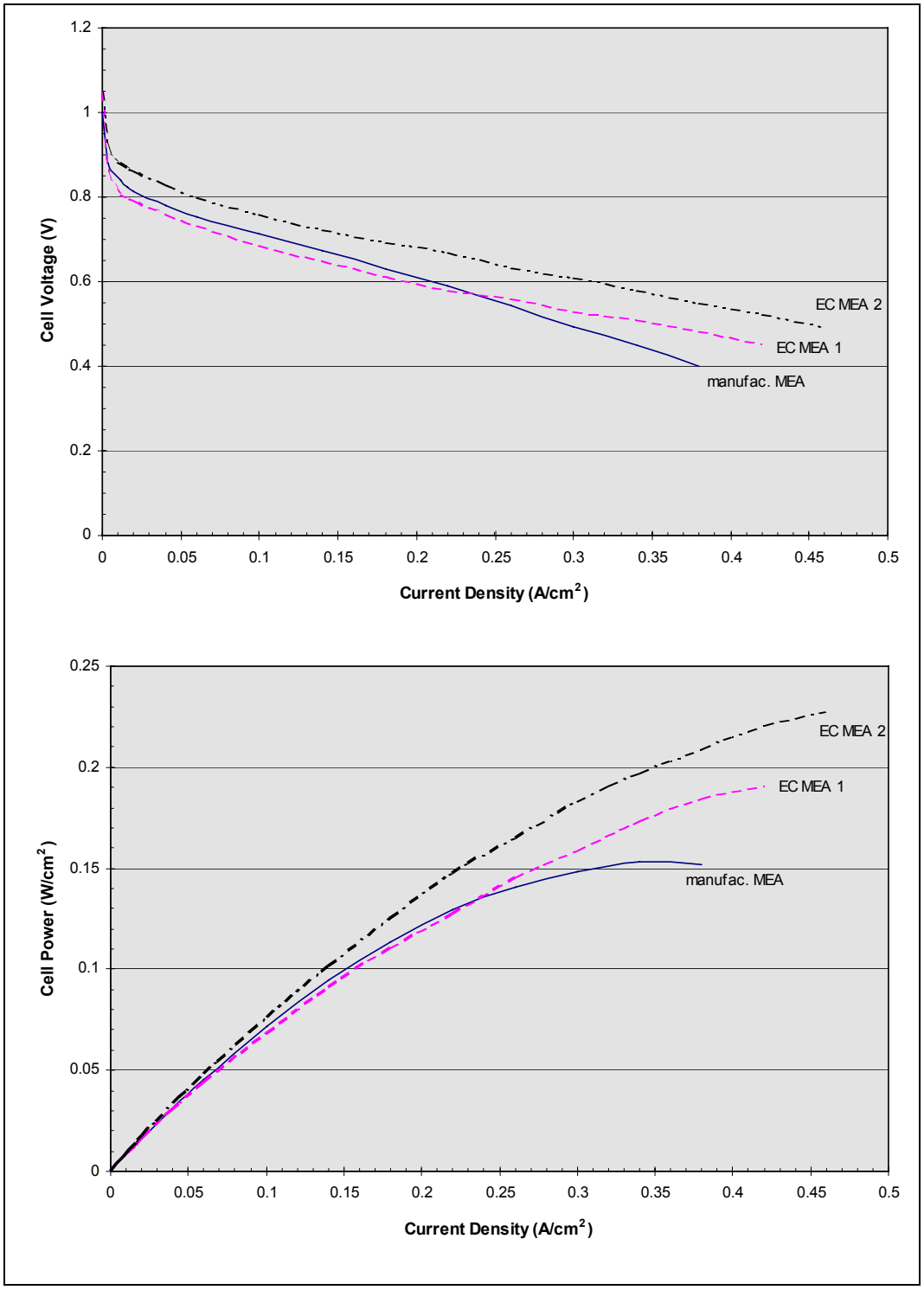

Figure 11.9 : Comparison of the performance of the manufactured MEA and the ElectroChem (EC) MEAs using H_2 (humidified) and O_2 (humidified) at 1 atm (abs) and 40 °C

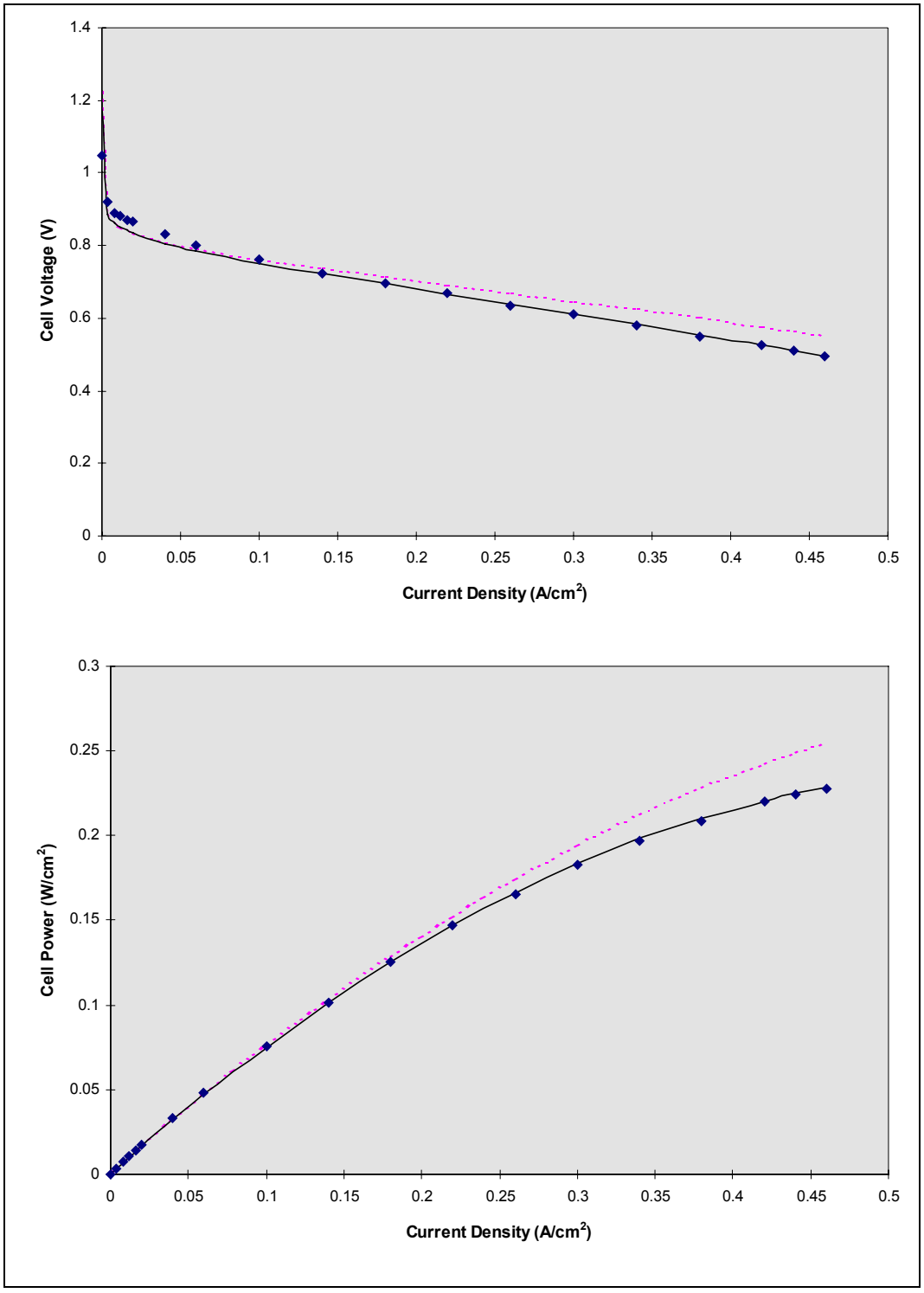

Figure 11.10 : Comparison of model and experimental result - (♦) experimental data using ElectroChem MEA (---) model prediction with inlet gases at 100 % saturation (−) model prediction with inlet gases at 87.5 % saturation. Operating conditions are H_2 and O_2 at 40 °C and 1 atm (abs)

CHAPTER 12 : DISCUSSION

12.1 Experimental Section

12.1.1 Set-up of experimentation station and equipment

The test station (photograph D3 on page D-3) was situated in a fume cupboard due to the potential danger of hydrogen gas. Hydrogen is a potentially explosive gas, hence the extraction fan in the fume cupboard was switched on after each run to prevent the build up of hydrogen gas. A flashback arrestor was fitted to the hydrogen gas cylinder as a safety requirement, preventing possible explosion of the gas cylinder in the event of a fire in the hydrogen line. Polyflow tubing was used for the inlet and the exit connections to the fuel cell because the polyflow tubing was more flexible than the copper tubing.

A variable resistor was used as a load and adjusted to alter the current. The lowest resistance achieved was about 0.15 ohms. A data logging programme, Quickstart, was used to log the data from the multimeter to a computer. The humidification units had to manufactured since the glass bottle humidifiers, that were already available, were not designed to withstand pressures higher than atmospheric pressure. The containers were placed on a heating pad, thus allowing the temperate of the water to be adjusted, depending on fuel cell operating temperature. The containers were filled to a maximum volume of 400 ml with distilled water. Filling the containers with a greater volume than this caused water to spurt out when the gas was bubbled through at high flowrates.

Flowmeters were calibrated using a bubble flowmeter. The calibration curves are shown in figures A1 to A3 (pages A-1 to A-3). The thermocouples were calibrated against a thermometer. The thermometer and thermocouples were placed in a beaker of water at different temperatures. The calibration chart is shown in figure A4 (page A-4). The thermocouples showed an average difference of approximately + 2 °C, relative to the thermometer.

12.1.2 Fuel cell operating procedure

An operating procedure was developed and due to observations made from the results using this initial procedure, the procedure was consequently modified. In the initial procedure, the cell was opened after a run to remove the water from the flow channels as it was thought that if there was any water in the flow channels, this would adversely affect the performance by decreasing the diffusion rate of reactants. When the cell was opened, it was noticed that the electrodes were beginning to separate from the MEA. A logged run was started immediately after the humidification stage.

However, it was noticed that when a run was repeated immediately after the first run, the performance improved. This was a result of the improved humidification of the membrane caused by the water produced by the reaction. Hence, the procedure was modified by not opening the cell and starting a logged run after an initial 'humidifying' run. By not opening the cell after each run, the MEA was kept in a relatively intact and undamaged state.

The extractor fan was switched on at the end of every run as a safety precaution, to preventing the build-up of hydrogen gas.

12.1.3 Test Cells

ElectroChem Cell

The FC05 fuel cell was shipped with one gasket, instead of two. It was decided to obtain the gasket locally, rather than order it from ElectroChem, as it would reduce cost and delivery time significantly. The ElectroChem gasket was 0.3 mm thick but the minimum thickness of the silicon rubber that could be obtained locally was 1 mm. The 1 mm gasket would be too thick and would prevent contact between the graphite block and the electrode, which is essential for electronic conduction, hence the gasket was ordered from ElectroChem.

The cell was assembled using a torque of 3 N.m on the bolts, as recommended by the manufacturer. The cell was connected to the load after the initial humidifying stage. The performance of the cell was very poor. The maximum current produced was 0.8 A. The cell was opened and the thickness of the individual components was measured. The 10 mil gasket was 0.27 mm thick. When tightened, the gaskets compress to approximately 85 % of the uncompressed thickness, which meant a final

thickness of 0.23 mm. The thickness of the ElectroChem MEA was measured to be 0.56 mm and that of the Nafion® membrane was 0.18 mm. Thus, the thickness of a single electrode was calculated to be 19 mm. This showed that since the 10 mil gasket were thicker than the electrode. Hence, the gaskets were preventing good electronic contact between the electrode and graphite block. The cell could not be tightened using a torque greater than 3 N.m (which was recommended by the manufacturer) as this damages the washers.

It was attempted to make a thinner gasket (see chapter 9 'Fuel Cell Manufacturing') but the manufactured gaskets were too weak and tore easily. Hence, a backing electrode, which was simply a piece of untreated carbon paper, was placed in-between the electrode and graphite block to ensure good electronic contact between the electrode and graphite block. With the backing electrode, the maximum current increased to 2 A. This confirmed that the gaskets were too thick. Higher currents were not attainable due to the resistance limitation of the load, which had a lowest resistance of 0.15 ohms.

The ElectroChem MEA was not square, that is, the electrodes were not squarely pressed onto the membrane, hence when placed in the cell, the gasket tended to overlap onto the electrode and prevented good contact with graphite block. The gaskets were trimmed to allow the electrode to fit inside the gasket.

When the cell was opened after the initial run, it was noticed that the MEA was separating. The membrane was bubbly and hence causing the electrodes to separate from the membrane, especially at the edges of the electrode. When the membrane came into contact with water it bubbled and flexed as it absorbed the water. The electrodes were water proofed to prevent water from readily escaping from the membrane and hence cause a decrease in the conductivity of the membrane. Hence the water formed on the cathode side was not readily absorbed by the electrode. The backing electrode helped with flooding by absorbing some of the water and preventing the build up of water. Build-up of water on the flow channels would decrease the diffusion rate of oxygen to the reaction site. Experimental observations, as discussed in the operating procedure above, showed that the advantages of higher membrane conductivity and hence performance caused by the water formed by the

reaction, were greater than the disadvantage of any decrease in the diffusion rate of oxygen.

Dais Cell

The Dais cell, which was kindly donated to us by Dais Corporation, was a single test cell. It was an air cathode cell, that is, the cathode reactant was ambient air. The cell had a maximum pressure rating of 2 psi. There was no temperature control for the cell. The experiments were conducted at atmospheric pressure and room temperature, which was approximately 25 °C. The cell was tightened using a torque of 2.5 N.m, which was the lowest torque rating on the torque wrench. The exact torque on the bolts is not given by the manufacturer. The specification, that is, cell area and catalyst loading of the cell were not known. Contact with the company was attempted without success.

12.2 Results

The results from the experiments performed, as detailed in chapter 8 'Experimentation', on the commercial cells (ElectroChem and Dais cells), the comparison test between the manufactured MEA and the ElectroChem MEA, and the model results are discussed below.

12.2.1 ElectroChem Cell

Effect of Temperature

Figure 11.1 (page 11-1) shows the effect of the operating temperature on the performance of the cell. There was an average increase of 1.6 % in the maximum current density and 1.5 % in the maximum power density for a 10 °C increase in temperature. The cell was run on humidified hydrogen and oxygen at 1 atm. Since the reactant gases were humidified and at 1 atm, the partial pressure of the reactants was less than unity, hence the second part of equation 10.53 would be negative, and would become more negative as the temperature increased, however the standard electrode potential would increase at the higher temperature. Overall we see a small increase in the equilibrium potential at increased temperature. From a diffusion point of view, the higher temperature increased the diffusion rate of reactants to the reaction site (equations 10.25 and 10.28), hence the concentration of reactants at the reaction site was higher, which increased the reaction rate. The increase in temperature also

increased the reaction rate constants, which are functions of temperature as given by equation 10.55, and hence increased the exchange current density (see equations 10.61 and 10.73). This increase in the reaction kinetics caused a decrease in activation overpotential (equations 10.67 and 10.76). A decrease in activation overpotential meant the reaction was able to proceed at a faster rate so there was less loss of potential from the reaction kinetics. Hence the cell voltage increased as temperature increased due to the decrease in the losses. Also the reactants were humidified, hence the saturated pressure of water increased with increasing temperature, as given by the Antoine equation (equation 10.1). The higher water content improved the membrane conductivity (equation 10.79), which meant protons were more easily conducted through the membrane and decreased the resistance of the membrane and hence the ohmic loss through the membrane. Due to the decreased ohmic losses, the performance of the fuel cell increased. On the negative side, higher temperature, greater than 60 °C, dehydrated the membrane if the gas streams were not sufficiently humidified (as shown by the humidification tests).

Effect of Pressure

The effect of pressure on performance is shown in figure 11.2 (page 11-2). Increasing the cell pressure by 1 atm caused an average increase in the maximum current density of 9 % and 15 % in the maximum power density. When the pressure was increased, the equilibrium potential (equation 10.53) increased due to the increased partial pressure of the reactants. From the reaction kinetics point of view, the increased partial pressure of the reactant gases increased the reaction kinetics and exchange current density as seen by equations 10.61 and 10.73. This decreased the activation overpotential, as given by equation 10.67 and 10.76. The decrease in activation overpotential meant the reaction was proceeding at a faster rate and hence the losses due to reaction kinetics were less. As a result of the lower losses in the cell, the cell voltage increased.

Effect of Humidification

Figure 11.3 (page 11-3) shows that humidification at low temperature, 30 °C, showed little or no improvement in the performance of the cell. Any improvement was noticed only in the low current range. At medium to high currents, the water produced by the reaction is sufficient to humidify the membrane hence the performance is similar to

that of humidified run. Figure 11.4 (page 11-4) shows the effect of humidification at 60 °C Humidification resulted in a 10 % increase in the maximum current density and a 26 % increase in the maximum power density at 60 °C. The increased performance can be explained by the higher conductivity of the membrane (equation 10.79) as a result of the increased water content of the membrane. The increased conductivity of the membrane meant that the protons were more easily conducted through the membrane and this decreased the ohmic losses through the membrane. The decreased ohmic losses resulted in a higher cell voltage. The unhumidified run, at 60 °C, showed an increase in performance at approximately 0.3 A/cm^2. This was due to the hydrating effects of the water produced by reaction 10.11. As the current increased, the water produced increased. An unhumidified run at 80 °C was attempted but the performance was very poor indicating that humidification and proper water management is of crucial importance in the operation of the PEMFC, especially at high temperatures.

Effect of Oxidant (Air *vs*. Oxygen)

Figure 11.5 (page 11-5) shows the effect of air *vs.* oxygen, as the oxidant, in the cathode stream. The cell had a significantly better performance when oxygen was used rather than air. There is a 21 % increase in the maximum current density and a 50 % increase in the maximum power density when oxygen was used as compared to air. Since air contains 20 % oxygen, the lower mole fraction of oxygen in the air resulted in a lower partial pressure of oxygen and thus lowered the equilibrium potential (equation 10.53). The diffusion rate of oxygen (equation 10.28) was decreased due to the reduced oxygen concentration, which decreased the amount of oxygen reaching the reaction site. The lower oxygen concentration decreased the reaction kinetics by decreasing the cathodic exchange current density (equation 10.73) and hence, increasing the activation overpotential of the cathode (equation 10.76). The increased activation overpotential resulted in a decreased cell voltage. While oxygen gave a better performance than air, the cost of oxygen makes it’s use uneconomical in most circumstances.

Effect of Carbon Dioxide Dilution

The effect of carbon dioxide dilution of the anode on cell performance can be seen in figure 11.6 (page 11-6).. There was approximately a 17% decrease in maximum current density and a 31 % decrease in the maximum power density between the 0 % and 50 % carbon dioxide mole fractions. Carbon dioxide was an inert and acted as a diluent and effectively decreased the mole fraction of hydrogen (equation 10.18). The decreased hydrogen mole fraction meant a decreased hydrogen partial pressure, hence the equilibrium potential decreased. Carbon dioxide decreased the diffusion rate of hydrogen gas to the reaction site as given by equation 10.25. The consumption of hydrogen is a linear function of current as seen by Faraday equation (equation 10.15). At high currents, the diffusion rate of hydrogen to the reaction site becomes increasingly important. The carbon dioxide, in decreasing the diffusion rate of hydrogen, reduced the amount of hydrogen reaching the reaction site and hence caused a decrease in the reaction kinetics due to limited hydrogen supply, thus the performance decreased.

12.2.2 Dais Cell

Effect of Humidification

Figure 11.7 (page 11-7) shows the effect of humidification (at 25 °C), of the anode, on the Dais cell. Humidification resulted in a 1.6 % increase in the maximum current density and a 7.5 % increase in the maximum power density. Only the anode stream could be humidified because the anode was an enclosed compartment with inlet and outlet connections. Since the Dais cell was an air cell, that is, the oxidant was air, the cathode was open to the atmosphere and hence could not be humidified. To improve the cathode humidification level, the cell was run at medium to high current to allow the water formed by reaction 10.11 to increase cathode humidification. The tests were then performed on the cell in this relatively higher state of hydration. There was an increase in performance of the fuel cell, as was expected, due to the enhanced conductivity of the membrane. The higher proton conductivity resulted in lower ohmic losses through the membrane and thus increased cell voltage or performance.

Effect of Air flow

The effect of air flowrate is shown in figure 11.8 (page 11-8). There was a 25 % increase in the maximum current density and a 36 % increase in maximum power density for the higher air flowrate run. The flowrate of air across the cell was increased by switching on the extractor fan in the fume cupboard. Although the exact flowrate of air was not known, the results showed that increasing the airflow increased the performance. The increased airflow maintained a higher oxygen concentration gradient than that of the stagnant air, thus increasing the diffusion rate of oxygen to the reaction site. This higher oxygen concentration increased the reaction kinetics and hence caused a decrease in the activation overpotential. The lower activation overpotential meant the cell voltage was higher.

12.2.3 Comparison Test (manufactured MEA *vs.* commercial MEA)

Figure 11.9 (page 11-9) shows the comparison test between the ElectroChem MEA's and the manufactured MEA. The individual ElectroChem MEA's varied in performance, with a difference of 0.04 A/cm^2 in the maximum current density and approximately 0.04 W/cm^2 in the maximum power density. The manufactured MEA compared favourably with the two ElectroChem MEA's up until a current density of about 0.23 A/cm^2. The performance curve of the manufactured MEA lies in-between that of the two ElectroChem MEA's. After 0.23 A/cm^2 the performance of the manufactured MEA dropped below that of the two ElectroChem MEA's. The manufactured MEA showed an average decrease of 23 % in the maximum current density and 26 % in the maximum power density as compared to the ElectroChem MEA's.

The electrode and MEA preparation methods for the ElectroChem MEA could not be obtained, since this was proprietary information, hence, a comparison of preparation methods, especially for electrode preparation, cannot be drawn. As a result, the lower performance of the manufactured MEA was attributed to the hot-pressing procedure. With conventional hot-presses, the MEA was assembled at approximately 5 MPa and 120 °C for 30 seconds. The G-clamp hot-press used was very limited in terms of the clamping pressure and the MEA was under a significantly lower pressure than that used in conventional hot-press. Also, due to the design of the G-clamp hot-press, the MEA was clamped and placed in the oven for about 1 hour to allow the metal plates

to reach the desired temperature. As a result the MEA was exposed to high temperature for a significantly longer time than the conventional hot-press.

This difference in the hot-pressing methods could result in poorer contact between the MEA manufactured using the G-clamp hot-press as compared to the conventional hot-press. The poor MEA contact resulted in increased resistance of the MEA and thus lower performance. The micrographs of the ElectroChem and manufactured MEA (figure E1 on page E-1) show the different regions in the MEA. The micrograph showed that the ElectroChem MEA appeared to have better contact between the catalyst and the membrane. The catalyst layer of the manufactured MEA showed a greater degree of cracking than that of the ElectroChem MEA. The micrograph of the surface of the catalyst layer (figure E2 on page E-2) showed that the catalyst surface of the ElectroChem MEA appears smoother and more uniform than the manufactured MEA.

12.2.4 Model results

Figure 11.10 (page 11-10) shows the performance comparison between the model prediction and the experimental result. At saturation of the inlet gases, the model predicts a higher performance than what is experimentally observed. As explained in the discussion on the operating procedure, the performance of the cell increased when a run was repeated, indicating that the cell was not completely humidifed or saturated. Simulating the run with the inlet gases at 87.5 % saturation, gave a better fit between the model prediction and the experimental data. The results of the experiments simulated using the model are shown in figures 11-11 to 11-13 (pages 11-11 to 11-13). The profiles predicted by the model are in agreeance with the experimental results. A more complex model would yield better results in terms of comparison to experimental results, but the aim of the modelling analysis was to provide a relatively simple model which was able to predict (relatively accurately) the performance of the fuel cell.

12.3 Manufacturing Section

In manufacturing of the fuel cell, it was preferred to obtain the materials required from a local supplier, rather than order these from fuel cell companies overseas. This would significantly reduce cost as well as delivery time. However, materials like the

Nafion® solution, membrane and carbon paper (specifically 0.17 mm thick) were not available locally. Teflon® products (FEP, PTFE) were available through a local Dupont® branch, but the minimum amounts that these were sold in were too large, and as a result, too expensive for our purposes. Thus the materials were obtained from a fuel cell manufacturer (ElectroChem Inc.) based in the United States.

The different methods for manufacturing of the electrodes are outlined in chapter 9 'Fuel Cell Manufacturing'. The main criteria used for selecting a method was that it had to be simple and not require very specialised, expensive equipment.
In manufacturing of the MEA, it was decided to keep the platinum loading and electrode area the same as the ElectroChem cell so as to be able to compare the performance of the two MEA's. The ElectroChem cell had a platinum loading of 1 mg/cm^2 and an electrode area of 5 cm^2. Platinum (20 weight percent platinum supported on Vulcan XC-72R) was used as the catalyst.

12.3.1 Preparation Methods

The methods as outlined in chapter 9 'Fuel Cell Manufacturing' are discussed below.

12.3.1.1 Preparation of Carbon Paper

The carbon paper was cut into 5 cm^2 pieces (2.2 cm x 2.3 cm) and wet-proofed using FEP solution. The carbon paper electrodes had to be water-proofed to prevent excessive water loss from the cell, thus dehydrating the membrane and reducing performance. The FEP solution was painted onto the electrode using a small, artists paint brush. The carbon paper was dried as outlined in the method. The average FEP loading was 51 weight percent.

12.3.1.2 Preparation of catalyst paste

Small catalyst samples (approximately 20 to 30 mg) were used to test the different methods. Small masses were used so as not to waste the catalyst. The catalyst (Pt-C) particles, which are quite large, were first crushed to a fine powder using a glass rod. The fine powder ensured better mixing of the catalyst paste during ultrasonic treatment. The well mixed paste resulted in a uniform catalyst paste and made it easier to paint onto the electrode. A micrograph of the catalyst is shown in figure E3 on page E-3.

Trial runs

The catalyst paste and electrode preparation methods as outlined in chapter 9 'Fuel Cell Manufacturing' were tested (trial runs) to compare the different methods and consequently select a method for further study.

Method 1

First run

The catalyst (30 mg) and PTFE are mixed at 50 °C for 10 minutes. A solution formed, which tended to dry if insufficient PTFE solution was added. A 40 weight percent PTFE loading is suggested, but this was insufficient for good mixing with the catalyst, hence PTFE was added as required to form a well-mixed paste. After cooling to room temperature, isopropyl alcohol was added to the mixture. A sticky flocculate formed. The treated carbon paper was placed in a mould made from masking tape. The flocculate was screen printed onto the carbon paper using a glass rod.

The electrodes were placed in the oven and dried at 70 °C for 30 minutes, then dried at 180 °C for 30 minutes. After the drying process the catalyst layer was cracked and appeared flaky. The layer appeared quite thick (approximately twice the thickness of the carbon paper itself). The electrodes had an average platinum loading of 0.4 mg/cm^2. The cracking may be a cause of the drying process. For the second run, the method was attempted at a lower initial drying temperature for a longer period of time as well as vacuum drying.

Second run

Catalyst (28 mg) and PTFE were mixed at 55 °C. The mixture was cooled and isopropyl alcohol was added which resulted in the formation of a flocculate. A small amount was screen printed onto an electrode using a glass rod. The electrode was then dried in oven at 70 °C for 30 minutes then at 100 °C for 15 minutes and vacuum dried at 100 °C for 1 hour. The catalyst layer seemed slightly wet and sticky after the 70 °C heating stage. After the vacuum drying the catalyst paste was still slightly moist and sticky. The electrode was placed in oven at 200 °C for 30 minutes. After drying the catalyst layer was cracked and flaky.

The layer of the catalyst paste that is screen printed onto the carbon paper was relatively thick and due to thermal stresses during drying, causes cracking of the catalyst surface.

Method 2

The method was tested using the literature concentrations. The catalyst (25.6 mg), 1 ml H_2O and 0.6 ml Nafion® (5 weight percent) solution were mixed together and treated ultrasonically for 1 hour. The catalyst paste, after ultrasonic treatment, appeared well mixed and of a thicker, uniform consistency. The catalyst solution was painted onto the electrode using a small paint brush. Due to the water-proofing of the electrodes the paste tended to run off the electrode. The painted electrode was dried in the oven for 30 minutes and vacuum dried for 1 hour at 75 °C. The catalyst layer after drying was a thin, smooth coating on the electrode. The catalyst layer seemed to be uniformly applied without any cracking. The electrodes were weighed and found to contain an average platinum loading of 0.2 mgPt/cm^2. The entire solution needed to obtain a platinum loading of 1 mg/cm^2 was too much to paint onto the electrode at once. Hence, it had to be applied in stages, that is, paint the electrode, allow to dry and repeat the process until the desired platinum loading was obtained.

Method 3

Solvents with a dielectric constant ranging from 3 to 10 form colloids forms colloids. Acetic acid (99 % pure) was used as the solvent since it had a dielectric constant of 6.15 and was readily available. The acetic acid and Nafion® solution were added together in weight ratio 1 : 6 Nafion® : solvent. On addition of the Nafion® solution to the acetic acid, there was no colloid formation as reported in the literature. A solution formed. Water was added to dilute the acid but no colloid formation was observed. Ethyl acetate (dielectric constant of 6.02) was used as the solvent but, as with the acetic acid, a solution and not a colloid formed. The catalyst powder was added to the acetic acid / Nafion® solution and treated ultrasonically for an hour. After ultrasonic treatment, the catalyst mixture was a weak solution. The catalyst solution was painted onto the electrode. Due to the water proofing and weakness of the solution, the catalyst solution tended to run off the electrode. After drying, the catalyst layer was powdery and non-uniform.

From the above trial runs, method 2 yielded the best results in terms of application of the catalyst paste as well as the uniformity and texture of the catalyst layer.

Thus, method 2 was selected and tests performed to try and optimise the consistency of the catalyst paste and test the effect of different drying temperatures. In addition, the effects of the type of brush used for painting of the catalyst paste, the material used for electrode backing, as well as wet-proofing of the backing layer were also tested.

(i) Effect of solvent concentration

The effect of the solvent (water) concentration on the catalyst paste was tested. The Nafion® concentration or rather the ratio of Nafion® solution (volume) to catalyst mass was kept at a constant value, as used in the original method. The solvent volume was adjusted. Two solvent volumes (concentrations) were tested:-

- twice the original concentration
- half the original concentration

When the solvent concentration was doubled, the catalyst paste was much weaker than the original concentration. It was more difficult to paint the weaker paste onto the electrode due to the wet-proofing of the carbon paper. The catalyst paste tended to run off the carbon paper. As a result of the higher solvent concentration the drying time was increased. The large amount of solvent resulted in uneven distribution of catalyst particles. Thus, certain areas of the electrode had more catalyst particles than others resulting in a gap in the catalyst layer.

When the solvent concentration was halved, the catalyst paste was thicker and easier to paint onto the carbon paper. Drying time was quicker with the reduced solvent concentration.

Solvent concentration tests showed that the consistency and ease of application of the catalyst paste increased with decreasing solvent concentration. However, a minimum quantity of solvent was needed to ensure good mixing during ultrasonic treatment.

(ii) Effect of drying conditions

The electrodes were dried at various temperatures and pressures to obtain the best drying conditions, that is, when cracking was eliminated.

Drying conditions:

- room temperature (approximately 25 °C), atmospheric pressure
- 50 °C, atmospheric pressure
- room temperature, vacuum
- 50 °C, vacuum

The electrodes dried at room temperature and atmospheric pressure gave the best results in that the catalyst layer showed less cracking. Slower drying reduces the tendency of catalyst layer to crack.

(iii) Effect of type of brush used

Two types of brushes, a soft, thin bristled brush and a stiffer, thicker bristled brush were tested (see photograph D7 on page D-7).

The soft bristled brush gave the best results in that the catalyst layer was less prone to cracking. The length of the bristles had a significant effect on the thickness of the cost applied. If the bristles were too long, a thicker coat results. The thicker coating was more likely to crack due to thermal stresses during drying. As a result the length of the bristles on the soft bristled brush was shortened, resulting in an increase in the rigidity of the bristles. Results were significantly improved with the modified brush. In addition to the thickness of the coat applied, if too much air was entrapped in the paste during painting, pitting of the catalyst layer results during drying. Thus, the optimum coat applied was a thin, smooth and continuous film without any air bubbles entrapped.

It was noticed that cracking or pitting tended to occur after a loading of about 0.5 mg/cm^2.

(iv) Effect of wet-proofing

An untreated piece of carbon paper was painted with catalyst paste. The liquid (Nafion® solution and solvent) in the catalyst paste seeps through the untreated carbon paper. The catalyst layer was unevenly dispersed and rubbed off very easily. Hence, wet-proofing of the carbon paper was necessary.

(v) Effect of electrode backing material

Carbon paper and carbon cloth (Toray®) were used as the backing for the catalyst paste. The carbon cloth which was initially soft (untreated state) became stiff and rigid after treating with FEP, but was still more flexible than the carbon paper. The carbon cloth tended to bend and lose its 'flatness' after wet-proofing, however this could be solved by placing cloth under a weight for a period of time. The carbon paper gave marginally better results in terms of the catalyst surface.

(vi) Nafion® loading

The Nafion® loading in the electrode was an important factor in the performance of the electrode. The Nafion® increased the ionic conductivity of the protons from the catalyst layer to the membrane. The Nafion® solution used contains 5 weight percent dry Nafion®. To calculate the loading of dry Nafion® after drying, the drying characteristics of the Nafion® solution need to be known. By this we mean what fraction of the dry Nafion® was lost in the drying process. According to DuPont, the manufacturer of Nafion®, the solvent evaporates without any loss of the Nafion®. Experiments conducted (Marsh) at Anglo American Research Laboratory confirmed this. Marsh conducted drying tests in a moisture analyser and found that the mass dry Nafion® remaining after drying was approximately the same as that in the solution originally. The fraction of dry Nafion® remaining on the electrode affected not only the Nafion® loading but obviously the catalyst loading as well. The ratio of Nafion® to catalyst used in method 1 yields a Nafion® loading of about 5 mg/cm^2, which according to Poltarzewski *et al* (1992) was too high. They have shown that after a loading of 1 mg/cm^2, the Nafion® forms a layer on the catalyst surface which increased the resistance of the catalyst layer and decreased the performance of the electrode.

As a result, the catalyst preparation method (method 2) was further modified by using a catalyst mass to Nafion® solution volume ratio of 0.21 g(Pt/C) : 1 ml Nafion® solution. This ratio resulted in both a dry Nafion® and platinum loading of 1 mg/cm^2, assuming that no dry Nafion® was lost during the ultrasonic and drying processes. The water content was kept the same, that is, 19 ml water per gram Pt-C powder. The mixture was placed in the ultrasonic bath for approximately 15 minutes. If the mixture was left in ultrasound bath for too long, most of the organic solvent in the Nafion® solution evaporated leaving a mixture that had a high water content. Due to the water-proofing on the electrodes, it was difficult to paint this high water content paste onto the carbon paper. A lower Nafion® loading not only improved the performance of the electrode but reduced the cost as well. The Nafion® loading on the ElectroChem electrodes could not be obtained, as this was proprietary information.

Table C1 (page C-1) shows the calculations for the electrode loading. In the calculation of the loading, it was assumed that the catalyst and Nafion® were well mixed, such that the ratio of catalyst to Nafion® was constant for the entire catalyst paste.

12.3.2 MEA Assembly

Hot-Pressing -Trial run

First run:

The metal plates were heated to 100 °C, but as a result of the heating, handling of the plates was difficult. Electrodes manufactured using method 2 for catalyst preparation were used. In an actual size MEA the membrane is 9.6 cm x 9.6 cm, but since these were trial runs to test the hot-pressing technique, the membrane was cut into smaller pieces (4 cm x 4 cm) so that the membrane is not wasted. The membrane was placed in hot water (50 °C) for a 30 minutes to hydrate the membrane. The electrode was placed centrally on the bottom plate. When the membrane was placed on top of the electrode, it started to flex due to the heat from the plate. Consequently, placing the second electrode in line with the first was difficult. The top plate was placed on the MEA assembly and clamped in the G-clamp. The unit was clamped to 35 N.m. When the unit was tightened, twisting of the plates occurred. The clamp was placed in the oven for about 1 hour at 120 °C. The clamp was allowed to cool before opening it.

When opening the clamp the metal plates twisted slightly. The MEA did not make good contact, that is, the electrodes were easily separated from the membrane.

Second run:
Electrodes prepared using method 1 for catalyst preparation were used. The MEA was placed in-between the plates without preheating the plates. As a result, handling of plates and placing of the MEA was much easier. The unit was clamped using a torque of 35 N.m. Twisting of the plates occurred when tightening. The clamp was placed in oven set at 120 °C for 3 hours. When the clamp was opened, twisting of the plates occurred. The MEA seemed to have good contact. The electrodes were not separating from the membrane as before. The MEA was slightly 'twisted' due to the twisting of the metal plates. The membrane appeared brownish due to the heating, compared to being clear, colourless before hot-pressing.

A major problem encountered during hot-pressing was slippage (twisting) of the two metal plates when the unit is tightened and opened. The twisting of the plates was a result of the twisting action of the G-clamp. This resulted in "twisting" of the MEA. As a result the electrodes were not aligned. Since the flow channels are naturally square, a MEA that was not square would not fit properly (or squarely) onto the flow channel, with the result that the entire electrode was not exposed to the reactant gases. This decreased the catalytic surface area resulting in a decrease in the reaction rate and thus, performance. In addition, the gaskets would not fit properly (squarely) around the entire electrode, which would result in poor sealing of the cell. Due to the overlapping of the electrodes onto the edges of the flow channel as well as the overlapping of the gasket on the electrode, the electrodes would be damaged when the cell was tightened.

A metal bracket (see photograph D8 on page D-8) was made, into which the metal plates are placed. The bracket holds the plates firmly and does not allow them to twist when the plates are clamped.

In MEA manufacturing from literature, the MEA was clamped under high pressure (4 MPa) and at high temperature (120 °C) for a short time (40 seconds), however with the G-clamp this was not possible. The entire clamp was inserted into the oven and hence it had to heat up to the required temperature. As explained, the plates could not

be preheated as this makes handling of the plates very difficult and more importantly causes flexing of the membrane and makes aligning of the electrodes very difficult. The clamp was normally placed in the oven for about 1 hour. Figure E1 (page E-1) shows the micrographs of the manufactured MEA and the ElectroChem MEA. The catalyst layer of the manufactured MEA shows a greater degree of cracking than that of the ElectroChem MEA.

12.3.3 Gasket manufacturing

Gaskets are used to seal the cell, preventing gas leaks. A mould was made using masking tape (0.2 mm thick) and marking out an area (10 cm by 20 cm) on a piece of glass. The glass was coated with a thin layer of polish to prevent the silicon from sticking to the glass when removing it. The silicon rubber solution (prepared using the method detailed in chapter 9 'Fuel Cell Manufacturing') was poured into the mould and a glass rod was used to screen print the silicon solution. A second piece of glass was placed on top.

The mixture was left to dry for 1 week. The gasket was very fragile, tore easily and lacked the strength and durability of the ElectroChem gaskets.

12.3.4 Machining of flow channels

The flow channels were machined into the graphite blocks using a drilling machine with a 1 mm drill bit. Photograph D2 (page D-2) shows the machined blocks.

12.4 Modelling

The models predict the performance of the fuel cell under various operating conditions. The models differ depending on the inlet composition and whether the water flux across the membrane was taken into account.

The variations in the models developed included :

- fuel, water / oxidant, water
- fuel, water / oxidant, inert, water
- fuel, inert, water / oxidant, water

Both zero and non-zero water flux was used for each of the above variations.

The models are one dimensional and isothermal. A non-isothermal case was also looked at. The average flow in the flow channel was taken as a log mean average of the inlet and outlet flows, as was suggested by Amphlett *et al*, 1995.

The diffusion through the carbon paper backing of the electrode was modelled using the Stefan-Maxwell equation (equation 10.19) for multicomponent diffusion. The binary diffusion coefficient term was converted to an effective binary coefficient (equation 10.20) by multiplying the binary diffusion coefficient by the effective porosity, ε. The porosity factor accounts for the porosity of the carbon paper backing, which constitutes the diffusion layer. A micrograph of the diffusion layer is shown in figure E5 (page E-4). The micrograph showed the diffusion path for the reactants and products. For the multicomponent system (fuel/oxidant, inert, and water), the equations were solved numerically using the Euler algorithm.

The reaction kinetics were modelled using the Butler-Volmer equation (equation 10.56). Equations for the exchange current densities (equations 10.61 and 10.73) and activation overpotentials (equations 10.67 and 10.76) were derived. The temperature and pressure dependence of the exchange current density was obtained by fitting equations to the data from Parthasarathy *et al* (1992a,b), who experimentally investigated these dependencies. The non-zero water flux models incorporate the 'alpha' term, which is the net flux of water across the membrane per proton flux. This was basically the difference between the water dragged by the protons across the membrane from the anode to the cathode (electro-osmosis) and the back diffusion of water from the cathode to the anode. The solution for this net water flux involved an iterative procedure. The details of the procedure, as is the model development are, explained in chapter 10 'Model Development'.

The ohmic overpotential was calculated as a function of the activity of the water at the anode. The water content at the anode will be lower than that at the cathode due to the migration effect and the formation of water at the cathode. A cautious approach was taken and the activity and hence ohmic overpotential was based on the anode water content rather than an average water content of the membrane. The concentration overpotential was included in the model for completeness, although this term was very small and was generally ignored.

In the equation for the equilibrium potential (equation 10.53), the activity or rather fugacity of the gas species was approximated by the respective partial pressure. This approximation was used since the gases are assumed to be ideal. Also for the relatively low pressures (usually atmospheric) used, the fugacity coefficient was approximately unity and the difference in equilibrium potential as a result of using the partial pressure instead of the fugacity is negligible. A flow diagram of the model algorithm is shown in figure 10.1 (page 10-20).

The increase in cell temperature was calculated by equation 10.83. The entropy change term of the thermodynamic relation (equation 10.82), which was the difference between the enthalpy of the reaction and the Gibbs energy, causes an increase in the temperature of the cell. The model predicted the average (between the anode and the cathode) increase in the temperature of the inlet stream (inlet temperature of 40 °C) was approximately 5 °C.

The electrical efficiency of the fuel cell was also developed in the modelling section. The efficiency calculations showed that the fuel cell had a potentially much higher electrical efficiency than conventional energy converters, which were governed by the Carnot cycle. The maximum electrical efficiency of the fuel cell in terms of the fraction of the total energy of the reaction (reaction 10.11) that is converted to electrical energy was approximately 0.95. The electrical efficiency in terms of the fraction of the total energy of the fuel that was converted to electrical energy is 0.83.

CHAPTER 13 : CONCLUSIONS AND RECOMMENDATIONS

13.1 Conclusions

In terms of the aims, as detailed in each of the relevant sections, the following conclusions were reached.

13.1.1 Experimental section

Increasing the temperature of the cell resulted in an increase in the performance of the cell due to a decrease in the activation losses since the reaction kinetics increased at the higher temperature. Similarly, increasing the cell pressure resulted in an increase in the cell performance due to a higher reactant concentration at the reaction site and increased reaction kinetics, which resulted in lower activation losses and hence increased performance of the cell. Humidification of the reactants increased performance of the cell, especially in the higher temperature range. This was due to the higher water content, which resulted in an increased conductivity of the membrane and hence a reduction in the ohmic losses through the membrane. It was observed that humidification of the cell was essential for temperatures greater than 40 °C. In addition, proper water management was crucial to the performance of the membrane. Oxygen, as the oxidant, improved the performance significantly compared to air due to the higher oxygen content in pure oxygen as opposed to air, which resulted in higher oxygen concentration at the reaction site and increased reaction kinetics so the activation losses decreased. Carbon dioxide acts as a diluent in the system effectively decreased the hydrogen concentration. This caused a decrease in the reaction kinetics and increased the activation losses and resulted in decreased performance of the cell. Good electronic contact between the graphite block and the electrode was very important for good performance.

13.1.2 Manufacturing section

It was concluded that specialised materials like the Nafion® products, electrode backing (specific thickness needed), gaskets (specific thickness needed) were not available locally and must be obtained from fuel cell companies overseas. Teflon products (PTFE, FEP) were available locally, but minimum quantities sold were too large for testing purposes and had to be obtained from overseas suppliers.

A simple, effective method for catalyst preparation has been demonstrated. Cracking of the catalyst layer was a major problem and was affected by various factors such as drying temperature, thickness of catalyst paste and the type of brush used to paint the catalyst paste. Lower drying temperature, thicker paste and a soft, yet rigid brush gave the best results.

A hot-press was manufactured and a hot-pressing procedure developed. Twisting of the MEA during hot-pressing is a major concern, although with a proper bracket this can be eliminated. MEA twisting was expected to be restricted to the G-clamp type of hot-press and should be eliminated if a commercially obtained hot-press was used.

13.1.3 Modelling section

A one-dimensional, multicomponent model has been developed. The model prediction showed a good fit to the experimental data. The results from the model were in aggreeance with the profiles from the experimental section. That is to say, they showed the same trends. The modelling work helped to give a better understanding of the operation of the fuel cell and to explain the experimental results.

13.2 Recommendations

The following recommendations are made:-

- testing the effect of adding PTFE to the catalyst paste.
- investing in a better humidification unit to ensure good humidification of reactant gases.
- if a humidification unit is too expensive then the feasibility of having a direct water injection system, where liquid water can be injected into the cell at regular intervals should be investigated.
- having a moisture trap in the exit line to remove excess liquid water from the cell, especially the cathode and hence, reduce flooding of the electrode.
- redesigning the bracket to allow for the G-clamp itself to be securely bolted to the bracket. This would make tightening of the G-clamp easier, especially using high torque. The G-clamp would be held securely in place and not have to be held by the operator.
- increasing the complexity of the model, by including the resistance of the catalyst layer.

APPENDIX A : CALIBRATION CHARTS

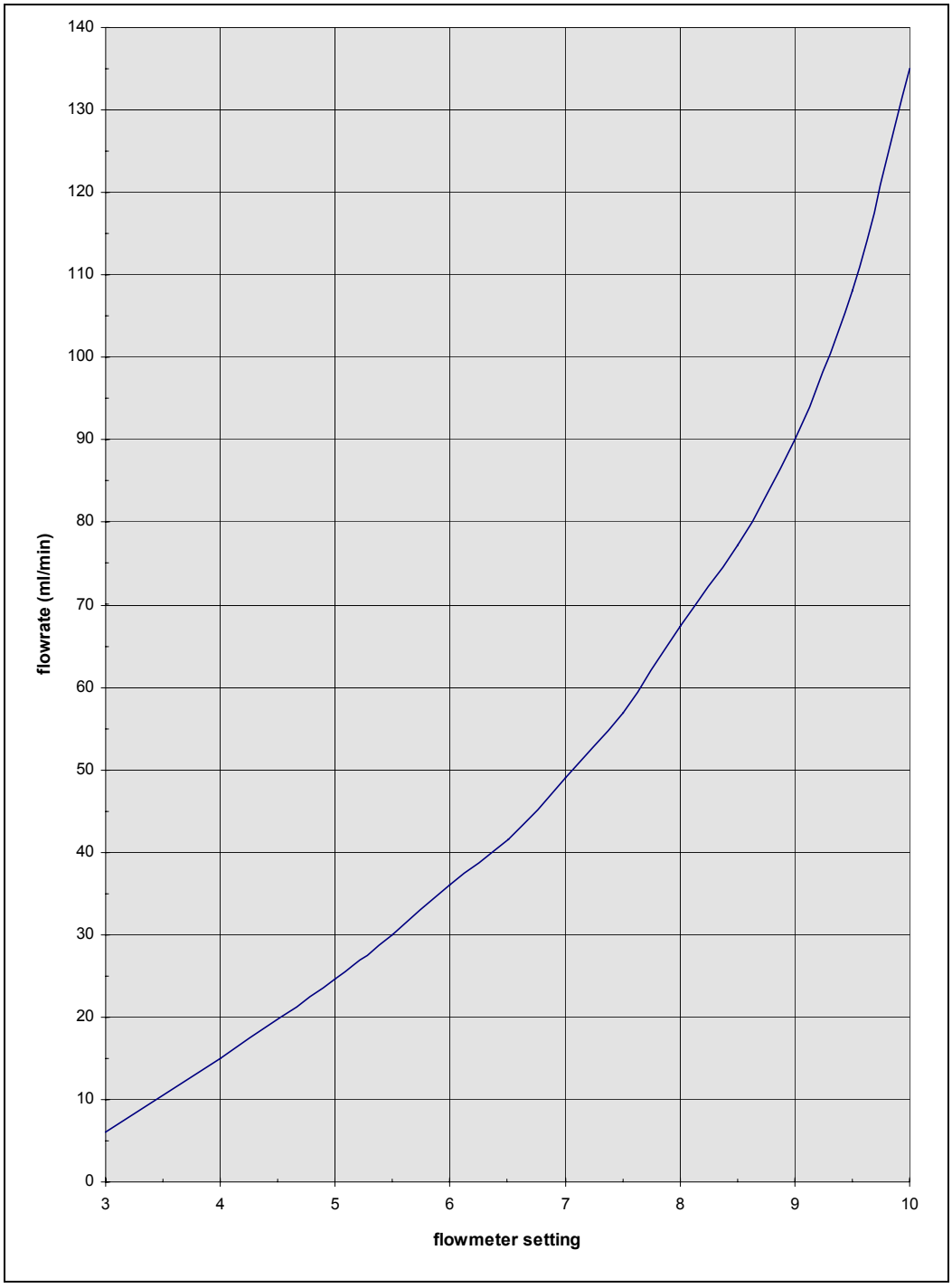

Figure A1 : Calibration chart for H_2 flowmeter

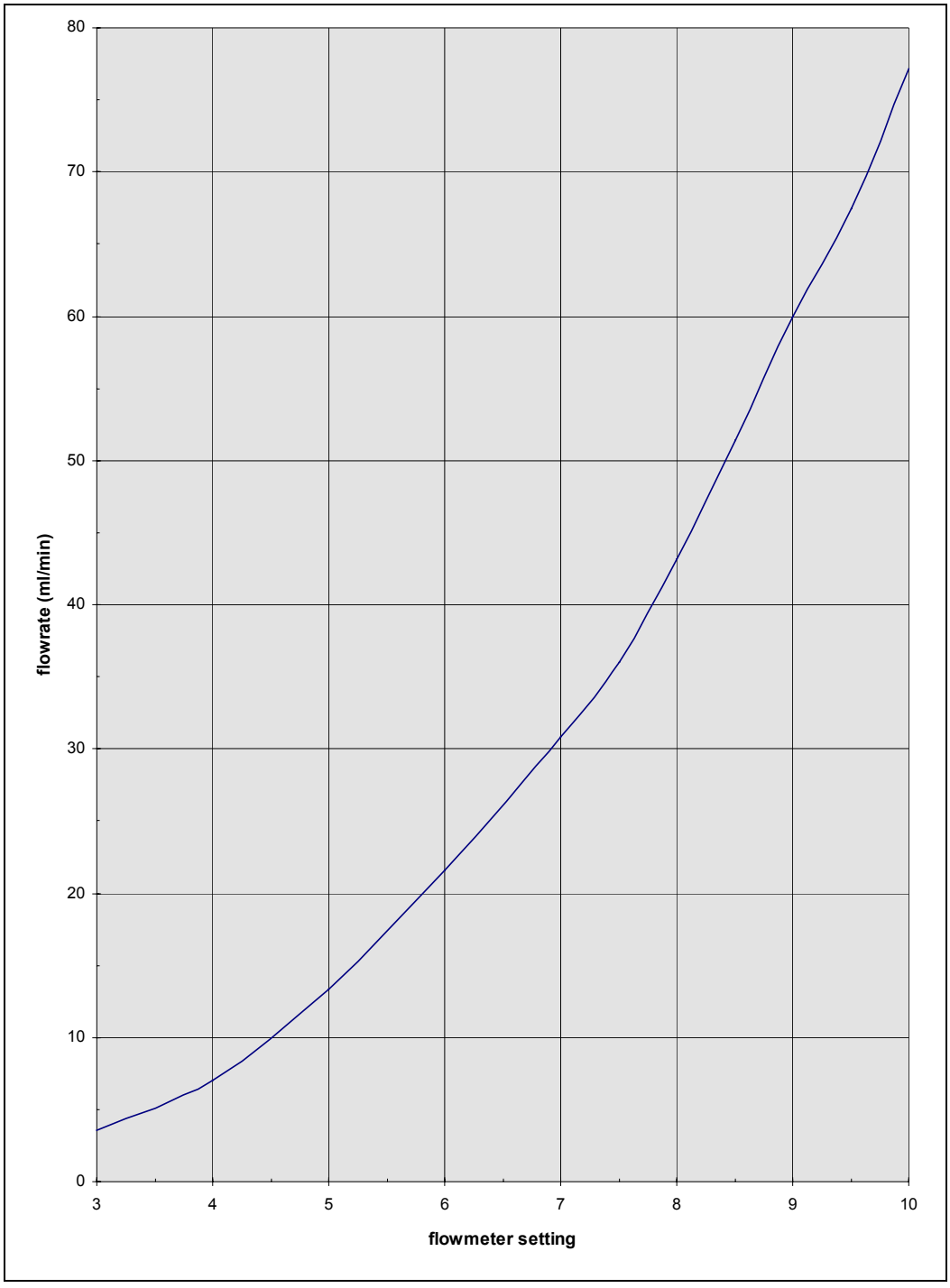

Figure A2 : Calibration chart for O_2 flowmeter

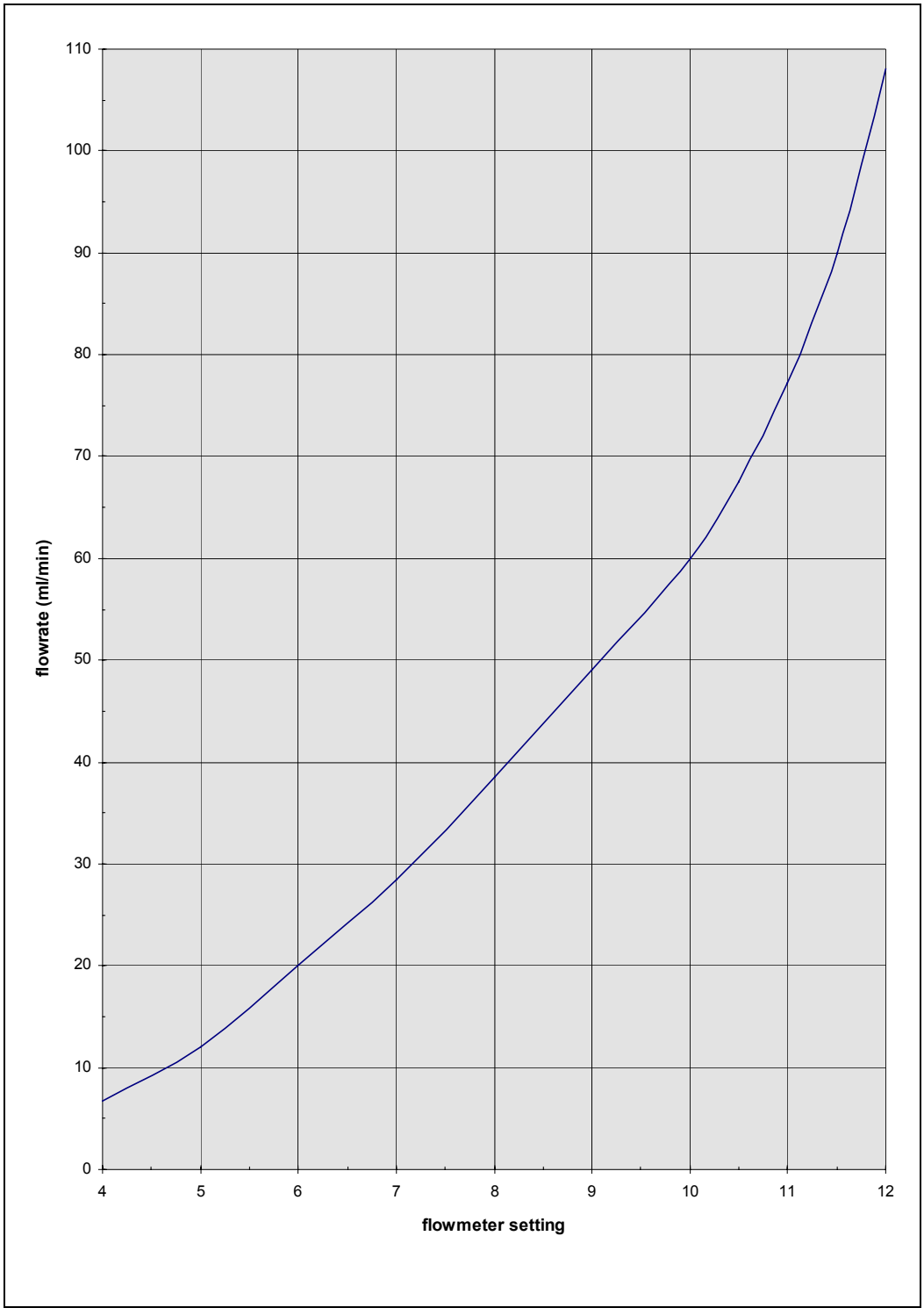

Figure A3 : Calibration chart for CO_2 flowmeter

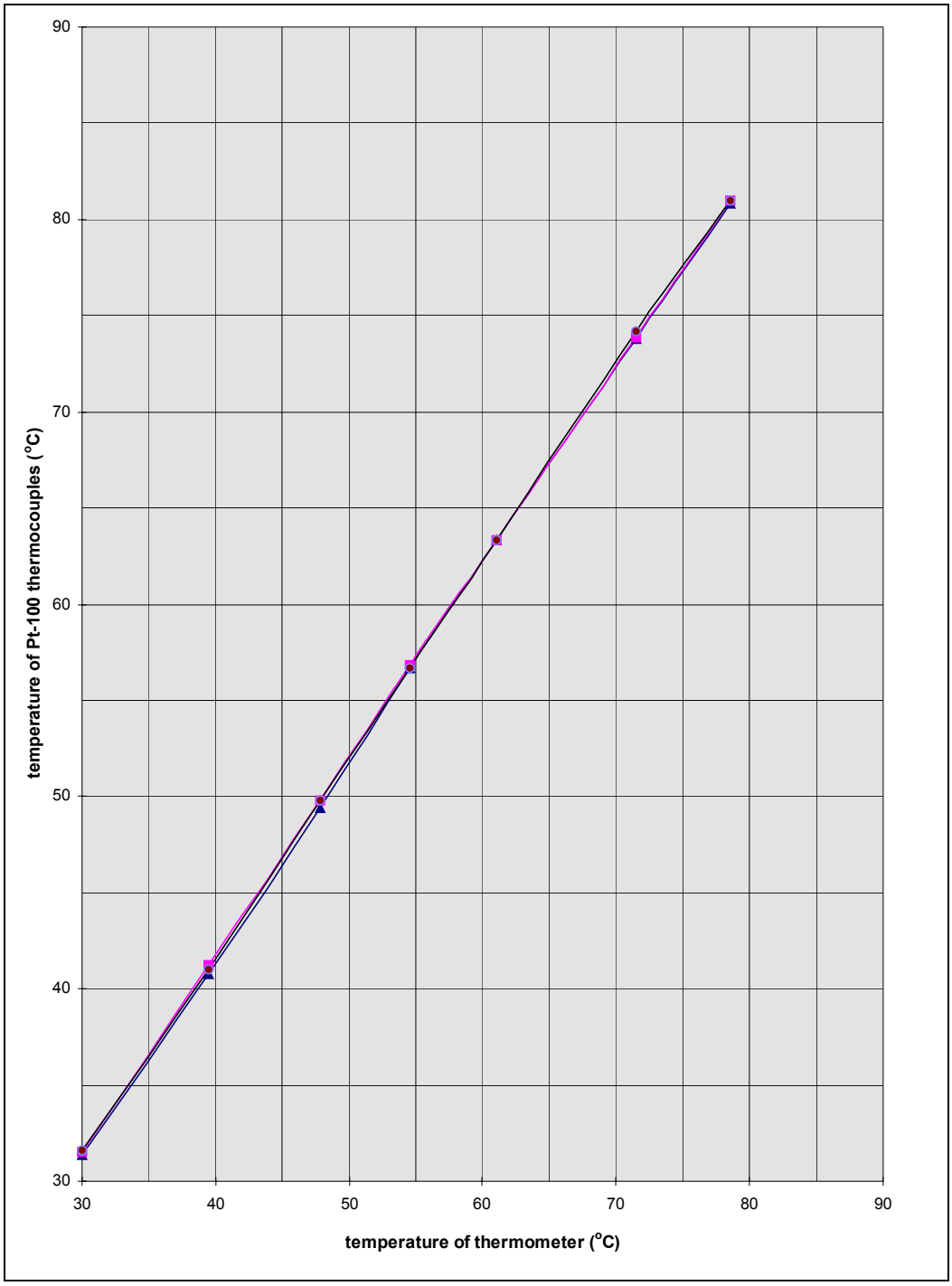

Figure A4 : Calibration chart for Pt-100 thermocouples - calibrated against thermometer

Legend - (▼) thermocouple 1 (■) thermocouple 2 (●) thermocouple 3

APPENDIX B : SPECIFICATION SHEETS

Nafion® Solution

Nafion® solutions are solutions of perfluorosulphonic acid/PTFE copolymerin (acid form). The typical composition (DuPont, USA) of the solution is shown in the table below.

Table B1 : Typical composition of Nafion® solution

Component	Composition (wt %)
polymer	5.0 min, 5.4 max.
water	45 ± 15
VOC	50 ± 15
1- propanol	15-30
2-propanol	15-30
methanol	< 5
mixed ethers and other VOCs	< 5
solution density (lbs/gallon)	7.75

Nafion® 117 Membrane

Nafion® membranes are non-reinforced films based on Nafion® resin, a perfluorosulphonic acid/PTFE copolymerin (acid form).

Table B2 : Typical properties of Nafion® 117 membrane

Property	Value
thickness (mm)	0.183
density (g/cm^3)	2.0
conductivity (S/cm)	0.083
water uptake (% water)	38
thickness change (% increase)	10
linear expansion (% increase)	10

NB: water uptake measured from dry membrane to water soaked at 100 °C for 1 hour

thickness and linear expansion measured from 50 % relative humidity (23°C) to water soaked at 23 °C

APPENDIX C : ELECTRODE LOADING CALCULATIONS

Table C1 : Calculations for the catalyst, FEP and Nafion® loadings of the manufactured electrodes

		electrode 1	**electrode 2**
mass carbon paper	g	0.0510	0.0507
area of carbon paper	cm^2	5	5
mass carbon paper + FEP	g	0.1069	0.1025
% FEP loading		**52.3**	**50.5**
mass catalyst powder (platinum + carbon support)	g	0.0225	0.0225
mass platinum catalyst (20 wt. %)	g	0.0045	0.0045
volume Nafion® solution used	ml	0.1000	0.1000
density Nafion®	g/ml	0.9290	0.9290
mass Nafion® solution used	g	0.0929	0.0929
mass catalyst + Nafion® solution	g	0.1154	0.1154
mass dry Nafion® (5 wt. %)	g	0.0046	0.0046
% dry Nafion® in electrode after drying		100.00	100.00
mass dry Nafion® in electrode after drying	g	0.0046	0.0046
ratio of mass catalyst : mass dry Nafion®		4.8439	4.8439
mass electrode after drying	g	0.1370	0.1325
mass carbon paper before painting	g	0.1069	0.1025
mass catalyst + mass dry Nafion®	g	0.0301	0.0300
mass catalyst powder	g	0.0249	0.0249
mass platinum catalyst	g	0.0050	0.0050
mass dry Nafion®	g	0.0052	0.0051
mass dry Nafion®/area electrode	g/cm^2	0.0010	0.0010
mass platinum catalyst/area electrode	g/cm^2	0.0010	0.0010
Nafion® loading	**mg Nafion®/cm^2**	**1.0301**	**1.0267**
Catalyst loading	**mg Pt/cm^2**	**0.9980**	**0.9947**

NB : Colour Coding :-

values in dark grey are measured values

values in black are calculated values (except for Nafion® density - obtained from supplier)

values in **bold** are calculated loadings

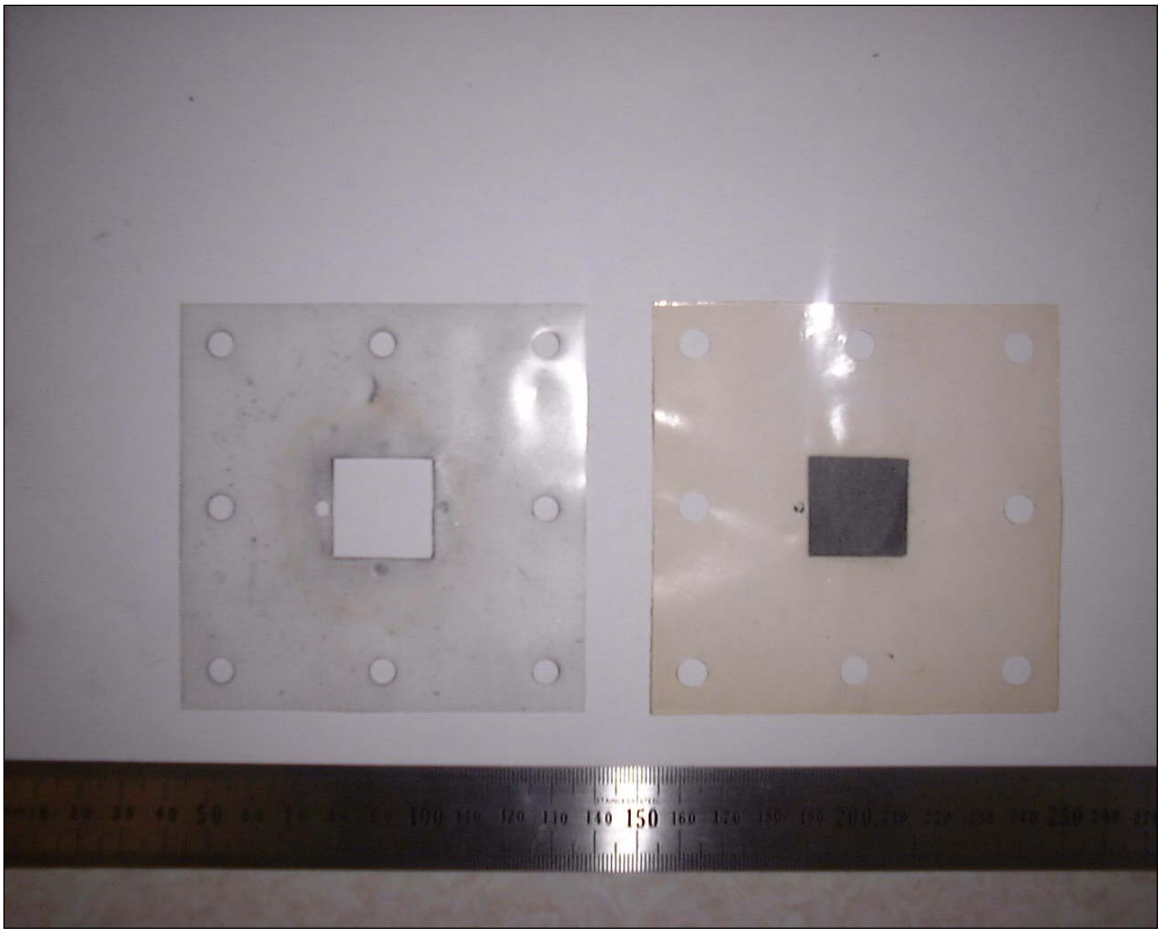

Figure D5 : Photograph of ElectroChem MEA and gasket

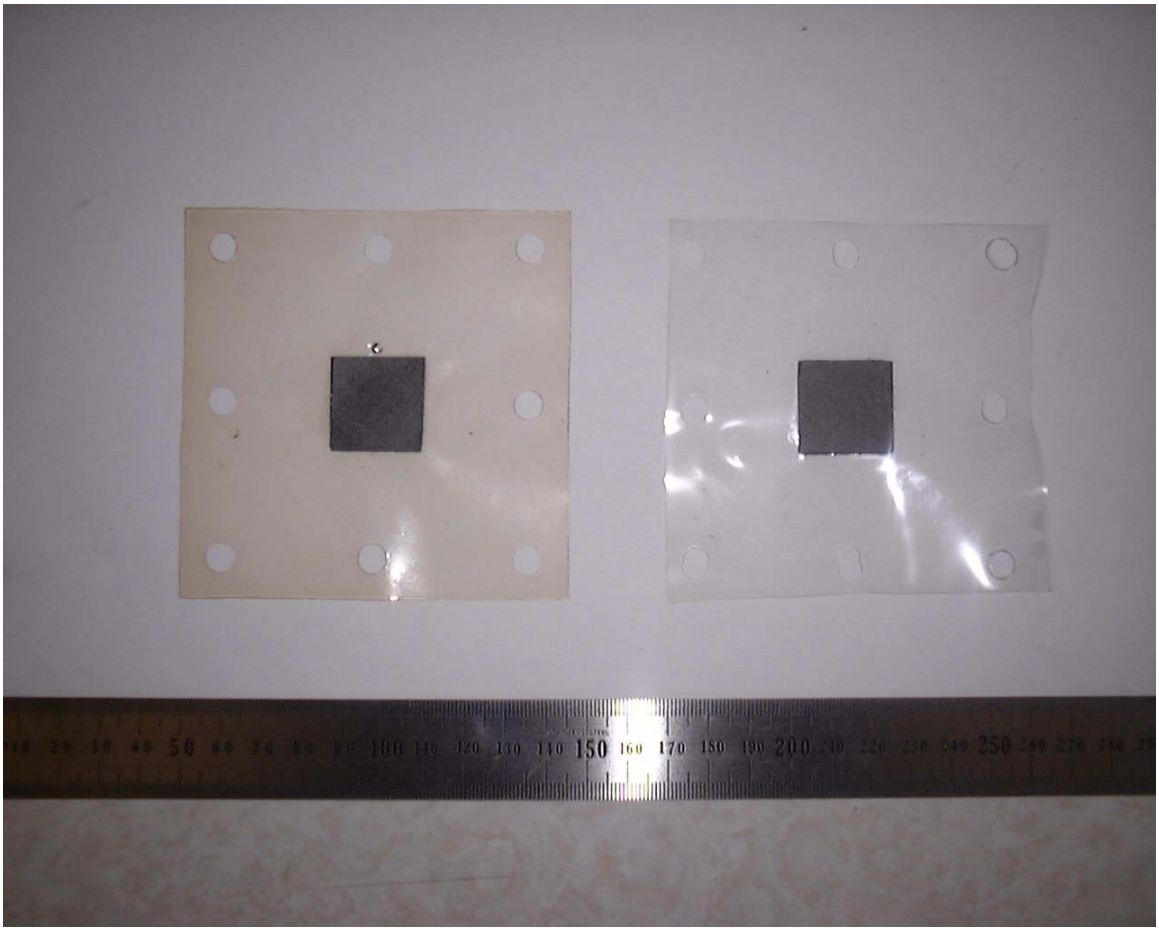

Figure D6 : Photograph of ElectroChem MEA (left) and manufactured MEA (right)

Figure D7 : Photograph of paint brushes

Figure D8 : Photograph of G-clamp hot-press

APPENDIX E : SCANNING ELECTRON MICROGRAPHS

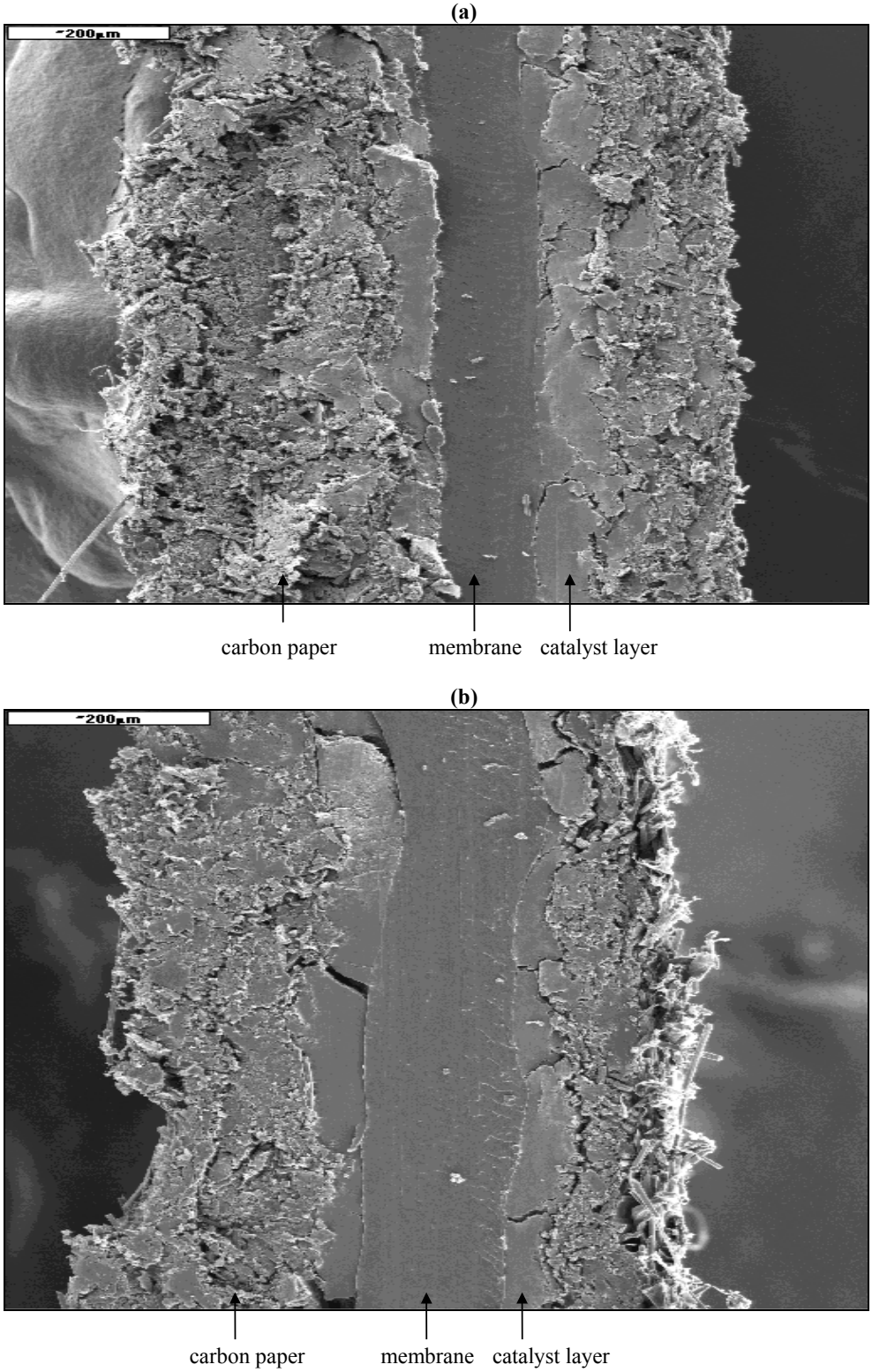

Figure E1 : Micrograph of the cross sectional view of the MEA - (a) ElectroChem MEA (b) manufactured MEA

(a)

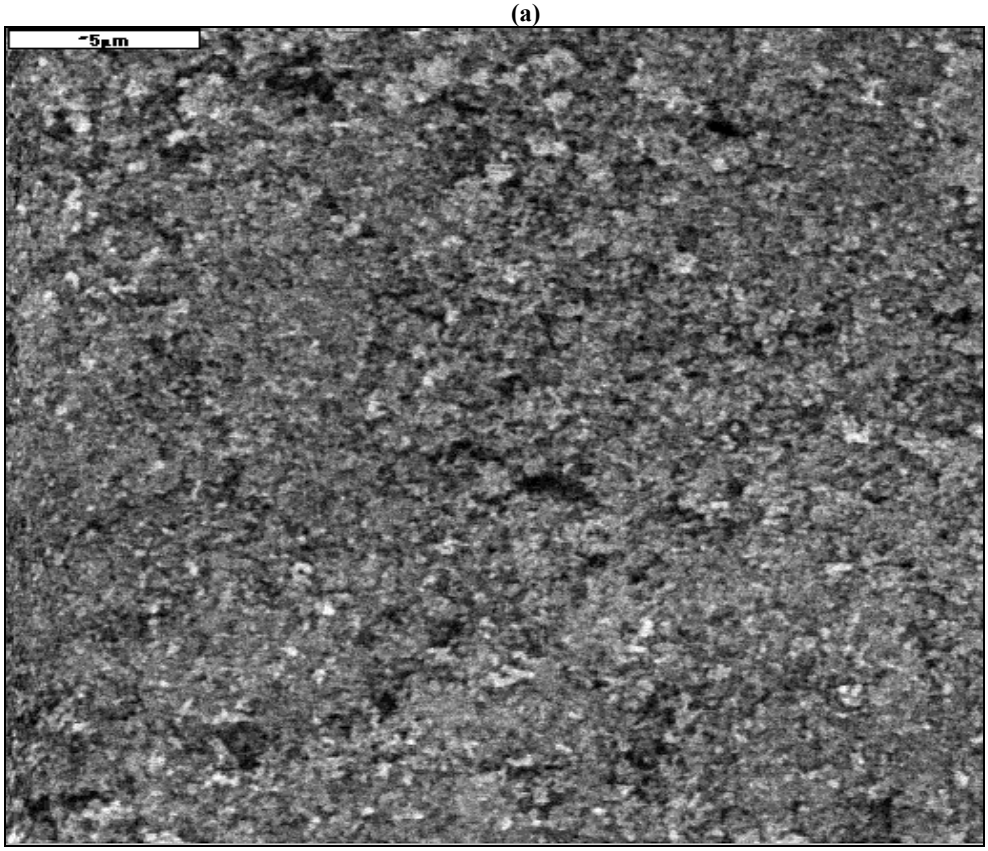

(b)

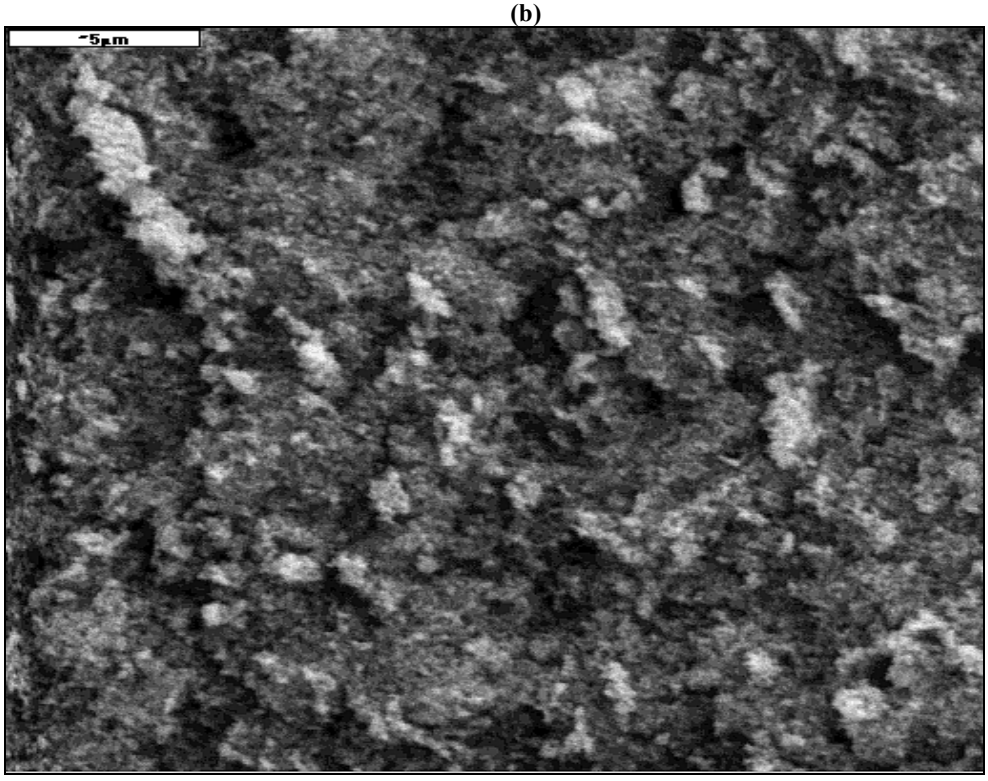

Figure E2 : Micrograph of the surface of the catalyst layer - (a) ElectroChem MEA (b) manufactured MEA

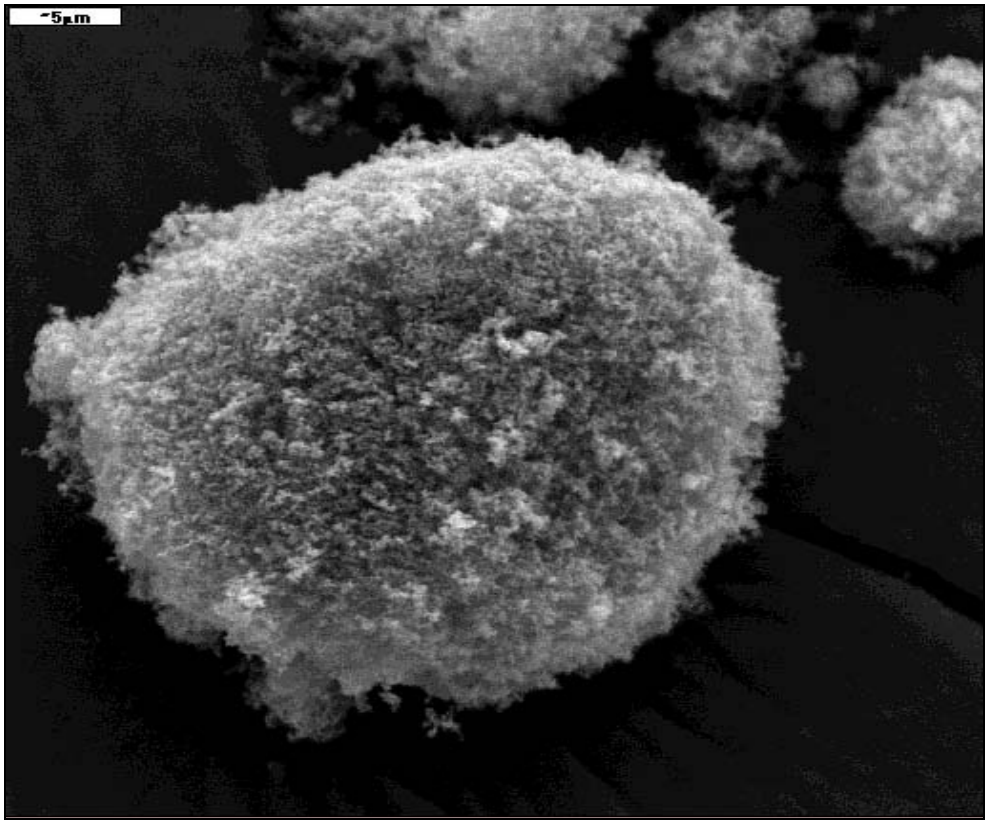

Figure E3 : Micrograph of the catalyst powder (20 wt. % Pt supported on Vulcan XC-72R carbon support)

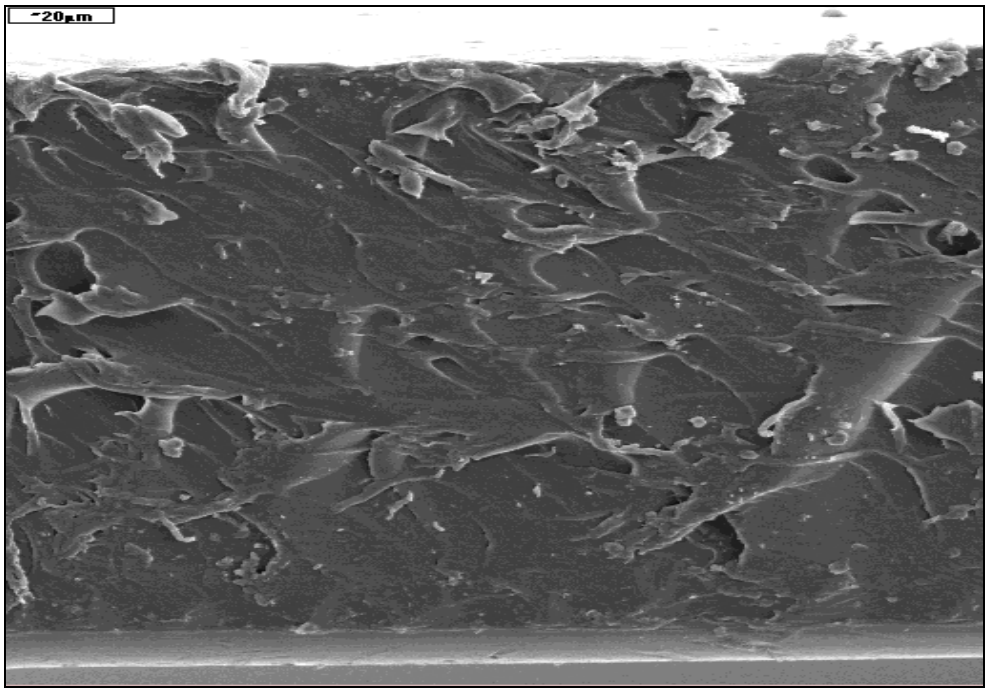

Figure E4 : Micrograph of Nafion® 117 membrane - cross-sectional view

(a)

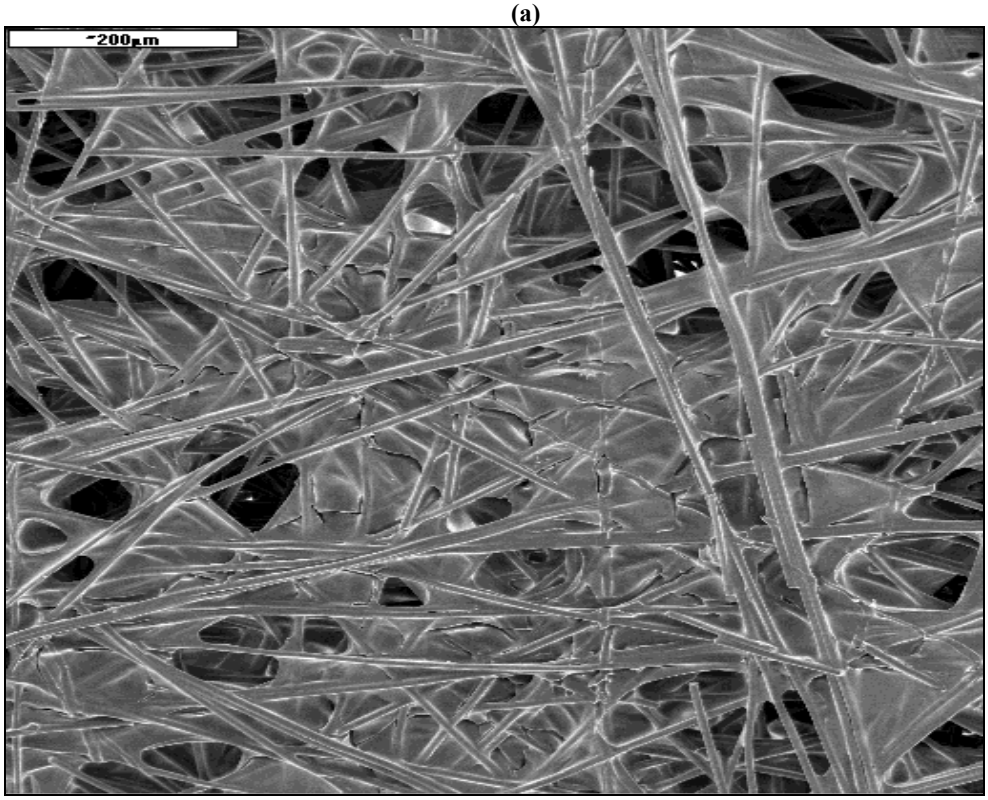

(b)

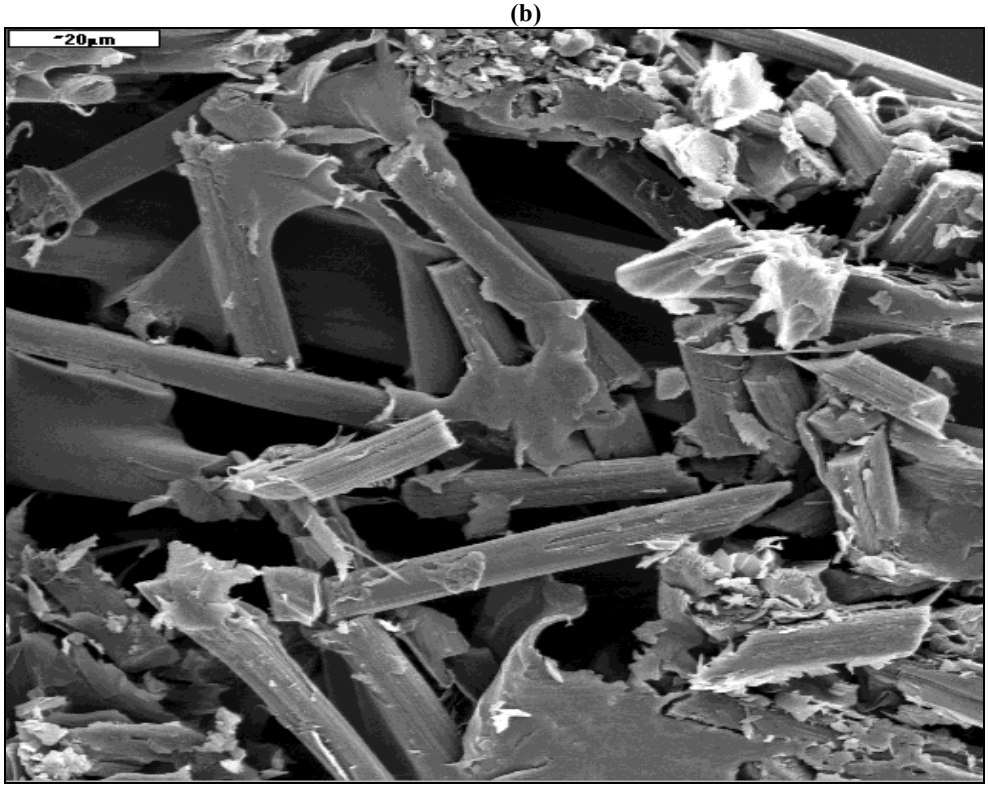

Figure E5 : Micrograph of treated (wet-proofed) carbon paper - (a) surface view (b) cross-sectional view showing the diffusion path for reactants / products

APPENDIX F : FUEL CELL MODEL PROGRAM

The fuel cell model program was written using matlab® (version 3.1). The programme for the model using humidifed hydrogen and humidified oxygen is shown here.

NOMENCLATURE

Symbol	Definition	Units
a_i	activity of species i	
A_e	electrode area	cm^2
A_i	symbol representing reactant / product formula	
C_i	concentration of species i	mol/cm^3
C_{p_i}	heat capacity of species i	J/mol.K
D_{ij}^{eff}	effective binary diffusion coefficient of pair i-j	cm^2/s
E_{eqm}	equilibrium voltage	V
E_k	activiation energy	J/mol.K
F	Faraday's constant	C/mole electron
F_i	molar flow of species i	mol/s
F_{cons,H_2}	hydrogen consumption rate	mol/s
G_{cons,H_2}	hydrogen consumption rate	g/s
i	current density	A/cm^2
i_o	exchange current density	A/cm^2
I	current	Ampere
M_i	molecular mass of species i	g/mol
n	number of electrons	
n_{drag}	flux water molecules dragged per proton flux	
$n_{in,i}$	inlet number of moles of species i	mol
N_i	molar flux of species i	$mol/cm^2.s$
p_i	partial pressure of species i	atm
p_i^{sat}	saturated pressure of species i	atm
p_i^{crit}	critical pressure of species i	atm
P	total pressure	atm
P_{cell}	cell power density	W/cm^2
q_{H_2}	hydrogen consumption rate	moles(H_2)/min
R	universal gas constant	J/mol.K
s_i	stoichiometric coefficent of reactants / products	

t	temperature	°C
ta	thickness of anode	cm
tc	thickness of cathode	cm
tm	thickness of membrane	cm
T	temperature	K
T_i^{crit}	critical temperature of species i	K
V	potential	V
V°	equilibrium potentail	V
V_{cell}	overall cell potential	V
x_i	mole fraction of species i	
z	distance along fuel cell co-ordinate	cm
z_a	distance along anode	cm
z_c	distance along cathode	cm
z_m	distance along membrane	cm
z_i	charge number on species i	
ΔH	enthalpy of formation or reaction	J/mol.K
ΔG	Gibbs free energy of formation	J/mol.K
Φ	electric potential	V
α	net H_2O flux through membrane per proton flux	
β	cathodic transfer coefficient	
ε	voidage	
η_s	surface overpotential	V
η_c	concentration overpotential	V
η_{ohm}	ohmic overpotential	V
γ , $\gamma`$	phase boundaries for anode and cathode	
κ	conductivity	1/ohm.cm
λ	water content of membrane (no. of H_2O molecules/ SO_3H site)	
μ_i	chemical potential of species i	J/mol
ρ	density	g/cm^3
τ	torque	N.m

subscript

a	anode
c	cathode
i	species or component
k	refers to anode or cathode
m	membrane
H_2	hydrogen
O_2	oxygen
CO_2	carbon dioxide
N_2	nitrogen
H^+	proton

superscript	
a	anode
c	cathode

REFERENCES

Ahmed, S., Krumpelt, M., Kumar, R., Lee, S.H.D., Carter, J.D., Wilkenhoener, R. and Marshall, C., (1998), Catalytic Partial Oxidation Reforming of Hydrocarbon Fuels, Argonne National Laboratory, Illinois

Amphlett, C., Baumert, R.M., Mann, R.F., Peppley, B.A. and Rogerge, P.R., (1995 a), Performance Modeling of the Ballard Mark IV Solid Polymer Electrolyte Fuel Cell: 1. Mechanistic Model Development, *Journal of Electrochemical Society*, vol. **142**, no.1, p.1

Amphlett, C., Baumert, R.M., Mann, R.F., Peppley, B.A. and Rogerge, P.R., (1995 b), Performance Modeling of the Ballard Mark IV Solid Polymer Electrolyte Fuel Cell: 2. Empirical Model Development, *Journal of Electrochemical Society*, vol. **142**, no. 1, p. 10

Anderson, A.B., Grantscharova, E. and Seong, S., (1996), Systematic Theoretical Study of alloys of Platinum for Enhanced Methanol Fuel Cell Performance, *Journal of Electrochemical Society*, vol. **143**, no. 6, p. 2075

Anon,. **The Chemical Engineer**, (1999), issue 689, 7 October, p. 8

Appleby, A.J. and Foulkes, F.R., (1993), **Fuel Cell Handbook**, Krieger Publishing Co., Florida

Argyropoulos, P., Scott, K. and Taama, W.M., (1999), Gas evolution and power performance in direct methanol fuel cells, *Journal of Applied Electrochemistry*, vol. **29**, p. 661

Arico`, A.S., Creti`, P., Kim, H., Mantegna, R., Giordano, N. and Antonucci, V., (1996), Analysis of the Electrochemical Characteristics of a Direct Methanol Fuel Cell Based on a Pt-Ru/C Anode Catalyst, *Journal of Electrochemical Society*, vol. **143**, no. 12, p. 3950

Arico`, A.S., Creti`, P., Antonucci, P.L. and Antonucci, V., (1998), Comparison of Ethanol and Methanol Oxidation in a Liquid-Feed Solid Polymer Electrolyte Fuel Cell at High Temperature, *Electrochemical and Solid-State Letters*, vol. **1**, no. 2, p. 66

Arico`, A.S., Shukla, A.K., El-Khatib, K.M., Creti`, P. and Antonucci, V., (1999), Effect of carbon-supported and unsupported Pt-Ru anodes on the peformance of solid-polymer-electrolyte direct methanol fuel cells, *Journal of Applied Electrochemistry*, vol. **29**, p. 671

Astanovsky, D., (1998), Advanced Process for Hydrocarbon Production By Steam Conversion of Hydrocarbons, National Hydrogen Association Newsletter, vol. **3**, no. 2

Baldwin, R., Pham, M., Leonida, A., McElroy, J. and Nalette, T., (1990), Hydrogen-Oxygen Proton -Exchange Membrane Fuel Cells and Electrolyzers*, Journal of Power Sources*, vol. **29**, p.399

Barbir, F., Gomez, T., (1996), Efficiency and Economics of Proton Exchange Membrane (PEM) Fuel Cells, Energy Partners Inc., Florida

Barton, S.A.C, Murach, B.L., Fuller, T.F. and West, A.C, (1998), A Methanol Sensor for Portable Direct Methanol Fuel Cells, *Journal of Electrochemical Society,* vol. **145**, no.11, p. 3783

Bellows, R.J., Marucchi-Soos, E. and Reynolds, R.P., (1998), The Mechanism of CO Mitigation in Proton Exchange Membrane Fuel Cells Using Dilute H_2O_2 in the Anode Humidifier, *Electrochemical and Solid-State Letters*, vol. **1**, no. 2, p. 69

Bernardi, D.M., (1990), Water-Balance Calculations for Solid-Polymer-Electrolyte Fuel Cells, *Journal of Electrochemical Society*, vol. **137**, no. 11, p. 3344

Bernardi, D.M. and Verbrugge M.W., (1991), Mathematical Model of a Gas Diffusion Electrode Bonded to a Polymer Electrolyte, *AIChE*, vol. **37**, no. 8, p. 1151

Bernardi, D.M. and Verbrugge M.W., (1992), A Mathematical Model of the Solid-Polymer-Electrolyte Fuel Cell, *Journal of Electrochemical Society*, vol. **139**, no. 9, p. 2477

Bird, B., Stewart, W.E., Lightfoot, E.N., (1960), **Transport Phenomena**, John Wiley and Sons, Inc., London, p. 570

Broka, K., Ekdunge, P., (1997), Modelling the PEM fuel cell cathode, *Journal of Applied Electrochemistry*, vol. **27,** p. 281

Büchi, F. N. and Srinivasan, S., (1997), Operating Proton Exchange Membrane Fuel Cells Without External Humidification of the Reactant Gases. Fundamental Aspects, *Journal of Electrochemical Society*, vol. **144**, no. 8, p. 2767

Cha, S.Y., Lee, W.M., (1999), Performance of Proton Exchange Membrane Fuel Cell Electrodes Prepared by Direct Deposition of Ultrathin Platinum on the Membrane Surface, *Journal of Electrochemical Society*, vol. **146,** no. 11, p. 4055

Chen, R.S., Stallworth, P.E., Greenbaum, S.G., Fontanella, J.J. and Wintersgill M.C., (1995), High Pressure NMR and Electrical Conductivity Studies in Acid Form Nafion® Membranes, *Electrochemica Acta*, vol. **40**, no. 3, p. 309

Cole, B,. (1998), Chicago's Fuel Cell Buses Mobilized, National Hydrogen Association Newsletter, vol. **3**, no. 1

Creamer, M., (1999), Mining Weekly, vol. **5**, no. 30, August 13-19, p. 22

Delime, F., Le′ger , J.M. and Lamy, C., (1998), Optimization of platinum dispersion in Pt-PEM electrodes: application to the electroxidation of ethanol, *Journal of Applied Electrochemistry*, vol. **28**, p. 27

Dhar, H.P, Christner, L.G, Kush A.K. and Maru H.C., (1986), Performance Study of a Fuel Cell Pt-on-C Anode in Presence of CO and CO_2, and Calculation of Adsorption Parameters for CO Poisoning, *Journal of Electrochemical Society*, vol. **133**, no. 8, p. 1574

Eisman, G.A., (1990), The Application of Dow Chemical's Perfluorinated Membranes in Proton -Exchange Membrane Fuel Cells, *Journal of Power Sources*, vol. **29**, p. 389

Faubert, G., Guay, D. and Dodelet, J.P., (1998), Pt Inclusion Compounds as Oxygen Reduction Catalysts in Polymer-Electrolyte Fuel Cells, *Journal of Electrochemical Society*, vol. **145**, no. 9, p. 2985

Fisher, A., Jindra, J. and Wendt, H., (1998), Porosity and catalyst utilization of thin layer cathodes in air operated PEM-fuel cells, *Journal of Applied Electrochemistry*, vol. **28**, p. 277

Fournier, J., Faubert, G., Tilquin, J.Y., Cote`, R., Guay, D., Dodelet, J.P., (1997), High-Performance, Low Pt Content Catalyst for the Electroreduction of Oxygen in Polymer-Electrolyte Fuel Cells, *Journal of Electrochemical Society,* vol. **144**, no. 1, p. 145

Fuller T.F. and Newman, J., (1992), Experimental Determination of the Transport Number of Water in Nafion® 117 Membrane, *Journal of Electrochemical Society*, vol. **139**, no. 5, p. 1332

Fuller, F.T., Newman, J., (1993), Water and Thermal Management in Solid-Polymer-Electrolyte Fuel Cells, *Journal of Electrochemical Society,* vol. **140**, no. 5, p. 1218

Fuller T.F., (1997)., Is a Fuel Cell in Your Future? A look at the past and future performance of Fuel Cell Technology, *The Electrochemical Society Interface*, p. 26

Gibson, G.L. and Merten, G.P., (1997), 200 kW Fuel Cell Monitoring and Evaluation Program, New York State Energy and Research and Development Authority, New York

Gottesfeld, S. and Pafford, J., (1988), A New Approach to the Problem of Carbon Monoxide Poisoning in Fuel Cells Operating at Low Temperatures, *Journal of Electrochemical Society*, vol. **135**, no. 10, p. 2651

Gupta, S., Tryk, D., Zecevic, S.K., Aldred, W., Guo, D. and Savinell, R.F., (1998), Methanol-tolerant electrocatalyst for oxygen reduction in a polymer electrolyte membrane fuel cell, *Journal of Applied Electrochemistry*, vol. **28**, p. 673

Gurau, V., Liu, H. and Kakac, S., (1998), Two-Dimensional Model for Proton Exchange Membrane Fuel Cell, *AIChE*, vol. **44**, no. 11, p. 2410

Hirschenhofer, J.H., Strauffer, D.B., Engleman, R.R., (1994), Fuel Cells A Handbook, revision 3, U.S Department of Energy, West Virginia, p. 1-8, 16-17

Ianniello, R., Schmidt, V.M., Stimming, U., Stumper, J. and Wallau, A., (1995), CO Adsorption and Oxidation on Pt and Pt-Ru Alloys: Dependence on Substrate Composition, *Electrochemica Acta*, vol. **39**, no. 11, p. 1863

Kim, J., Lee, S.M., Srinivasan, S. and Chamberlin, C.E., (1995), Modelling of Proton Exchange Membrane Fuel Cell Performance with an Empirical Equation, *Journal of Electrochemical Society*, vol. **142**, no. 8, p. 2670

Kumar, G.S., Raja, M. and Parthasarathy, S., (1995), High Performance Electrodes with Very Low Platinum Loading for Polymer Electrolyte Fuel Cells, *Electrochemica Acta*, vol. **40**, no. 3, p. 285

Lalande, G., Tamizhmani, G., Cote`, R., Dignard-Bailey, L., Trudeau, M.L., Schulz, R., Guay, D. and Dodelet, J.P., (1995), Influence of Loading on the Activity and Stability of Heat-Treated Carbon-Supported Cobalt Phthalocyanine Electrocatalysts in Solid Polymer Eelctrolyte Fuel Cells, *Journal of Electrochemical Society*, vol. **142**, no. 4, p. 1162

Lancaster, P., (1996), Daimler-Benz's New Prototype Vehicle Powered by Fuel Cells, National Hydrogen Association Newsletter, vol. **1**, no. 2

Ledjeff, K., Mahlendorf, F., Peinecke, V. and Heinzel, A., (1995), Development of Electrode/Membrane Units for the Reversible Solid Polymer Fuel Cell (RSPFC), *Electrochemica Acta*, vol. **40**, no. 3, p. 315

Lloyd, A.C., (1991), California Clean Air Initiatives-The Role of Fuel Cells, Second Grove Fuel Cell Symposium, Royal Institution, London

Lombard, R., De Mattos, G.W.P., Williams, N.M., (1999), Practical Landfill Gas Extraction at Bisasar Road in Durban, Lombard, de Mattos and Associates, Durban

Lufrano, F., Passalacqua, E., Squadrito, G., Patti, A. and Giorgi, L., (1999), Improvement in the diffusion characteristics of low Pt-loaded electrodes for PEFCs, *Journal of Applied Electrochemistry*, vol. **29**, p. 445

Nahmias, D., (1999), Fuel Choice for Fuel Cell Vehicles, National Hydrogen Association Newsletter, vol. **4**, no. 3

Nguyen, V., (1993), A Gas Distributor Design for Proton-Exchange-Membrane Fuel Cells, *Journal of Electrochemical Society,* vol. **143**, no.5, p. L103

Nguyen, T.V. and White, R.E., (1993), A Water and Heat Management Model for Proton-Exchange-Membrane Fuel Cells, *Journal of Electrochemical Society*, vol.**140**, no. 8, p. 2178

Newman, J.S., (1991), **Electrochemical Systems**, Prentice Hall, Inc., New Jersey, chapters 2, 8

Oetjen, H.F., Schmidt, V.M., Stimming, U. and Trila, F., (1996), Performance Data of a Proton Exchange Membrane Fuel Cell using H_2/CO as Fuel Gas, *Journal of Electrochemical Society*, vol. **143**, no. 12, p. 3838

Okada, T., Nakamura, N., Yuasa, M. and Sekine, I., (1997), Ion and Water Transport Charateristics in Membrane for Polymer Electrolyte Fuel Cells Containing H^+ and Ca^+ Cations, *Journal of Electrochemical Society*, vol. **144**, no. 8, p. 2745

Paik, W., Springer, T.E. and Srinivasan, S., (1989), Kinetics of Fuel Cell Reaction at the Platinum/Solid Polymer Electrolyte Interface, *Journal of Electrochemical Society*, vol. **136**, no. 3, p. 644

Parthasarathy, A., Srinivasan, S., Appleby, A.J. and Martin, C.R., (1992 a), Temperature Dependence of the Electrode Kinetics of Oxygen Reduction at the Platinum/Nafion® Interface: A Microelectrode Investigation, *Journal of Electrochemical Society,* vol. **139**, no. 9, p. 2530

Parthasarathy, A., Srinivasan, S., Appleby, A.J. and Martin, C.R., (1992 b), Pressure Dependence of the Oxygen Reduction Reaction at the Platinum Microelectrode/Nafion® Interface: Electrode Kinetics and Mass Transport, *Journal of Electrochemical Society,* vol. **139**, no. 10, p. 2856

Patel, P.S., (1994), Ethanol Fuel Cells for Rural Power Generation, Energy Research Coporation, Connecticut

Perry, H., Green, D., (1984), **Perry's Chemical Engineers Handbook**, sixth edition, McGraw- Hill Book Co.

Poltarzewski, Z., Staiti, P., Alderucci, V., Wieczorek, W., and Giordano, N., (1992), Nafion® Distribution in Gas Diffusion Electrodes for Solid-Polymer-Electrolyte - Fuel-Cell Applications, *Journal of Electrochemical Society,* vol. **139**, no. 3, p. 761

Pyle, W., Spivak, A., Cortez, R. and Healy, J., (1994), Making Electricity with Hydrogen, Home Power Magazine, issue no. 35, p. 42

Ralph, T.R., Hards, G.A., Keating, J.E., Campbell, S.A., Wilkinson, D.P., Davis, M., St-Pierre, J. and Johnson M.C., (1997), Low Cost Electrodes for Proton Exchange Membrane Fuel Cells: Performance in Single Cells and Ballard Stacks, *Journal of Electrochemical Society*, vol. **144**, no. 11, p. 3845

Ravikumar, M.K. and Shukla, A.K., (1996), Effect of Methanol Crossover in a Liquid-Feed Polymer-Electrolyte Direct Methanol Fuel Cell, *Journal of Electrochemical Society*, vol. **143**, no. 8, p. 2601

Ren, X., Wilson, M.S., Gottesfeld, S., (1996), High Performance Direct Methanol Polymer Electrolyte Fuel Cells, *Journal of Electrochemical Society*, vol. **143,** no. 1, p. L12

Ren, X., Henderson, W. and Gottesfeld, S., (1997), Electro-osmotic Drag of Water in Ionomeric Membranes: New Measurements Employing a Direct Methanol Fuel Cell, *Journal of Electrochemical Society*, vol. **144**, no. 9, p. L267

Rho, Y.W., Velev, O.A. and Srinivasan, S., (1994 a), Mass Transport Phenomena in Proton Exchange Membrane Fuel Cells Using O_2/He, O_2/Ar, and O_2/N_2 Mixtures. I. Experimental Analysis, *Journal of Electrochemical Society*, vol. **141**, no. 8, p. 2084

Rho, Y.W., Srinivasan, S., Kho, Y.T., (1994 b), Mass Transport Phenomena in Proton Exchange Membrane Fuel Cells Using O_2/He, O_2/Ar, and O_2/N_2 Mixtures. II. Theoretical Analysis, *Journal of Electrochemical Society*, vol. **141**, no. 8, p. 2089

Samms, S.R., Wasmus, S. and Savinell., (1996), Thermal Stabality of Nafion® in Simulated Fuel Cell Environments, *Journal of Electrochemical Society*, vol. **143**, no. 5, p. 1498

Schmidt, V.M., Oetjen, H.-F. and Divisek, J., (1997), Performance Improvemennt of a PEMFC Using Fuels with CO by Addition of Oxygen-Evolving Compounds, *Journal of Electrochemical Society*, vol. **144**, no. 9, p. L237

Schmidt, T.J., Noeske, M., Gasteiger, H.A., Behm, R.J., Britz, P. and Bönnemann, H., (1998), PtRu Alloy Colloids as Precursors for Fuel Cell Catalyst. A Combined XPS, AFM, HRTEM, and RDE Study, *Journal of Electrochemical Society*, vol. **145**, no. 3, p. 925

Schmidt, T.J., Gasteiger, H.A., Behm, R.J., (1999), Methanol electrooxidation on a colloidal PtRu-alloy fuel-cell catalyst, *Electrochemistry Communications*, vol. **1**, no. 1, p. 1

Scott. K., Taama, W. and Cruickshank, J., (1998 a), Performance of a direct methanol fuel cell, *Journal of Applied Electrochemistry*, vol. **28**, p. 289

Scott, K., Taama, W.M. and Argyropoulos, P., (1998 b), Material aspects of the liquid feed direct methanol fuel cell, *Journal of Applied Electrochemistry*, vol. **28**, p. 1389

Smith, J.M. and Van Ness, H.C., (1987), **Introduction to Chemical Engineering Thermodynamics**, 4th ed., McGraw-Hill Book Co., Singapore

Springer, E., Zawodzinski, T.A. and Gottesfeld, S., (1991), Polymer Electrolyte Fuel Cell Model, *Journal of Electrochemical Society*, vol. **138**, no. 8, p. 2334

Springer, T.E., Wilson, M.S., and Gottesfeld, S., (1993), Modelling and Experimental Diagnostics in Polymer Electrolyte Fuel Cells, *Journal of Electrochemical Society*, vol. **140**, no. 12, p. 3513

Srinivasan, S., (1989), Fuel Cells for Extraterrestrial and Terrestrial Applications, *Journal of Electrochemical Society*, vol. **136**, no. 2, p. C41

Srinivasan, S., Manko, D.J., Koch, H., Enayetullah, M.A. and Appleby A.J., (1990), Recent Advances in Solid Polymer Electrolyte Fuel Cell Technology with Low Platinum Loading Electrodes, *Journal of Power Sources*, vol. **29**, p. 367

Sun, G.Q., Wang, J.T. and Savinell, R.F., (1998), Iron(III) tetramethoxyphenylporphyrin(FeTMPP) as methanol tolerant electrocatalyst for oxygen reduction in direct methanol fuel cells, *Journal of Applied Electrochemistry*, vol. **28**, p. 1087

Tamizhmani, G. and Capuano G.A., (1994 a), Improved Electrocatalytic Oxygen Reduction Performance of Platinum Ternary Alloy-Oxide in Solid-Polymer-Electrolyte Fuel Cells, *Journal of Electrochemical Society*, vol. **141**, no. 4, p. 968

Tamizhmani, G. and Capuano G.A., (1994 b), Life Tests of Carbon-Supported Pt-Cr-Cu Electrocatalysts in Solid-Polymer Fuel Cells, *Journal of Electrochemical Society*, vol. **141**, no. 9, p. L132

Taylor, J., Anderson, E., Vilambi, N.R.K., (1992), Preparation of High-Pt-Utilisation Gas Diffusion Electrodes for PEM Fuel Cells, *Journal of Electrochemical Society,* vol. **139**, no.5, p. L45

Ticianelli, A., Derouin, C.R., Redondo, A., and Srinivasan, S., (1988), Methods to Advance Technology of Proton Exchange Membrane Fuel Cells, *Journal of Electrochemical Society,* vol. **135**, no.9, p. 2209

Uchida, M., Fukuoka, Y., Sugawara, Y., Ohara, H. and Ohta A., (1998), Improved Preparation Process of Very-Low Platinum-Loading Electrodes for Polymer Electrolyte Fuel Cells, *Journal of Electrochemical Society*, vol. **145**, no. 11, p. 3708

Uchida, M., Aoyama, Y., Eda, N., and Ohta, A., (1995), New Preparation Method For Polymer-Electrolyte Fuel Cells, *Journal of Electrochemical Society,* vol. **142**, no.2, p. 463

Uchida, M., Fukuoka, Y., Sugawara, Y., Eda, N. and Ohta, A., (1996), Effects of Microstructure of Carbon Support in the Catalyst Layer on the Performance of

Polymer-Electrolyte Fuel Cells, *Journal of Electrochemical Society*, vol. **143**, no. 7, p. 2245

Verbrugge, M.W., (1989), Methanol Diffusion in Perfluorinated Ion-Exchange Membranes, *Journal of Electrochemical Society*, vol. **136**, no. 2, p. 417

Voss, H.h., Wilkinson, D.P., Pickup, P.G., Johnson, M.C. and Basura, V., (1995), anode Water Removal: A Water Management and Diagnostic Technique for Solid Polymer Fuel Cells, *Electrochemica Acta*, vol. **40**, no. 3, p. 321

Wakizoe, M., Velev, O.A. and Srinivasan, S., (1995), Analysis of Proton Exchange Membrane Fuel Cell Performance with Alternative Membranes, *Electrochemica Acta*, vol. **40**, no. 3, p. 335

Wang, J., Wasmus, S., Savinell, R.F., (1995), Evaluation of Ehtanol , 1-Propanol, 2-Propanol in a direct Oxidation Polymer-Electrolyte Fuel Cell. A Real-Time Mass Spectrometry Study, *Journal of Electrochemical Society*, vol. **142,** no. 12, p. 4218

Wang, J.T., Savinell, R.F., Wainright, J., Litt, M. and Yu, H., (1996), A H_2/O_2 Fuel Cell Using Acid Doped Polybenzimidazole as Polymer Electrolyte, *Electrochemica Acta*, vol. 41, no. 2, p. 193

Watanabe, M., Uchida, H. and Emori, M., (1998), Analyses of Self-Humidifying and Suppression of Gas Crossover in Pt-Dispersed Polymer Electrolyte Membranes for Fuel Cells, *Journal of Electrochemical Society*, vol. **145**, no. 4, p. 1137

Watanabe, M,. Igarashi, H. and Yosioka, K., (1995), An Experimental Prediction of the Preparation Condition of Nafion®-Coated Catalyst Layers for PEFCs, *Electrochemica Acta*, vol. **40**, no. 3, p. 329

Watanabe, M., Uchida, H., Seki, Y., Emori, M., Stonehart, P., (1996), Self-Humidifying Polymer Electrolyte Membrane for Fuel Cells, *Journal of Electrochemical Society* vol. **143**, no. 12, p. 3847

Wilson, M.S., Valerio, J.A. and Gottesfeld, S., (1995), Low Platinum Loading Electrodes for Polymer Electrolyte Fuel Cells Fabricated Using Thermoplastic Ionomers, *Electrochemica Acta*, vol. **40**, no. 3, p. 355

Wilson, M.S., Gottesfeld, S., (1992 a), Thin-film catalyst layers for polymer electrolyte fuel cell electrodes, *Journal of Applied Electrochemistry*, vol. **22,** p. 1

Wilson, M.S., Gottesfeld, S., (1992 b), High Performance Catalyzed Membranes of Ultra-Low Pt Loadings for Polymer Electrolyte Fuel Cells, *Journal of Electrochemical Society*, vol. **139**, no. 2, p. L28

Wilson, M.S., Garzon, F.H., Sickafus, K.E. and Gottesfeld, S., (1993), Surface Area Loss of Supported Platinum in Polymer Electrolyte Fuel Cells, *Journal of Electrochemical Society*, vol. **140**, no. 10, p. 2872

www.clp-energy.com

www.fetc.doe.gov

Ye, S., Vijh, A.K. and Dao, L., (1996), A New Fuel Cell Electrocatalyst Based on Highly Porous Carbonaized Polyacrylonitrile foam with Very Low Platinum Loading, *Journal of Electrochemical Society,* vol. **143**, no.1, p. L7

Yi, J.S. and Nguyen, T.V., (1998), An Along-the-Channel Model for Proton Exchange Membrane Fuel Cells, *Journal of Electrochemical Society*, vol. **145**, no. 4, p. 1149

Zawodzinski, T.A, Derouin, C., Radzinski, S., Sherman, R.J., Smith, V.T., Springer, T.E. and Gottesfeld, S., (1993 a), Water Uptake by and Transport Through Nafion® 117 Membranes, *Journal of Electrochemical Society*, vol. **140**, no. 4, p. 1041

Zawodzinski, T.A., Springer, T.E., Davey, J., *Journal of Electrochemical Society*tel, R., Lopez, C., Valerio, J. and Gottesfeld, S., (1993 b), A Comparative Study of Water Uptake By and Transport Through Ionomeric Fuel Cell Membranes, *Journal of Electrochemical Society*, vol.**140**, no. 7, p. 1981

Zawodzinski, T.A., Davey, J., Valerio, J. and Gottesfeld, S., (1995), The Water Content Dependence of Electro-Osmotic Drag in Proton-Conducting Polymer Electrolytes, *Electrochemica Acta*, vol. **40**, no. 3, p. 297